Structure formation of amphiphilic molecules at the air/water interface and after film transfer

Dissertation

zur Erlangung des Grades
„Doktor der Naturwissenschaften“
am Fachbereich Chemie, Pharmazie und Geowissenschaften
der Johannes-Gutenberg-Universität in Mainz

vorgelegt von

Rabea Keller
geboren in Mainz

Mainz, den 4. Juni 2012

Tag der mündlichen Prüfung: 25.06.2012
Dekan:

1. Berichterstatter:
2. Berichterstatter:

“Doktorarbeiten können in vielen Gestalten erscheinen.”

Walter Moers, Dr. Oztafan Kolibril (Rumo)

Zusammenfassung

Eines der Grundkonzepte der molekularen Selbstaggregation ist, dass die Morphologie der Aggregate in direktem Bezug zu Struktur und Wechselwirkung der aggregierenden Moleküle steht. Dies gilt nicht nur für die Aggregation in flüssiger Phase sondern ebenfalls für die Bildung sogenannter Langmuir Filme an der Luft/Wasser Grenzfläche. Entsprechend bilden Moleküle an der Grenzfläche nicht zwangsläufig einen flachen monomolekularen Film sondern können ebenso zu Mehrfachschichten oder Oberflächenmizellen aggregieren. In diesem Zusammenhang wurden verschiedene neuartige synthetische Moleküle in Hinblick auf ihre Strukturbildung an der Luft/Wasser Grenzfläche sowie im Filmübertrag untersucht. Beispielsweise wurden semifluorierte Alkane bezüglich ihrer Selbstaggregation und molekularen Orientierung an der Luft/Wasser Grenzfläche bzw. in übertragenen Filmen mittels Rasterkraftmikroskopie (SFM) und Kelvinsondenmikroskopie analysiert. Es konnte gezeigt werden, dass die untersuchten semifluorierten Alkane runde Oberflächenmizellen mit einem Durchmesser von 30 nm bilden, welche sich wiederum aus kleineren Muffin-förmigen Untereinheiten mit einem Durchmesser von 10 nm zusammensetzen. Des Weiteren konnte gezeigt werden, dass der Einbau eines aromatischen Kerns in die molekulare Struktur zur Ausbildung länglicher Aggregate führt und somit zu einer gerichteten Selbstaggregation. In weiteren Experimenten wurde die Selbstaggregation zweier unterschiedlicher amphiphiler Hybridmaterialien bestehend aus kurzkettigen Einzelstrang-Desoxyribonukleinsäure(DNA)-Sequenzen an der Luft/Wasser Grenzfläche studiert. Bei dem ersten der beiden Moleküle handelte es sich um eine Einzelstrang-DNA (11mer) mit zwei hydrophob modifizierten 5-(dodec-1-ynyl)uracil Nukleobasen am 5'-Ende der Oligonukleotid-Sequenz. Durch die Messung von Kompressions-Isothermen konnte die Bildung von semi-stabilen Filmen an der Luft/Wasser-Grenzfläche nachgewiesen werden. SFM Aufnahmen von Filmen, welche mittels der Langmuir-Blodgett Technik übertragen wurden, unterstützten diese Ergebnisse und deuteten auf die Bildung von Mono-, Doppel- und Mehrfachschichten in Abhängigkeit vom Oberflächendruck beim Übertrag hin. In diesen Schichten war die hydrophile DNA-Sequenz mit einer Oberflächenbelegung von 95% zur Luft ausgerichtet. Ähnliche Resultate wurden auch für die zweite amphiphile Verbindung - ein DNA-Blockcopolymer, bestehend aus einem kovalent an Polypropylenoxid gebundenen DNA(11mer)-Strang gefunden. Weiterhin wurde das Potential dieser DNA hybrid Materialen für die Durchführung molekularer Erkennungsexperimente an der Luft/Wasser Grenzfläche evaluiert. Dritter Schwerpunkt der vorliegenden Arbeit war die Untersuchung von schaumbildenden Polyglycerolestern (PGE). Ziel hierbei war die Aufklärung der molekularen Struktur von PGE an der Luft/Wasser Grenzfläche zum besseren Verständnis der Schaum-Stabilisation. Verschiedene Modelsysteme, welche die Luft/Wasser-Grenzfläche eines PGE Schaums imitieren, sowie Methoden für einen nicht invasiven Übertrag der Filme wurden durch SFM-Messungen charakterisiert. Es konnte gezeigt werden,

dass PGE durch Bildung von Mehrfachschichten die Luft/Wasser-Grenzfläche einer Schaumblase stabilisiert. Zusätzlich wurde eine neue Transfer-Methode, der sogenannte "Bubble-Film-Transfer" entwickelt und durch Aufnahmen mit einer High-Speed Kamera untersucht. Sämtliche Ergebnisse demonstrieren die Vielfalt möglicher Strukturen, die von amphiphilen Molekülen an der Luft/Wasser-Grenzfläche ausgebildet werden können, sowie den Einfluss der chemischen Struktur auf die Aggregat-Morphologie.

Abstract

One of the basic concepts of molecular self-assembly is that the morphology of the aggregate is directly related to the structure and interaction of the aggregating molecules. This is not only true for the aggregation in bulk solution, but also for the formation of Langmuir films at the air/water interface. Thus, molecules at the interface do not necessarily form flat monomolecular films but can also aggregate into multilayers or surface micelles. In this context, various novel synthetic molecules were investigated in terms of their morphology at the air/water interface and in transferred films. First, the self-assembly of semifluorinated alkanes and their molecular orientation at the air/water interface and in transferred films was studied employing scanning force microscopy (SFM) and Kelvin potential force microscopy. Here it was found, that the investigated semifluorinated alkanes aggregate to form circular surface micelles with a diameter of 30 nm, which are constituted of smaller muffin-shaped subunits with a diameter of 10 nm. A further result is that the introduction of an aromatic core into the molecular structure leads to the formation of elongated surface micelles and thus implements a directionality to the self-assembly. Second, the self-assembly of two different amphiphilic hybrid materials containing a short single stranded desoxyribonucleic acid (DNA) sequence was investigated at the air/water interface. The first molecule was a single stranded DNA (11mer) molecule with two hydrophobically modified 5-(dodec-1-ynyl)uracil nucleobases at the terminal 5'-end of the oligonucleotide sequence. Isotherm measurements revealed the formation of semi-stable films at the air/water interface. SFM imaging of films transferred via Langmuir-Blodgett technique supported this finding and indicated mono-, bi- and multilayer formation, according to the surface pressure applied upon transfer. Within these films, the hydrophilic DNA sequence was oriented towards air covering 95% of the substrate. Similar results were obtained with a second type of amphiphile, a DNA block copolymer. Furthermore, the potential to perform molecular recognition experiments at the air/water interface with these DNA hybrid materials was evaluated. Third, polyglycerol ester molecules (PGE), which are known to form very stable foams, were studies. Aim was to elucidate the molecular structure of PGE molecules at the air/water interface in order to comprehend the foam stabilization mechanism. Several model systems mimicking the air/water interface of a PGE foam and methods for a noninvasive transfer were tested and characterized by SFM. It could be shown, that PGE stabilizes the air/water interface of a foam bubble by formation of multiple surfactant layers. Additionally, a new transfer technique, the bubble film transfer was established and characterized by high speed camera imaging. The results demonstrate the diversity of structures, which can be formed by amphiphilic molecules at the air/water interface and after film transfer, as well as the impact of the chemical structure on the aggregate morphology.

Contents

1 Introduction

Insoluble monolayers at the air/water interface are ubiquitous in our every day life. They are formed by amphiphilic molecules, which combine a hydrophilic and a hydrophobic moiety within one molecule (Figure 1.1 A). These molecules usually align at the air/water interface according to these preferences, with the hydrophilic moiety facing water and the hydrophobic moiety facing air. Typical representatives of this molecule class are surfactants in soaps or lipids in cell membranes. The history of insoluble monolayers at the air/water interface can be traced back to the ancient Greeks, where Aristole noted the calming effect of an oil film on a water surface, and even further back to the Babylonians and Japanese[1]. Later on, in the 18th century, Benjamin Franklin made first attempts to treat this phenomenon scientifically [3]. After him, Lord Rayleigh was the first scientist to suspect that the oil film was only one molecule thick [4]. Agnes Pockels confirmed this theory by experiments, which had actually been carried out in her kitchen sink [5]. Her simple apparatus became the model for the instrument, which today is termed *Langmuir trough*. In 1917 Irving Langmuir introduced new theoretical concepts and experimental methods to investigate the film formation on water interfaces further [6]. He described his film balance and showed, as Pockels had done earlier, that it could be utilized to elucidate the shapes and sizes of molecules and their orientation at the air/water interface. In 1932 he was awarded the Nobel prize in chemistry "for his discoveries and investigations in surface chemistry". After him, insoluble monolayers at the air/water interface are also termed *Langmuir films*. Together with Katherine Blodgett he developed a technique to transfer insoluble monolayers onto substrates to investigate them even

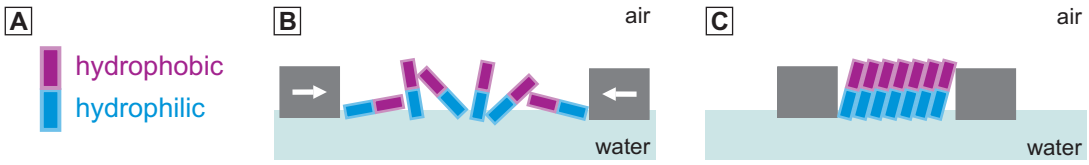

Figure 1.1: (A) Sketch illustrating an amphiphilic molecule. (B) Random orientation of amphiphilic molecules at the air/water interface. (C) Alignment of amphiphilic molecules upon compression at the air/water interface.

[1]The historical background is based on the reviews of Roberts et al. [1] and Oliveira et al. [2]

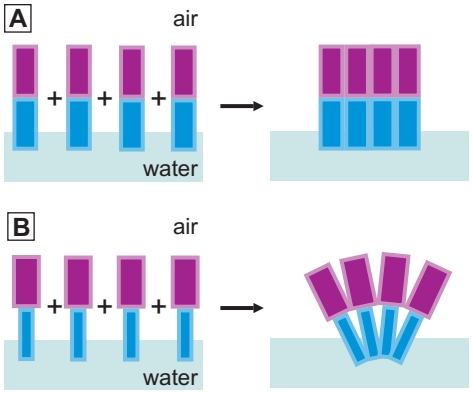

Figure 1.2: Sketch illustrating different molecular shapes resulting in the formation of different self-assembled structures like (A) monolayers or (B) surface micelles.

further [7]. This transfer is also called *Langmuir-Blodgett* (LB) *transfer* and the generated films *Langmuir-Blodgett films*. From this point, research in the field of insoluble monolayers has been manifold. Examples are the establishment of Langmuir monolayers as model systems for biological membranes [8] or fundamental investigations of structure and phase behavior of amphiphilic molecules at the air/water interface and after film transfer [9]. A significant upturn in LB research activity was related to the idea to utilize these thin films in electronic devices [10, 11]. Here, the aim is to always develop smaller and more efficient devices. The controlled fabrication of molecular films was and is seen as a promising possibility of molecular engineering: Monomolecular films with tunable molecular alignment and density (Figure 1.1 B and C) can be fabricated by LB transfer. Additionally, the film thickness is adjustable accurately by deposition of a specific number of layers forming a defined film with a multilayered structure. Next to surface pressure versus area isotherms, direct studies at the air/water interface can be performed by optical methods like fluorescence microscopy [12] or Brewster angle microscopy [13], X-ray reflectivity [14] and surface potential measurements [15]. These provide information about the molecule density and orientation of the molecules at the air/water interface, according to the molecule dipole moment. Transferred films can be investigated employing Fourier transform infrared spectroscopy, Raman or scanning electron spectroscopy, ellipsometry as well as scanning probe microscopy. This technique allows the investigation of the film structure and quality at high resolutions [16]. Scanning force microscopy is considered to be nondestructive and cannot only provide precise information about the film morphology, but also about the local frictional and elastic properties of the film with nanometer resolution. Molecular self-assembly is an important strategy to for the design of new innovative materials. The variety of possible structures, which can be formed by molecular self-assembly, is beyond the scope of ordinary chemical

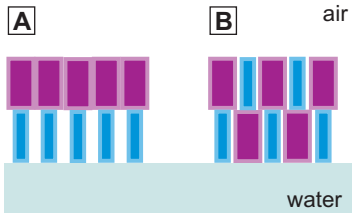

Figure 1.3: Possible orientations of the semifluorinated alkane molecules. (A) Parallel orientation. (B) Antiparallel orientation.

synthesis [17]. One of the basic concepts of molecular self-assembly is the direct relation between the morphology of the aggregate and the structure and interaction of the aggregating molecules [18]. As an example, Israelachvili et al. related the formation of a vesicle or micelle, respectively, from lipids dissolved in water to the molecular geometry of the lipid molecule itself [19, 20]. The geometry of the lipids as building blocks is thus directly related to the geometry of the aggregate (Figure 1.2). To comprehend exactly this relation is a crucial step for the design of new customized functional materials. Langmuir and LB films provide a suitable platform for this investigation, because they resemble a simplified two-dimensional model system for the aggregation in bulk solution. To elucidate and understand the Langmuir and LB film morphology is therefore especially appealing as a basis for the design of nanostructures in two and three dimensions.

1.1 Aim and Motivation

Aim of my PhD thesis was to investigate the molecular self-assembly of various novel synthetic molecules in terms of their structural morphology at the air/water interface and in transferred films. This is of interest because the molecules at the interface do not necessarily form flat monomolecular films (Figure 1.2 A). Similar to amphiphiles in solution, which can aggregate into different shapes like micelles, lamellar structures or vesicles, molecules at the interface can aggregate into multilayers [21] or surface micelles (Figure 1.2 B) [22].

First in this context, semifluorinated alkanes ($C_nF_{2n+1}C_mH_{2m+1}$ abbreviated as Fn-Hm) with varying chemical structures were investigated. Despite of the hydrophobic character of these molecules, they form stable Langmuir films at the air/water interface. Incompatibility of the fluorocarbon and hydrocarbon molecule moieties generates nano phase separation and results in the formation of stable surface micelles at the air/water interface. The surface micelle shape has been shown by Zhang et al. to be subject to the molecular chemical structure of the investigated

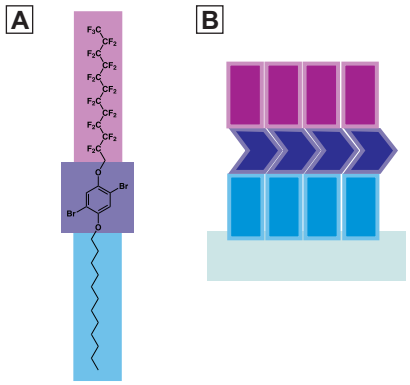

Figure 1.4: (A) Chemical structure of a core extended semifluorinated alkane molecule. (B) Illustration of the directionality induced by the aromatic moiety in the molecule core.

asymmetric molecules, forming circular surface micelles for shorter hydrocarbon chain lengths (F8H16) and elongated surface micelles for longer hydrocarbon chains (F8H20) [22,23]. However, Zhang et al. also found that variation of the fluorocarbon chain length had no significant influence on the micelle shape. The orientation and alignment of the molecules in the self-assemblies is a matter of discussion in this context, because a parallel as well as an alternating orientation of the fluorocarbon and hydrocarbon blocks has been proposed in literature (Figure 1.3) [24, 25]. Also, the correlation between shape of the self-assembly and chemical structure of the molecules is of interest. As an example, the implementation of directionality to the self-assembled structure by variation of the molecular chemical structure might offer the possibility to generate surface micelles with shapes beyond circular surface micelles. In my thesis, I have investigated the self-assembling properties of symmetric semifluorinated alkanes. Here, it is of general interest whether similar block lengths induce specific self-assembling properties different from the reported asymmetric cases. Moreover, the results on the purely alkyl-based semifluorinated alkanes are contrasted with those of two structurally related core-extended molecules, which combine aromatic with alkyl moieties. These aromatic moieties introduce a new kind of intermolecular interactions, the π-stacking, and are therefore promising candidates to introduce directional lateral organization of the molecules at the air/water interface (Figure 1.4). In order to investigate the structure formation and orientation of these molecules at the air/water interface and after film transfer I employed scanning force microscopy and Kelvin potential force microscopy. The respective experiments and results will be discussed in **Chapter 3**.

Second, amphiphilic DNA hybrid materials were examined, namely the DNA block-copolymer DNA-*b*-PPO and the nucleolipid dU11. Both materials consist of a single

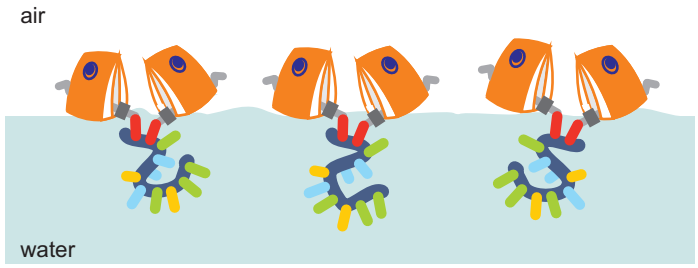

Figure 1.5: Sketch illustrating the anchoring of the single stranded DNA molecules by the hydrophobic moiety.

stranded DNA moiety, which is functionalized with hydrophobic components acting as arm floats to anchor the DNA moiety to the air/water interface (Figure 1.5). The air/water interface can thus be used as a confinement for the self-assembling process in order to prepare functional thin films. Additionally, structural changes in the molecules due to external stimuli like DNA hybridization will propagate along the air/water interface and can be detected e.g. by surface pressure - molecular area isotherms. Both DNA hybrid materials presented in **Chapter 4** and **5** theoretically offer the possibility to perform molecular recognition experiments at the air/water interface (Figure 1.6 A). Additionally, the formation of pristine films from these molecules at the air/water interface is new and appealing for the preparation of functional thin films, which are accessible for further modification by DNA hybridization (Figure 1.6 B). The structure formation of these amphiphilic DNA molecules is especially interesting, because they possess a very large hydrophilic head group, which might induce the formation of unorthodox structures rather than flat amphiphilic monolayers. The thin film structure of the nucleolipid dU11 will be discussed in **Chapter 4**. Furthermore, one part of my thesis was to investigate the practical potential for the performance of molecular recognition experiments at the air/water interface. The basic idea was to prepare a stable single stranded DNA (ssDNA) monolayer, which was anchored to the air/water interface and accessible by molecules from the subphase like complementary ssDNA. Aim was to detect the DNA hybridization at the air/water interface by changes in the isotherm shape and area per molecule. In order to do so, several practical aspects such as stability and film formation of the molecules at the air/water interface, influence of salt onto the Langmuir films, establishment of hybridization conditions and control experiments had to be investigated.

Third, I investigated polyglycerol esters, nonionic amphiphilic molecules, which exhibit a significant surface activity. The particular polyglycerol ester of interest for my thesis, PGE, consists predominantly of a hydrophilic triglycerol head group and an equimolar mixture of hydrophobic hexadecanoic acid and octadecanoic acid. This

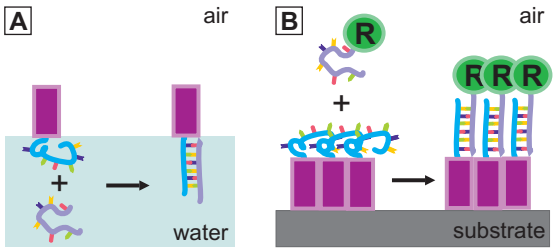

Figure 1.6: Sketch illustrating the potential applications of DNA hybrid material films. (A) The introduction of a hydrophobic component into the molecule offers the possibility to perform molecular recognition experiments directly at the air/water interface. (B) Transfer of the molecules onto solid substrates leads to the formation of functional thin films, which can be further modified by hybridization with a functionalized complementary DNA sequence (functionalization is indicated by R).

molecule has been shown to form exceptionally stable foams and is thus utilized readily in food industry [26]. Nowadays, food industry is especially interested in foams, because many food products like bread or ice cream owe their unique texture to the incorporation of gas bubbles stabilized by a surface active agent, thus forming a foam. Such a foam is supposed to be stable over a certain, preferably long period of time, because nobody wants his fresh ice cream to lose its creaminess after storage for one or two days. In other words, the stability of the foam in a food product is essential for the respective quality and life period. To understand the underlying molecular stabilization mechanism of a foam is crucial for the improvement of foam stability and for the design of new foaming agents. It was speculated from rheological experiments, that PGE molecules form a multilamellar structure upon adsorption to the air/water interface [27]. Scanning force microscopy is an especially valuable tool when it comes to the study of morphologies at the nano scale. It was thus employed on PGE films at the liquid/solid and air/solid interface in order to investigate them in terms of their molecular structure at the interface (**Chapter 6**). In this context, a new film preparation technique applicable for foam films, the *bubble film transfer*, was established and will be introduced in **Chapter 7**. My aim was to develop a transfer technique, which allows the investigation of real foam films rather than model systems in order to characterize the molecular structure inside the film. Real PGE foam films were investigated, as well as the applicability of the new film transfer technique for the characterization of other surfactants.

2 Fundamentals, materials and methods

2.1 Self-assembly of amphiphilic molecules

The term *amphiphile* originates from the greek words amphi "both sides" and philos "loving" and therefore entitles a molecule composed of a hydrophilic and a hydrophobic moiety. One characteristic property of amphiphilic molecules is that they spontaneously aggregate in water to form well defined structures such as micelles or vesicles [28]. In a micelle the molecules assemble into a spherical object with their polar head groups facing the water molecules while the hydrophobic apolar moieties are situated in the core of the object (Figure 2.1). The formation of these aggregates is energetically favorable and happens because of two competing effects [29]: The dissolution of the nonpolar hydrophobic part of the amphiphilic molecule causes the water molecules to adopt a highly ordered configuration around these moieties. This configuration is accompanied by a drastic decrease in entropy. An aggregation of the hydrophobic moieties into micelles is also accompanied by an entropy decrease, therefore both, the dissolution of unpolar groups and their aggregation are energetically unfavorable. The more unpolar groups aggregate, the less is the degree of order, which the polar water molecules have to adopt. Thus, the entropic gain due to the disorder of the water molecules is significantly larger than the loss due to

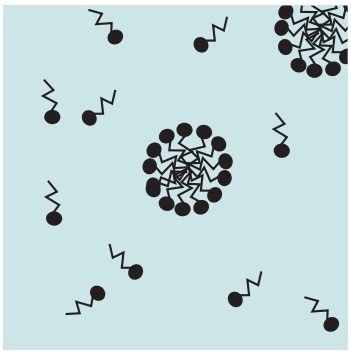

Figure 2.1: Schematic model of a micelle formed by amphiphilic molecules in water.

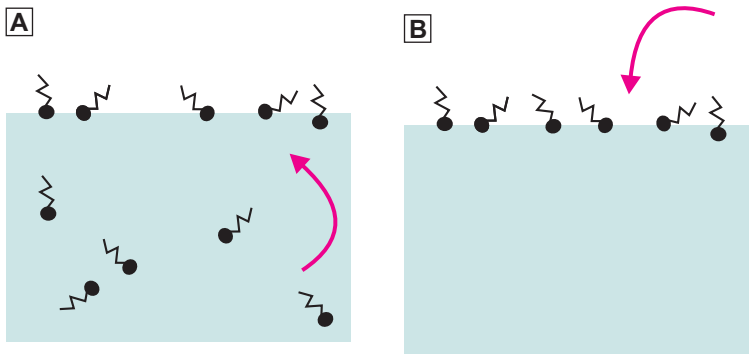

Figure 2.2: (A) Sketch of a Gibbs monolayer. The arrow indicates the adsorption of the molecules from bulk solution to the air/water interface. (B) Sketch of a Langmuir monolayer. The arrow indicates, that the molecules are brought explicitly to the air/water interface, they do not adsorb from the bulk solution.

the formation of micelles. This phenomenon is called *hydrophobic effect* [30]. An effect opposing the aggregation is the repulsion between polar head groups of the amphiphilic molecules, which is based on a complex interplay of several effects. In order to come into close proximity to each other, the head groups need to be dehydrated, which leads to a hydration repulsion [31]. The close proximity to other molecules reduces the molecular mobility and thus entropy, which also leads to a repulsion between the molecules. If the head groups are charged, additional electrostatic repulsion will come into play. The lateral repulsion between the hydrophilic head groups results in micelles with some hydrophobic inner parts being directly exposed to polar water molecules. The assembly into the micellar structures starts, when the amphiphilic molecules in solution exceed a certain concentration, the so called *critical micelle concentration* (cmc). An alternative to the aggregation into micelles in bulk solution is the adsorption of the amphiphilic molecules to the air/water interface. Here, the molecules can align into a monolayer with their hydrophilic moiety immersed in water while the hydrophobic moiety faces air. This film formed by adsorption of the amphiphilic molecules from bulk solution is called *Gibbs monolayer* (Figure 2.2 A). Amphiphilic molecules with a sufficiently hydrophobic moiety ($CH_3(CH_2)_{n-1}R$ with $n \geq 14$) form insoluble films at the air/water interface, which are called *Langmuir monolayers* (Figure 2.2 B). These Langmuir monolayers can be fabricated and characterized on an Langmuir trough.

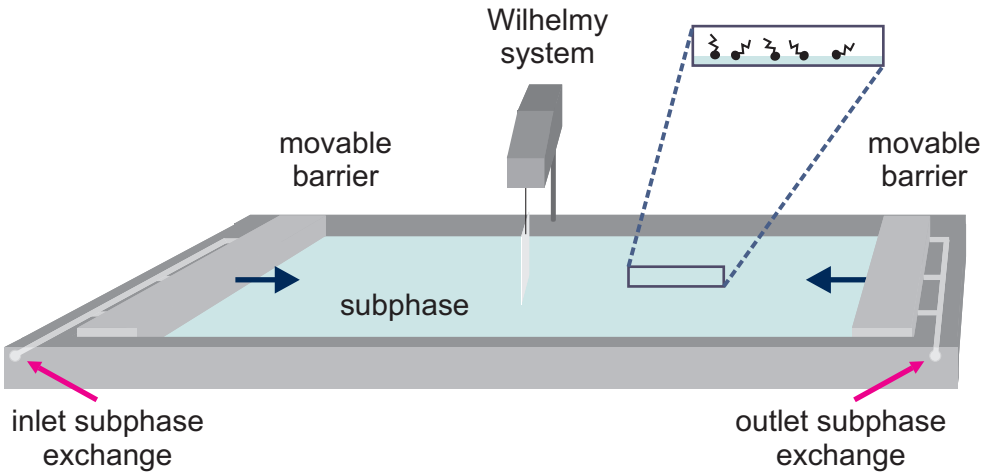

Figure 2.3: Sketch of a Langmuir trough equipped with two movable barriers and a Wilhelmy system for determination of the surface pressure.

2.2 Langmuir trough

The Langmuir trough is a so called film balance, which allows the preparation and characterization of monomolecular films at the air/water interface. The modern film balance is a teflon trough which is filled with an aqueous solution (typically ultrapure water, but also buffer solution depending on the application) (Figure 2.3). The temperature of the solution can be controlled by an externally attached thermostat with the heating system situated underneath the water reservoir. The aqueous solution inside the trough is also called the *subphase*. A defined monomolecular film can be prepared by dissolving the respective amphiphilic molecule at a known concentration in a volatile solvent, which is immiscible with the subphase, e.g. chloroform or hexane. Then, a certain volume of this solution is deposited at the air/water interface in tiny drops using a syringe. This process is called *spreading*. The volatile solvent evaporates while the amphiphilic molecules remain at the interface, forming a monomolecular film composed of a known number of molecules. The Langmuir trough is equipped with either one or two barriers, which can be moved to reduce the surface area. In the expanded state, the interaction between molecules spread at the interface is negligible. They behave like a two-dimensional gas and can move freely along the air/water interface. Upon compression of the barriers, the surface area is reduced and thus the surface concentration of the amphiphiles increases, which results in a significant lateral interaction between the amphiphiles and accordingly in a reduction of the surface tension. Illustratively, the surface tension decreases because the highly polar water surface (high surface tension) is converted into a nonpolar

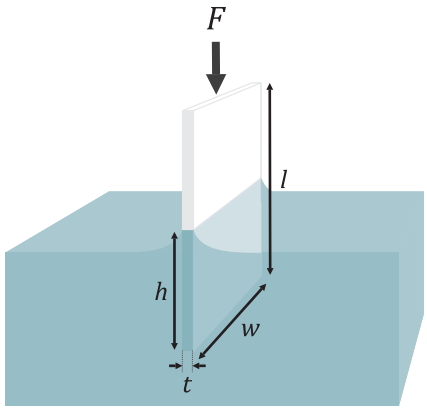

Figure 2.4: Sketch of a Wilhelmy plate immersed in water.

hydrocarbon surface (low surface tension). The Langmuir trough is equipped with a Wilhelmy plate which detects the variation of the surface tension.

2.2.1 Wilhelmy plate method

The Wilhelmy plate method [32] is widely used to measure the surface tension γ of liquids. A thin plate, in this particular case a filter paper [33], is vertically placed halfway through the liquid (Figure 2.4). The forces acting on the filter paper are surface tension and gravity pulling it downward into the solution while the buoyancy pushes it upward out of the solution. The force, which is required to prevent the filter paper from being drawn into the liquid is measured by a microbalance, to which the filter paper is attached via a wire. This net downward pulling force F for a rectangular Wilhelmy plate with a material density ρ_W, a width w, a thickness t and a length l, which is immersed to a depth h into the liquid of the density ρ_l is given by:

$$F = \rho_W glwt + 2\gamma\,(t + w)\cos\theta - \rho_l gtwh \tag{2.1}$$

where θ is the contact angle of the liquid on the filter paper and g the gravitational constant. In this equation, the second phase is neglected, because this is usually air with a negligible density. Equation 2.1 can be simplified by considering that the filter paper is wetted by the liquid and therefore the contact angle θ is considered to be 0°. In order to determine changes in the surface tension, the surface pressure π is measured, which is defined as $\pi = \gamma_0 - \gamma$. γ_0 is the surface tension of the pure subphase and γ the surface tension after spreading of the respective amphiphiles at

the air/water interface. The change in surface pressure can be calculated from the detected change in force:

$$\pi = \gamma_0 - \gamma = \frac{F_0 - F}{2(t + w)} \tag{2.2}$$

with F_0 the force acting on the Wilhelmy plate when immersed into the pure subphase and F the force acting after spreading of the amphiphiles. The thickness t of the Wilhelmy plate is negligible if $t \ll w$ resulting in

$$\pi = \gamma_0 - \gamma = \frac{F_0 - F}{2w} \tag{2.3}$$

A conventional Langmuir trough is used to determine the surface pressure against the surface area normalized by the absolute number of molecules at the air/water interface, the so called area per molecule A. The measurements are performed at a constant temperature, which is why the graph is also called *isotherm*.

Wilhelmy system calibration

The absolute force acting on the Wilhelmy plate can be determined by calibration of the Wilhelmy system. This can be achieved by measuring an isotherm of an arachidic acid monolayer, because the isotherm of this substance shows a sharp characteristic kink at $\pi = 25.6$ mN/m. In case the kink in a measured isotherm cannot be found at this surface pressure, the surface pressure can be calibrated as follows. An arachidic acid monolayer is compressed up to the surface pressure, at which the kink is visible in the isotherm. Then, the calibration potentiometer of the Wilhelmy system is used to regulate the actual surface pressure at the kink to the obliged surface pressure of 25.6 mN/m. This procedure is controlled by a renewed measurement of an arachidic acid isotherm and repeated, until the kink occurs at $\pi = 25.6$ mN/m. For the experiments in this thesis the calibration procedure was repeated upon exchange of the filter paper used as Wilhelmy plate. This was the case after approx. 20-30 measurements or upon exchange of the investigated substance in order to avoid contamination of the trough and the air/water interface.

2.2.2 Phases in monomolecular films

Monomolecular films show ordered phases similar to three-dimensional systems [34]. The measurement of an isotherm gives insight into the phase behavior of the respective substance (Figure 2.5). The phase behavior varies with the substance and is

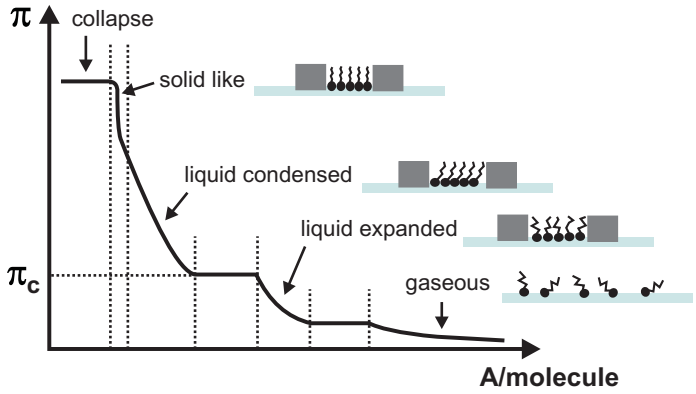

Figure 2.5: Schematic graph of a $\pi - A$ isotherm showing the different phases and the respective configuration of the molecules at the air/water interface. Not every molecule necessarily exhibits all phases.

mainly governed by the molecular structure and interaction between the amphiphilic molecules at the air/water interface. Typical phases for amphiphiles like fatty acids or phospholipids on water are the *gaseous* (G), *liquid* (L) and *solid* (S) state.

Amphiphiles at the air/water interface are in the gaseous state, when the average area per molecule available at the interface is larger than the molecule itself. Then, the molecules can move freely along the interface without interacting with each other in analogy to a three-dimensional gas. In this state, changes in surface tension are almost not detectable. A compression of the amphiphiles by a movement of the trough barriers can initiate a first-order phase transition into the liquid state. It is characterized by a significant lateral interaction between the molecules at the air/water interface. Here two liquid states have to be distinguished, the *liquid-expanded* (LE or L_1) and the *liquid-condensed* (LC or L_2) state. Molecules in the LE state are interacting with each other, but they do not exhibit a lateral order. The head group is highly hydrated and an extrapolation of the area per molecule yields values larger than the actual molecule. The LC phase is reached by compressing the monomolecular film even further. The transition from LE to LC is a first order phase transition. A plateau at the critical film pressure π_c can separate both states from each other, but is not mandatory. The amphiphiles are tilted against the surface normal and the tilt angle decreases upon compression. The film is relatively stiff, which is visible by a steeper slope, but there is still water present between the head groups. In the solid phase the $\pi - A$ isotherm lapse is linear. An extrapolation to $\pi = 0$ allows to determine the area per molecule which corresponds to the actual cross-sectional area of the molecule. In this state the head groups are largely dehydrated. Upon further film compression the monolayer collapses. This can be understood as the macroscopic failure of the monomolecular film: the

remaining surface area is too small to accommodate all amphiphiles, which have already adopted the closest possible configuration. The collapse is characterized by the formation of three-dimensional aggregates as well as by the loss of molecules diving into the subphase. The area per molecule which the amphiphiles occupy at the collapse point is called the *collapse area* A_c.

2.2.3 Monolayer stability

One possibility to investigate the stability of the amphiphilic monolayer at the air/water interface is the measurement of *compression-expansion cycles*. Here the monolayer is compressed up to a certain pressure and afterwards expanded completely. If the lapse of compression and expansion isotherm is congruent, this can be taken as a first indication for a stable monolayer and reversible aggregation. A hysteresis between compression and expansion isotherm is in contrast a clear indication that the compression process is not completely reversible. Possible reasons can be two-dimensional aggregation of amphiphiles, also called *raft formation* at the interface, but also the formation of three-dimensional aggregates or the loss of amphiphiles into the solution are possible scenarios. The compression and expansion are repeated, either with increasing or similar final surface pressure. The congruence of the first and second compression isotherm shows that the molecules have recovered completely from their first compression. If this is not the case, then again the two- or three-dimensional aggregation or molecular loss are possible explanations. Not all amphiphilic molecules form stable monolayers at the air/water interface. The better the amphiphile is actually soluble in the subphase, the higher is the probability that it will not stay at the interface upon compression. This molecule can either leave the interface and dissolve in the subphase or form a more stable three-dimensional aggregate at the interface, even before the actual collapse pressure is reached. The isotherm reversibility is a clear indication for the stability of a monomolecular film.

2.2.4 Subphase exchange

The Langmuir trough used for all experiments discussed in this thesis is equipped with a removable subphase exchange system. A peristaltic pump can be adjusted to introduce a certain liquid volume on one side of the trough and remove the same volume on the other side. Thus, a gradual exchange of the subphase can be achieved without disturbance of the monomolecular film. This system allows to investigate the influence of the subphase onto the monomolecular film or to introduce and remove molecules into the subphase. The system was also used to remove the subphase for the surface lowering film transfer, this time removing liquid at the in- and outlet.

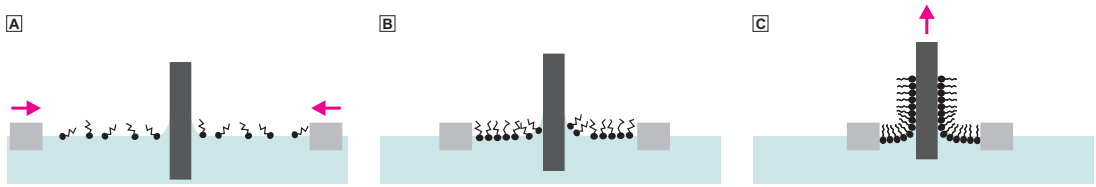

Figure 2.6: Illustration of the LB film transfer. (A) The hydrophilic substrate is immersed into the subphase and the molecules are spread. (B) The molecules at the interface are compressed to a designated surface pressure, which is then held constant. (C) The substrate is pulled out of the subphase and the compressed film is thus transferred.

2.3 Film transfer techniques

A monomolecular film can be transferred from the air/water interface onto a substrate. To achieve this, in this thesis several techniques have been employed:

2.3.1 Langmuir-Blodgett film transfer

The Langmuir-Blodgett (LB) film transfer is the oldest and best-established transfer technique for monomolecular films [7, 35]. A film can be transferred onto a hydrophilic substrate by immersing it vertically into the subphase before spreading of the amphiphilic molecules. After spreading the film can be compressed to a designated pressure, which is then kept constant by adjustment of the barrier position. Upon withdrawing of the substrate from the solution, the floating monomolecular film adsorbs to it retaining the molecular orientation with the hydrophilic head groups facing the hydrophilic substrate and the hydrophobic tails facing air (Figure 2.6). An alternative route yielding identical results is to compress the monomolecular film up to the designated pressure and to immerse the hydrophilic substrate afterwards. Due to the interaction between hydrophilic substrate and hydrophobic moieties of the molecules, no film will be transferred upon immersion but only upon withdrawal of the substrate. The film is transferred onto both sides of the immersed substrate, which is why the Si wafer used as substrate was polished on both sides, although only one side of the substrate could be investigated afterwards. Thus it can be ensured that the film transfer is not influenced by a contact angle difference between both sides of the substrate. Organized multilayered structures can be obtained by subsequent immersion and withdrawal of the substrate into the subphase.

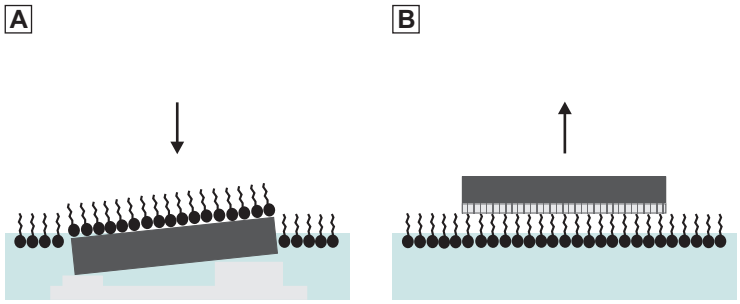

Figure 2.7: Illustration of the transfer techniques. (A) Surface lowering. (B) LS transfer onto a hydrophobic substrate. The shaded wafer surface illustrates the hydrophobic functionalization.

2.3.2 Surface lowering film transfer

A second technique to transfer a monomolecular film onto a hydrophilic substrate is via surface lowering (Figure 2.7 A) [36]. The hydrophilic substrate is placed on a sample holder immersed into the subphase with the hydrophilic side facing the air/water interface. After spreading of the amphiphiles, the subphase level is lowered placing the interfacial film onto the substrate. For the experiments discussed in this thesis, the subphase was removed by a peristaltic pump connected to the subphase exchange system of the Langmuir trough. The sample holder used is custom-made and holds the substrate at an inclination of 6° with respect to the air/water interface.

2.3.3 Langmuir Schaefer like transfer

The Langmuir Schaefer film transfer is a technique, which can be employed to transfer monomolecular films onto hydrophobic substrates like highly ordered pyrolytic graphite (HOPG) or hydrophobized Si wafers [37]: In the classical Langmuir Schaefer film transfer, the hydrophobic substrate is held parallel to the air/water interface and pushed through the monomolecular film into the subphase. Then, after the monomolecular film is removed from the interface, the substrate is removed from the subphase and left for drying. For experiments in this thesis a modified Langmuir Schaefer like approach was utilized: The substrate was held with tweezers and shortly dipped onto the monomolecular film at the air/water interface, instead of pushing it through the interface into the subphase (Figure 2.7 B). In contrast to the deposition techniques discussed before, the molecules in this film are oriented with the hydrophilic head group facing air while the hydrophobic tail faces the hydrophobic substrate, because the substrate approaches the film from the opposite side. The orientation with hydrophilic moieties of the monomolecular film facing air

is energetically less favorable than for the other transfer techniques, which is why it is possible that the film is removed from the substrate when withdrawing it from the subphase [38]. An alternative to overcome the unfavorable orientation is the formation of a bilayer, which results in a molecular orientation with hydrophobic moieties facing substrate and air.

2.3.4 Quality of transferred films

The quality of a transferred film is subject to several parameters such as compression speed, deposition speed, transfer pressure, nature of monolayer and substrate, as well as nature of the subphase. Preconditions for transfer of high quality films are a clean and dust free environment of the trough, the use of ultrapure water as basis for subphase solutions as well as clean and properly functionalized substrates. The determination of the ideal parameters for a film transfer is rather empirical [39]. Nevertheless, some general guidelines can be given: (i) The compression speed of the monomolecular film must be chosen slow enough to avoid local surface overpressure. This will be the case if the molecules have enough time to rearrange upon compression at the air/water interface. Upon too fast film compression, it can start to form ridges and can even collapse and form multilayers [40, 41]. (ii) Molecules must be in a close-packed state in order to transfer a film quantitatively onto a substrate. This state can be obtained at high surface pressures and the integrity of the transferred film is directly related to this transfer pressure [41]. If it is chosen too high, the film will start to collapse or to form small crystalline aggregates. If the transfer pressure is chosen too low, the film will not be continuous, covering the substrate incompletely. As a guideline, a transfer pressure of 80% of the collapse pressure is usually taken as starting point for further investigations. (iii) The transfer speed is usually chosen slow because the transfer requires strong interaction between the molecules and the substrate [42]. These interactions may involve a modification of the molecular packing [43]. It can therefore not generally be assumed, that the structure observed in a transferred film is similar to the structure at the air/water interface [16]. In order to draw reasonable conclusions on this topic, films have usually either been fabricated employing more than one transfer technique for comparison or the films at the air/water interface were directly investigated with complementary techniques like Brewster angle microscopy.

One parameter which gives a first impression on the film quality is the transfer ratio, which is defined as the decreased surface area on the trough divided by the coated area on the substrate. The closer this value is to one, the better is the quality of the transferred film. A transfer ratio bigger than one is a clear indication for collapse or dissolution of the monomolecular film at the air/water interface [41]. For experiments discussed in this thesis, the emphasis lay on the characterization of the

film morphology rather than on the production of defect free films. On the contrary, defects could often be utilized for analysis as reference for the determination of film thicknesses or surface potential differences.

2.4 Scanning force microscopy

Scanning force microscopy (SFM) is a tool to image surfaces beyond the resolution of optical microscopy. This is achieved by scanning a sharp tip (*probe*), which is attached to the end of a so called *cantilever*, over a surface, similar to the fingers of a blind person sensing Braille script. In analogy to the blind person feeling not only the elevations on the surface but also the roughness and texture, SFM is also capable of measuring not only the surface topography but also mechanical, viscoelastic and thermal properties as well as surface potentials and friction forces. This can be achieved because the probe experiences mechanical interaction with the sample surface, which is in contrast to optical microscopy. Attractive and repulsive forces act on the cantilever bending it. This movement can be detected by a photo diode using the optical lever principle (Figure 2.8). If the tip is in close proximity ($d < 0.1$ nm) to the sample, surface atoms of tip and sample will repel each other. Also, if higher forces are applied, elastic deformation in the contact area will cause repulsion of the tip. A water film, which forms under ambient conditions on the sample, exerts an attractive force onto the cantilever. Further away from the sample, long-ranged forces effect the cantilever. These include electrical forces, which can originate from work function differences, static surface charges or externally applied voltages. Van der Waals forces also belong to the group of long-ranged electrical forces. They include static and fluctuating dipole-dipole interactions between atoms and molecules of tip and sample. Forces acting on the cantilever can be determined for small cantilever deflections when considering the cantilever as a spring and applying Hooke's law $F = -k \cdot \Delta x$, where k is the spring constant and Δx the deflection of the cantilever. The distinct forces detected and the feedback control applied depend on the chosen measurement mode. The relevant measurement modes for this work are explained in detail in Section 2.4. The exact lateral and vertical movement of the cantilever is achieved with a piezo system. The information obtained about probe position and lever deflection is combined into a topographic map of the sample.

SFM modes

Contact mode

In *contact mode*, the SFM probe is in permanent repulsive contact with the sample surface. Usually, the force between tip and surface is kept constant. When the tip is

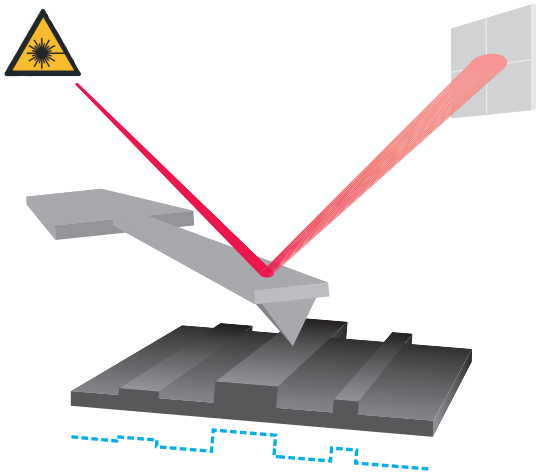

Figure 2.8: Sketch illustrating the basic principle of SFM. The movement of the cantilever is detected by a photo diode. A topographic profile is indicated by the dashed blue line.

scanned over the sample surface, changes in the sample topography initiate a change of the cantilever deflection, which is detected by the photo diode. The feedback control regulates the tip-sample distance by movement of the piezo in z-direction to again reach the initial, preset cantilever deflection. By recording this z-movement, a topographic image of the surface is obtained. Since the deflection of the cantilever and the force acting on the cantilever are directly related a constant force acts between probe and sample. Contact mode measurements have several drawbacks: (i) Friction between probe and sample generates a fast wear off of the probe, which reduces the image quality. (ii) The formation of a meniscus at the contact area between probe and sample under ambient measurement conditions results in attractive capillary forces acting on the cantilever [44]. This can cause manipulation of the sample surface. (iii) The lateral scanning of the sample induces shear forces, which can cause modification of the sample. (iv) The investigation of soft samples is problematic, because they can be easily indented with the probe, which can cause manipulation of the sample and contamination of the tip.

Tapping mode

A less intrusive alternative to contact mode measurements is the *tapping* or *intermittent contact mode*. Here the cantilever is excited to oscillate with a frequency close to its resonance frequency [45, 46]. This motion of the cantilever can be described as an harmonic oscillator. The force F_0 acting between tip and sample is represented in analogy to contact mode, as long as the cantilever is far away from the sample surface:

$$F_0 = k \cdot (z - z_0) \tag{2.4}$$

z_0 is the equilibrium position of the cantilever and z the deflection. If the cantilever moves closer to the surface, the tip-sample interaction F_{ts} will disturb the cantilever oscillation. The effective force F_{eff} acting on the oscillating cantilever close to the surface can then be expressed as:

$$F_{eff} = F_0 + \left(\frac{\partial F_{ts}}{\partial z}\right)_{z_0} \cdot (z - z_0) \tag{2.5}$$

With this equation, the effective spring constant k_{eff} is

$$k_{eff} = -\frac{\partial F_{eff}}{\partial z} = \left(k - \frac{\partial F_{ts}}{\partial z}\right)_{z_0} \tag{2.6}$$

The change of the effective spring constant results in a shift of the cantilever resonance frequency. The effective resonance frequency ω_{eff} is then [47]:

$$\omega_{eff} = \sqrt{\frac{k_{eff}}{m_{eff}}} = \sqrt{\frac{k - \left(\frac{\partial F_{ts}}{\partial z}\right)}{m_{eff}}} \tag{2.7}$$

The oscillation of the cantilever close to the surface is no longer elastic, meaning that it is damped by Van der Waals forces, electrostatics or capillary forces, which originate from a thin water layer usually covering the sample under ambient conditions. If the tip touches the sample a deformation of either of them will be possible. In case of this damping, the resonance frequency is shifted to lower frequencies. The dependence of amplitude $A(\omega)$ and excitation frequency is [47]:

$$A(\omega) = \frac{F_0/m_{eff}}{\left[(\omega_0^2 - \omega^2)^2 + (\omega\omega_0/Q)^2\right]^{1/2}} \tag{2.8}$$

with m_{eff} the effective mass of the cantilever, ω the resonance frequency and ω_0 the free resonance frequency. Q is the *quality factor* of the resonator and quantifies the energy dissipation per oscillation cycle [47], it is therefore a measure for the damping

of the oscillation. This damping also affects the resonance frequency. The effective resonance frequency ω_{eff} and free resonance frequency ω_0 are related by:

$$\omega_{eff} = \omega_0 \sqrt{1 - \frac{1}{2Q^2}} \tag{2.9}$$

With this oscillating cantilever several measurement techniques can be employed, which differ from each other in their the feedback control. One possibility is to approach the surface with a cantilever oscillating with a fixed frequency close to ω_0' until it reaches a preset amplitude, the amplitude setpoint. When scanning the surface, the height of the cantilever is adjusted to maintain the amplitude constant, which is called *amplitude modulation*. A second possibility is to maintain the frequency shift constant while oscillating the cantilever with a fixed amplitude, which is called *frequency modulation*.

The tip can vibrate vertically detecting only the long-range forces acting between tip and sample, which results in true non contact imaging. However, this can hardly be achieved in air and is mainly employed in ultra high vacuum.

If the probe touches the surface during each oscillation, this will result in a phase shift, meaning the difference between drive amplitude and actual amplitude of the cantilever oscillation. This shift is caused by energy dissipation due to probe-sample interactions and gives information about the local viscoelastic properties of the sample [48]. Amplitude modulation mode was used for the experiments in this thesis, if not denoted otherwise. Imaging of all samples was performed at the lowest possible tapping forces characterized by the ratio of free amplitude/amplitude set point [49], which was adjusted to be close to 1. A typical value reached in the experiments was 0.96. The free amplitude was determined to be the amplitude of the cantilever at peak maximum before approaching the surface. Even then I observed in some cases that material was dislocated or removed by the tip during the measurements.

Kelvin Probe Force Microscopy

Kelvin Probe Force Microscopy (KPFM) is an operation mode, which is sensitive to local variations in the *work function* ϕ of materials [50, 51]. The work function of a material is defined as the minimum energy needed to remove an electron from the solid. For a metal it represents the difference between the Fermi level and the vacuum level. In other types of materials, such as semiconductors or insulators, it can be regarded as the difference in energy between the vacuum level and the most loosely bound electron inside the sample. The work function depends on the specific

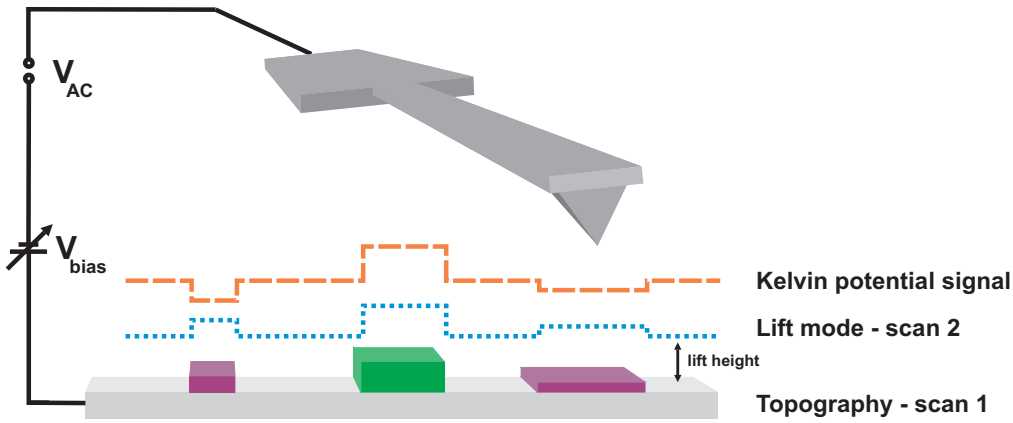

Figure 2.9: Sketch illustrating the basic principle of Kelvin probe force microscopy. Scan 1 determines the topography, scan 2 follows the surface profile determined in scan 1 in lift mode. The purple and green areas of the sample exhibit different surface potentials as can be seen in the detected KPFM signal.

material, adsorption layers (e.g. water), oxide layer thickness, dopant concentration, electrostatic charges, surface dipole moments and temperature [52].

When two different materials are brought into contact, then charge carriers can be exchanged at the interface. The same will be the case, if the materials are separated by a small distance, but electrically connected. The charge carriers move from the material with the higher Fermi level to the material with the lower Fermi level and as a consequence surface charges are generated, which give rise to an electric field. In equilibrium, the electric potential generated by the surface charges equals the energy difference between the Fermi levels. It is called *contact potential difference* V_{CPD}. The contact potential difference can be measured by using the vibrating capacitor method (Kelvin method): Two parallel plates are brought within a close proximity. One plate is made of the material under investigation (probe plate), while the second one consists of a reference material with a known work function (reference plate). One of the plates is periodically vibrated in the z-direction perpendicular to the other plate with a frequency ω and an amplitude z_0. This vibration results in a periodic current flow $I(t)$ [50]:

$$I(t) = \frac{\partial C}{\partial z} \cdot (V_{CPD} + V_{bias})\, \omega z_0 \cos(\omega t) \tag{2.10}$$

where C is the capacitance of the system defined by $C = \epsilon_0 A/d$ (A: surface area of the plates, ϵ_0: dielectric constant), $\frac{\partial C}{\partial z}$ is the change in capacitance with the distance

between the two plates and V_{bias} is the additionally applied constant potential. This additionally applied potential V_{bias} can be adjusted so that the periodic current flow $I(t)$ becomes zero and the space between the electrodes becomes field-free. This will be the case, if the externally applied bias is of the same magnitude as the contact potential difference, $V_{CPD} + V_{bias} = 0$. For KPFM measurements the identical principle is applied. The sample corresponds to the probe plate while the SFM tip acts as reference electrode. Now, the geometry of the system changes, because the SFM tip is very delicate with a tip radius of curvature of approximately 10 nm. As a consequence, the changes in the periodic current flow are too small to be detected significantly. It is however possible to detect the force F acting on the cantilever, which is induced by the charge accumulation at the tip and the sample surface. The total energy of the tip-substrate capacitor is $E = \frac{1}{2} \cdot C(V_{bias} + V_{CPD})^2$ and the force F can be derived as

$$F = \frac{1}{2} \cdot \frac{\partial C}{\partial z}(V_{bias} + V_{CPD})^2 \tag{2.11}$$

If $V_{CPD} + V_{bias} = 0$ is valid, the gap between tip and sample surface will be field free. Accordingly, the cantilever will not be bent. In all other cases, the cantilever will experience a force which results in a deflection of the cantilever. This force would be in the order of 1 pN leading to a very small deflection [53], which again is difficult to detect. The signal can be amplified by application of an additional AC bias $V_{AC} = V_0 \cdot \sin(\omega t)$ between tip and sample, with a frequency ω at or close to the resonance frequency of the cantilever. The force acting on the cantilever is therefore

$$F = \frac{1}{2} \cdot \frac{\partial C}{\partial z}(V_{bias} + V_{CPD} + V_0 \cdot \sin(\omega t))^2 \tag{2.12}$$

The force can be separated into its frequency components:

$$F_{dc} = \frac{1}{2} \cdot \frac{\partial C}{\partial z}\left((V_{bias} + V_{CPD})^2 + \frac{V_0^2}{2}\right) \tag{2.13}$$

$$F_{\omega} = \frac{\partial C}{\partial z} \cdot V_0 \cdot \sin(\omega t) \cdot (V_{bias} + V_{CPD}) \tag{2.14}$$

$$F_{2\omega} = -\frac{\partial C}{4\partial z} \cdot V_0^2 \cos(2wt) \tag{2.15}$$

The force at the angular resonance frequency F_ω will become zero when $V_{CPD} + V_{bias} = 0$. KPFM measurements can now be performed by regulating the externally applied voltage V_{bias} in such a way that oscillation of the cantilever is suppressed.

The contact potential difference between tip and sample can be determined in two different ways, either by *single-* or *dual-pass* data acquisition. For the dual pass method, which is also called *amplitude modulation* method, the topography is first scanned in tapping mode. Then, in a second scan the topographic profile is followed with the SFM tip at a defined distance from the surface, in the so called *lift mode* (Figure 2.9). During this scan the mechanical excitation of the cantilever is switched off and V_{AC} is applied to the tip while the sample remains grounded. An additional variable DC potential V_{bias} is applied at the tip in order to nullify the oscillation amplitude of the cantilever by a feedback control. This specific value is recorded at each raster point and is taken as the contact potential difference V_{CPD} between probe and sample surface. The technique is denoted as dual-pass measurement, because the sample is scanned twice, once in tapping mode and a second time in lift mode following the surface profile of the first scan. A second possibility is the single-pass data acquisition [53]. The resonance frequency f_0 of the mechanically excited cantilever in tapping mode is influenced by long-range forces like the electrical field gradient $\frac{\partial F}{\partial z}$ between tip and cantilever. The modified resonance frequency f_0' is

$$f_0' \approx f_0 \cdot \left(1 - \frac{1}{2k}\frac{\partial F}{\partial z}\right) \tag{2.16}$$

with k the spring constant of the cantilever. The application of an additional AC potential between tip and sample at a frequency ω (typically 3-10 kHz) results in the appearance of satellite peaks at $f_0 \pm \frac{\omega}{2\pi}$ and $f_0 \pm \frac{2\omega}{2\pi}$ as a consequence of the force gradient. The shift of the frequency at $f_0 \pm \frac{\omega}{2\pi}$ can be compensated by a feedback loop adjusting a bias potential V_{bias}, which enables to the record topography and contact potential difference V_{CPD} at the same time needing only one scan. The method is therefore called single-pass or *frequency modulation* method.

2.5 High speed camera

A high speed camera is capable of imaging fast processes at high recording rates, which allow the thorough investigation of these processes by replaying them in slow motion. For the experiments in this thesis the high speed camera was used to investigate the transfer of a bubble film onto a hydrophobic substrate. The high speed camera, which was used for all experiments is a Photron Fastcam SA-1, 4-6× magnification with backlighting. The typical recording rate was 5400 frames

per second (fps) at a resolution of 1000 pixel × 1000 pixel. A reduction of the resolution allows for an increase of the frame rate up to 675 000 fps. For more detailed investigation, some videos were recorded at 15 000 fps and a resolution of 700 pixel × 300 pixel.

2.6 Brewster angle microscopy

Brewster angle microscopy (BAM) [13,54] is a technique which allows *in-situ* imaging of film morphologies at the air/water interface, it is thus usually combined with a film balance. The principle is based on the effect that for a beam of light, which is polarized parallel to the plane of incidence, there is a an angle of incidence θ, at which no light reflection from a pure air/water interface occurs (Figure 2.10). This is called *Brewster angle* and satisfies the relationship

$$\tan(\theta) = \frac{n_2}{n_1} \tag{2.17}$$

where n_1 is the refractive index of air and n_2 is the refractive index of the subphase (usually water). The Brewster angle for an air/water system at 20°C is

$$\theta = \arctan\left(\frac{1.33}{1.00}\right) = 53.1^\circ \tag{2.18}$$

.

Introducing a thin film with a refractive index n_3 in between the the air and water phase changes the optical properties of the system because the relation for the Brewster angle is no longer fulfilled. As a consequence, the areas which are covered with the thin film now reflect parts of the incident light and can be detected by a detector like a CCD camera. In this way, areas, which are covered by a film can be visualized. The signal from the reflected light is relatively strong compared to the pure water surface, which does not reflect any light. The intensity of the detected light depends on the optical properties and the thickness of the film at the air/water interface. If the refractive index of the thin film is known, it will be possible to determine the thickness of the film by comparison of the intensity of the incident light I_0 and of the reflected light I_r. The reflectivity R is for single layered films directly related to the film thickness d, the wavelength of the incident light λ and the refractive indexes of the film n_3 and the suphase n_2 [55]:

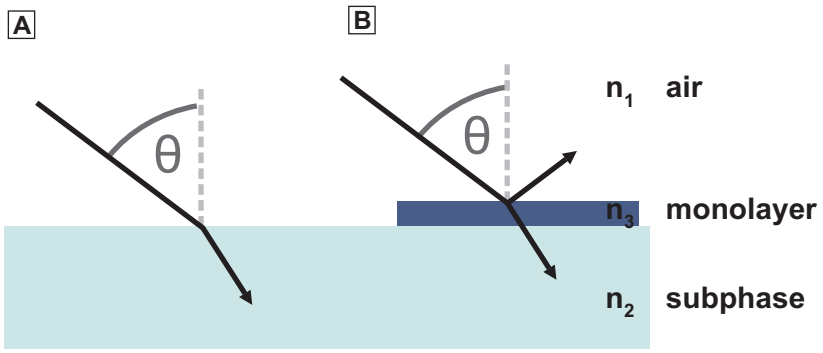

Figure 2.10: Sketch demonstrating the working principle of BAM (A) without and (B) with a monolayer at the air/water interface causing reflection of the incident light.

$$R = \frac{I_r}{I_0} = \left(\pi \cdot \frac{d}{\lambda}\right)^2 \cdot \frac{(n_3^2 - n_1^2 - 1 + n_2^2/n_3^2)^2}{1 + n_2^2} \tag{2.19}$$

Condition for the qualitative determination of the film thickness of a single layer is a precise photometric calibration of CCD camera and digital image processing system to obtain gray level information of selected image areas. Also, the film has to be optically isotropic and the refractive index has to be known or estimated. The reflectivity practically also relies on fluctuations at the air/water interface [13]. Phase transitions within the layer can be visualized by BAM, because the varying molecular density and molecule tilting in the respective phases results in optical anisotropy and thus in a varying contrast for each phase [56].

2.7 Photometric determination of nucleic acid concentration

The UV/Vis spectroscopy is a common tool to investigate light absorbing samples in terms of their concentration. This is possible, because the light absorption A at a sample specific wavelength λ is directly related to the concentration c of the investigated material, which can be described by Lambert Beer's law: $A = \epsilon \cdot c \cdot d$. ϵ is the extinction coefficient being characteristic for the substance investigated and d the thickness of the cuvette used for the measurement. Single stranded DNA is known to absorb light at the wavelength of $\lambda = 260$ nm [57]. The DNA hybrid materials DNA-*b*-PPO and dU11 both contain a single stranded

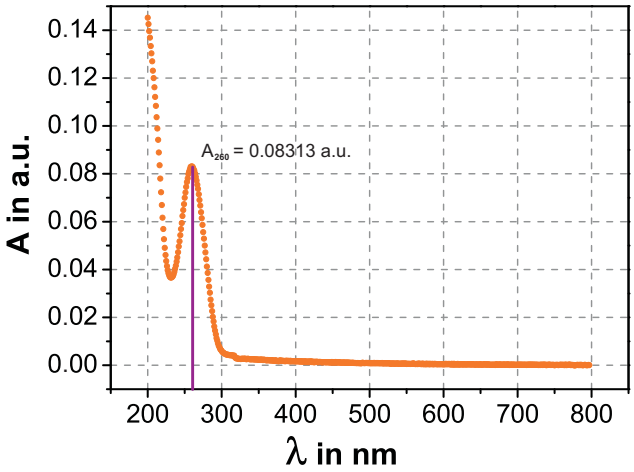

Figure 2.11: Exemplary UV/Vis spectrum of a DNA-*b*-PPO sample obtained in a cuvette with $d = 0.1$ cm. The purple line marks the absorption maximum at $\lambda = 260$ nm. The absorption A at this point is 0.08313 and the accordingly calculated DNA concentration of the solution is $c = 6.46$ µM.

DNA 11mer, which can be quantified by UV/Vis spectroscopy. The concentration of DNA in the solution was assumed to be similar to the concentration of the DNA hybrid material, which thus could be determined. Effects of light scattering due to micellation of the amphiphilic molecules on the light absorption have been neglected in this context, because the degree of micellation and thus the scattering can vary for each sample and cannot be quantified. The specific extinction coefficient ϵ for a given nucleic acid sequence can be determined using the nearest neighbor model, which was first introduced by Zimm et al. and Tinoco et al. [58,59]. The nearest neighbor model for nucleic acids assumes that the stability of a given base depends on the identity and orientation of neighboring bases [60]. The specific extinction coefficients for nucleic acid sequences investigated in this thesis have been predicted using an oligonucleotide property calculator called "OligoCalc" (http://www.basic.northwestern.edu/biotools/OligoCalc.html). The extinction coefficient $\epsilon_{DNA-b-PPO}$ for the DNA-*b*-PPO molecules with the following ssDNA sequence 5'-AAA GAT ATC TT-3' was determined to be $\epsilon_{DNA-b-PPO} = 128\ 667$ L/(mol · cm). Accordingly, the extinction coefficient ϵ_{dU11} for the following sequence 5'-UUT GGC GTC TT-3' is ϵ_{dU11} =103 327 L/(mol · cm). These specific extinction coefficient values allow to directly determine the concentration of a DNA containing sample by measurement of the light absorption at $\lambda = 260$ nm. An exemplary absorption spectrum is shown in Figure 2.11. DNA containing samples have been aliquoted accordingly for further experiments.

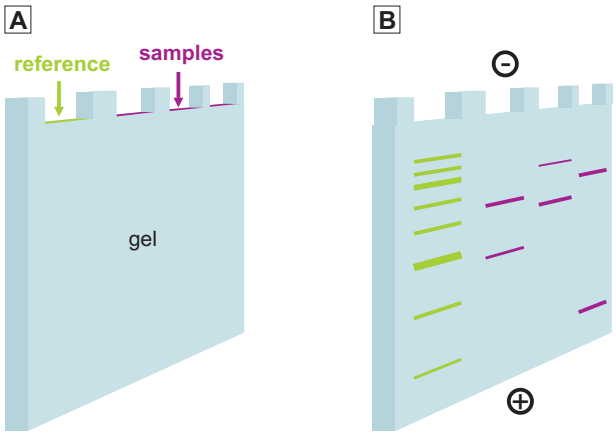

Figure 2.12: Sketch demonstrating the working principle of gelelectrophoresis: (A) Reference and samples are deposited in the wells of the gel. (B) Negatively charged reference and samples migrate in the gel due to application of an external electrical field.

2.8 Gelelectrophoresis

Gelelectrophoresis is an analytical method to separate different molecules in a mixture in terms of their size and charge. The mixture is applied onto a polymeric gel with a network-like structure, which is immersed in an ionic buffer solution (Figure 2.12 A). The degree of polymerization of the gel can be tuned according to the sample properties. The smaller the molecules in the mixture, the more finely-woven the network-like structure. An external electrical field is applied onto the gel upon which the molecules inside the mixture migrate through the gel. The molecules move with a speed according to their size and electric charge with the polymer network acting as a molecular sieve. Larger molecules move more slowly through the gel because they experience more constrain from the polymer network than smaller ones. The differently sized molecules form distinct bands in the gel (Figure 2.12 B). Gelelectrophoresis is a relative method, because the migration of the molecules is subject to the conformation of the migrating molecules, to the concentration of the buffer solution, to the degree of gel polymerization, to the strength of the external electrical field as well as to the duration of the electrical field application. Quantitative analysis of the molecular size is possible by comparison with reference samples. These are commercially available and can be chosen according to the investigated molecules. Gelelectrophoresis is typically applied on nucleic acids and protein molecules. The samples investigated in this thesis are hybrid nucleic acid materials containing 11 nucleic acid molecules. Thus, a reference sample with DNA molecule sizes ranging from 10-300 base pairs was used (GeneRuler Ultra low range DNA ladder). Aim of the gelelectrophoresis experiments discussed in this thesis was to investigate the

hybridization of these hybrid materials with their complementary DNA sequence. The ssDNA and double stranded DNA (dsDNA) can be distinguished from each other by their size, because dsDNA has a higher molecular weight and is stiffer than ssDNA. Therefore, ssDNA will migrate further in a gelelectophoresis experiment than dsDNA. Polyacrylamide was used as gel material for the experiments, which leads to the declaration of the methods as *polyacrylamide gelelectrophoresis* (PAGE). The ssDNA and dsDNA bands can be visualized by incubation of the gel in ethidium bromide solution in MilliQ water. This molecule is fluorescent when illuminated with UV light and intercalates into the major groove of the DNA helix. Distinct fluorescent bands are visible under illumination. The fluorescence intensity is proportional to the number of nucleic acids in the sample and can thus be used as a tool to quantify the amount of DNA in each band.

3 Effect of the molecular structure on the hierarchical self-assembly of semifluorinated alkanes

Semifluorinated alkanes (SFAs) with the molecular structure $C_nF_{2n+1}C_mH_{2m+1}$ (abbreviated as FnHm) are known to form stable Langmuir monolayers at the air/water interface despite the hydrophobicity of both the alkyl chain and the fluorinated moiety [61, 62]. The morphology of these self-assemblies is of special interest, because the molecules form stable surface micelles at the air/water interface.

SFAs have been widely studied in literature because of their unique properties: The F-chain is stiffer and more bulky than the H-chain, which is a consequence of the larger steric requirement of the fluorine atoms. This results in an *amphisteric* as well as *amphidynamic* character of FnHm molecules. Both chains exhibit different conformations, cross sections and space requirements (*amphisteric*) as well as distinct dynamic regimes: The F-chain is stiff and rod-like and tends to crystallize, while the H-chain is more flexible and therefore tends to build kinks and defects (*amphidynamic*) [62]. Both chains are basically hydrophobic, but the F-block additionally exhibits a lipophobic character, which is the reason for the strong incompatibility of fluorocarbon and hydrocarbon blocks and thus drives molecular phase separation of both chains. In this respect, these so-called *amphiphobic* molecules can be considered as molecular analogues of incompatible diblock copolymers. The strong difference in electronegativity of hydrogen and fluorine atoms induces a dipole moment along the -CF_2-CH_2- linkage, although the molecules are generally apolar in the sense that they neither exhibit a polar-hydrophilic-moiety nor dissolve in protic solvents [62]. The interplay of all these properties results in a significant surface activity of SFAs. SFA molecules find application as stabilizers of interfacial films to improve colloidal systems of biological interest, such as liposomes employed as drug carriers, or in the fluorocarbon-in-water emulsions used as blood substitutes [63, 64].

The molecular orientation and packing of an SFA carrying a hydrophilic head group could be elucidated to great detail, e.g., by grazing-incidence X-ray diffraction [65, 66]. Here the molecule is always oriented with hydrophilic head group facing the water interface. The situation is more ambiguous for amphiphobic SFA structures missing the hydrophilic head groups, because then both molecule moieties are

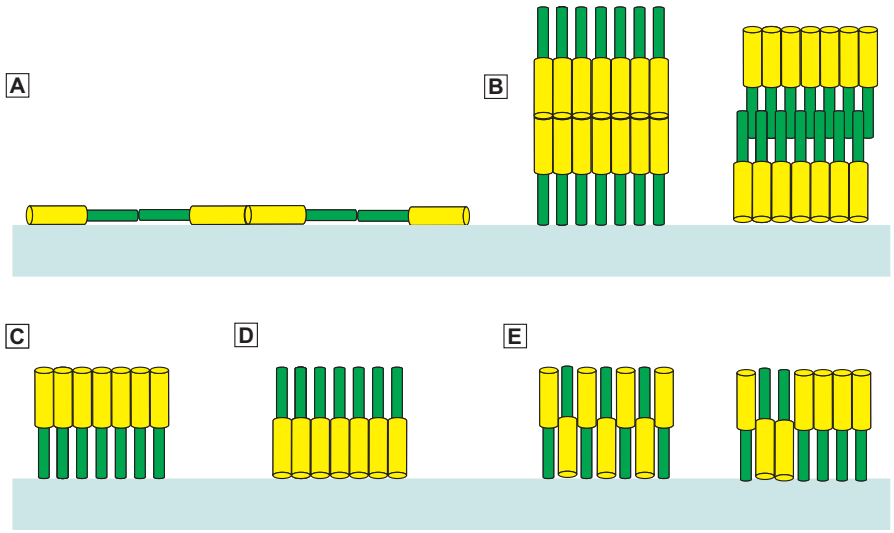

Figure 3.1: Different models for the F12H12 structure at the air/water interface (side view as cut through the water surface). Yellow: F-block, green: H-block. (A) Horizontal assembly, molecules lie flat on the surface. (B) Vertical multilayer. (C) Monolayer with F-block facing air. (D) Monolayer with H-block facing air. (E) Monolayer with antiparallel (left) or random (right) molecular orientation.

hydrophobic and thus do not like to face the water interface. Figure 3.1 shows the prominent orientation models with the molecules lying flat at the air/water interface (Figure 3.1 A), forming multilayers (Figure 3.1 B) and forming monolayers with either the hydrocarbon or fluorocarbon moiety facing water (Figure 3.1 C and D). The last options are an antiparallel or random orientation of the different molecule moieties (Figure 3.1 E). Significant efforts have been devoted to the investigation of the molecular orientation of SFA molecules at the air/water interface, still not giving a clear result. Semenov et al. proposed the formation of a flat phase (Figure 3.1 A) coexisting with vertically aligned molecules [67]. Abed et al. in 2002 proposed an upright antiparallel orientation of the SFA molecules (Figure 3.1 E), which he based on isotherm and surface potential measurements [24]. In contrast, from grazing-incidence X-ray diffraction and X-ray reflectivity studies on F12H18, Huang et al. concluded that the most probable molecular arrangement is a monolayer in which the hydrocarbon moieties are in contact with water and the fluorocarbon segments extend upwards away from the surface (Figure 3.1 C) [25]. Examination of diverse FnHm diblocks indicated that they tend to self-assemble spontaneously at different characteristic length scales into “surface micelles” (circular or elongated) as shown in Figure 3.2 [23,68]. The composition and formation of these micelles including the molecular orientation are major questions in this context. The surface micelle shape has been shown by Zhang et al. to be subject to the molecular chemical structure of

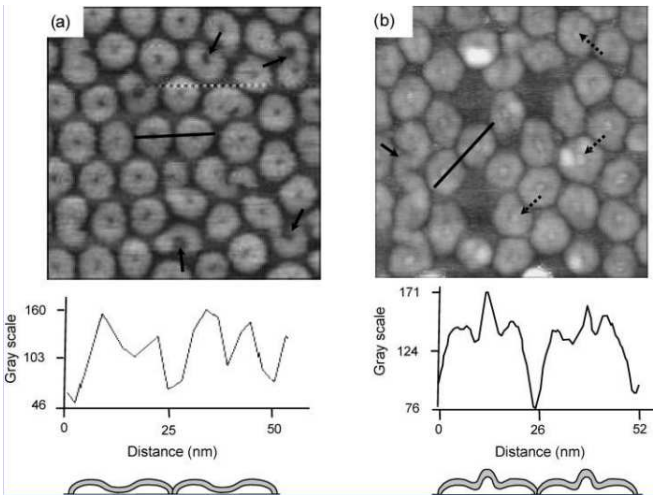

Figure 3.2: AFM images (336 × 336 nm) of films of F8H18 transferred at (a) 8 mN/m and (b) 12 mN/m . Below each panel are the corresponding image analyses of the AFM profiles along the solid lines shown in the images, as well as schematic representations of surface hemimicelles displaying (a) a pit and (b) a tip at their center. In (a), the arrows show doughnut-shaped surface micelles that are not completely closed up. In (b), the solid arrow shows an elongated micelle, and the dotted arrows show micelles with a tip at their center that may result from the protrusion of one of the edges during curling. Figure is adapted from [23].

the investigated asymmetric molecules, forming circular surface micelles for shorter hydrocarbon chain lengths (F8H16) and elongated surface micelles for longer hydrocarbon chains (F8H20) [22]. In contrast, Zhang et al. also found that variation of the fluorocarbon chain length had no significant influence on the micelle shape. In a later study Zhang et al. observed the formation of elongated and two different kind of circular micelles in SFM measurements [23]. He classified the circular micelles into ones exposing a pit or a tip in the center (Figure 3.2). As an explanation he suggested that all micelles are actually elongated and that circular micelles are formed by curling up of the elongated ones. Depending on the configuration of the curled up elongated micelles, either pits or tips in the middle of the circular micelle are formed (Figure 3.3).

These results give rise to the question of how the fluorinated molecules are assembled to form the surface micelles and how this assembly is correlated to the chemical structure of the molecules. If this relation is understood, it will be possible to utilize the novel organization motifs for the preparation of nanostructured surfaces. Therefore I have investigated new symmetric SFA molecules in terms of their self-assembly. It is of general interest whether similar block lengths induce specific

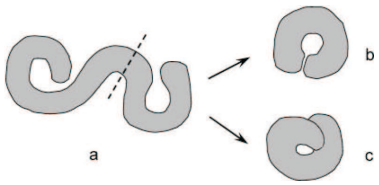

Figure 3.3: Schematic representation of the partition of an elongated micelle (a) to yield formation of (b) a pit-centered micelle and (c) a tip-centered micelle, depending on the conditions of transfer. Figure is adapted from [23].

self-assembling properties different from the reported asymmetric cases. Moreover, the results of a purely alkyl-based SFAs are contrasted with those of two different core extended SFA molecules, which combine aromatic with alkyl moieties. These aromatic moieties feature different modes of intermolecular interactions and therefore are promising candidates for the introduction of directional lateral organization of the molecules at the air/water interface.

This chapter deals with the aqueous surface-mediated self-assembly into molecularly thin films of SFAs, namely perfluoro(dodecyl)dodecane (F12H12) (Figure 3.4 A), perfluoro(dodecyl)eicosane (F12H20) (Figure 3.4 B), 1,4-dibromo-2-((perfluoroundecyl)methoxy)-5-(dodecyloxy)benzene (F11H1-core-H12) (Figure 3.4 C) and bis-(3-(1-perfluoroundecylmethoxy)-5-dodecyloxyphenyl)ethyne (bis-F11H1-core-H12) (Figure 3.17 A). The film structure was investigated by SFM on transferred films to image the film morphology and KPFM experiments were conducted to analyze the molecule orientation. The experiments have been conducted within the framework of a cooperation with xxx and xxx from the xxx.

3.1 SFA molecules at the air/water interface

All SFAs introduced were investigated at the air/water interfaces in terms π-A isotherms and compression-expansion cycles. Aim of the experiments was to investigate the phase behavior and stability of the SFA films at the air/water interface. Both, isotherms and compression-expansion cycles were recorded under identical conditions. For the compression-expansion cycles the film was compressed up to a designated surface pressure and afterwards fully expanded before recompression to a higher designated pressure.

The π-A isotherm of F12H12 is shown in Figure 3.5 A. It compromises a first sharp increase in surface pressure that occurs at a surface area A_0 of ca. 33-34 Å^2. A_0

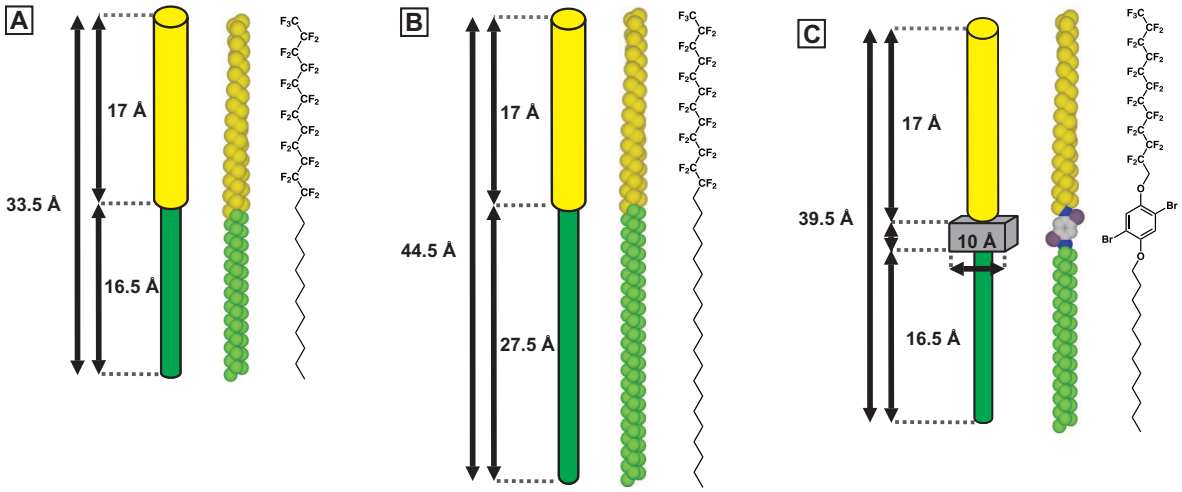

Figure 3.4: Chemical structures, molecular models, and schematic representations of (A) F12H12, (B) F12H20 and (C) F11H1-core-H12.

is the surface area at zero surface pressure extrapolated from the slope between 2 and 6 mN/m. A stable monolayer is formed up to the limiting area (collapse area) A_c = 31-33 Å^2. The measured A_0 and A_c values correspond to those found in the literature for other semifluorinated alkanes (for example F8H16 [69]). The values are consistent with the cross section (projection area) of a fluorocarbon chain, which lies between 27 and 30 Å^2 [62]. Under the given experimental conditions a phase transition is detected for F12H12 as a small change in the slope of the isotherm at a surface pressure of about 3 mN/m (inset of Figure 3.5 A, indicated by an arrow). Similar phase transitions have been reported previously for other, asymmetric semifluorinated alkanes and alkanoic acids [70–73]. Broniatowski et al. attributed the analogous phase transition of F12H14 as a transition from LE to LC phase [70]. Although the structure of the F12H12 monolayer was investigated in detail, a structural correlation to the phase transition in the isotherm is not clear [74]. The collapse at a surface pressure of 10 mN/m marks the macroscopic failure of the monolayer, meaning that at this point molecules from the film either dive into the subphase or start to form three-dimensional aggregates. The former is due to the strong hydrophobic character of the SFA molecules rather unlikely. After the collapse of the F12H12 monolayer, the surface pressure remains almost constant at 10 mN/m down to an area of 13 Å^2, forming a plateau region. Then, a second steep pressure increase occurs at an area of approx. 10 Å^2, which is approximately one-third of the monolayer collapse area A_c. A similar behavior was reported recently by Gracia Lux et al. [75] for several semifluorinated alkanes with different block lengths (F8H16, F8H18, F8H20, and F10H16), which was explained by the buildup

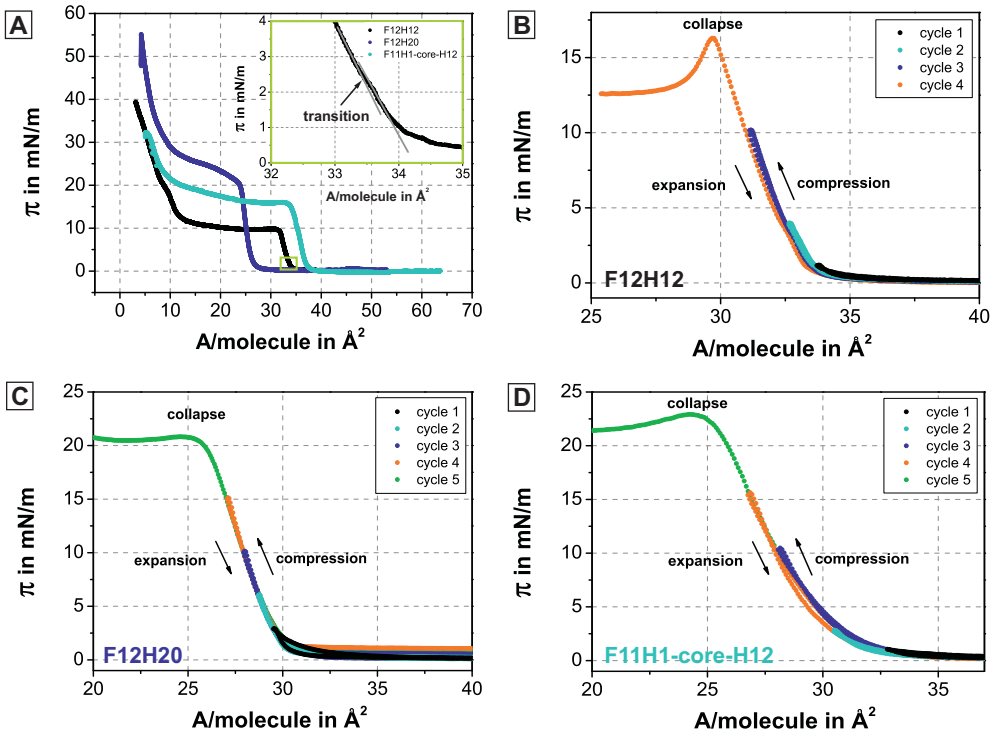

Figure 3.5: (A) Full isotherms of F12H12, F12H20 and F11H1-core-H12 spread from hexane. The inset shows the phase transition for F12H12 visible at a surface pressure of 3 mN/m indicated by an arrow. (B) F12H12 compression-expansion cycles. (C) F12H20 compression-expansion cycles. (D) F11H1-core-H12 compression-expansion cycles.

of a three-dimensional aggregation system. The authors showed that the two- and three-dimensional systems coexist in the plateau region.

The course of the F12H20 and F11H1-core-H12 isotherms is similar to that of F12H12 (Figure 3.5 A). They also comprise a first sharp increase of the surface pressure at A_0 = 27-32 Å^2 for F12H20 and A_0 = 35-37 Å^2 for F11H1-core-H12. In contrast to F12H12, both isotherms do not exhibit any phase transition and the monolayers collapse at A_c = 25-28 Å^2 for F12H20 and A_c = 33-34 Å^2 for F11H11-core-H12. The plateau region after the collapse can also be observed for both molecules and is characterized by a slight pressure and slope increase.

Aim of the measurement of compression-expansion cycles was to determine the film stability on the one hand and reversibility of the film deformation on the other hand (Figure 3.5 B-D). The isotherms for all three molecules are completely reversible, without hysteresis, for compression-expansion cycles before the collapse of the monolayer. These results indicate that the film deformation is under these experimental

conditions reversible. Also the phase transition of F12H12 was not affected by the repeated layer compression and reoccurred in each run at about 3 mN/m.

3.2 Film transfer

3.2.1 F12H12

In order to characterize the two-dimensional self-assembly structure of the F12H12 monolayers, SFM measurements were performed on films, which were transferred from the air/water interface via surface lowering (Figure 3.6). In order to do so, a hydrophilic substrate was placed on the sample holder, which was immersed in the subphase, a film was spread and the molecules were compressed to a designated surface pressure. Then, the subphase was removed with a peristaltic pump and the film was thus lowered onto the substrate and left for drying.

Figure 3.6 A shows the SFM topographic image of a monolayer of F12H12 transferred to a silicon wafer at a lateral pressure of 2 mN/m. Imaging conditions had to be adjusted to the lowest possible tapping forces characterized by the ratio of free amplitude/amplitude set point [49] of 0.96 and a peak offset of -3%. Otherwise micelles where either removed from the substrate or featureless blurry images were obtained. The image (Figure 3.6 A) depicts an array of surface micelles (circles, spirals, and wormlike structures) as previously reported and rationalized for similar derivatives with asymmetric fluorocarbon and hydrocarbon block lengths [23, 68]. These two-dimensional micelles were observed at all surface pressures investigated (from 1 mN/m up to the collapse) with a diameter of 35.2 ± 7.1 nm determined by measurement of the center to center distance between two neighboring surface micelles. Their average thickness was determined to be 2.1 ± 0.2 nm by surface profile analysis (Figure 3.6 D). The higher-resolution image in Figure 3.6 B exhibits features within the surface micelles (white arrows), which suggests that the surface micelles are composed of individual more uniform substructures. Their diameter of 12.2 ± 2.4 nm has been estimated by measuring the distance between the centers of adjacent substructures in the SFM images. At 2 mN/m, the micelles are partially arranged in close-packed hexagonal arrays (dotted circle in Figure 3.6 C). According to literature, the micelle size varies slightly with the surface pressure for other SFA molecules in the range of 1-10 mN/m, but the micelles progressively move closer together with increasing surface pressure [23]. However, for the F12H12 molecule in this surface pressure regime, the relative compression ($\Delta A/A_0$) is only approx. 7% and the applied surface pressure barely influences the micelle packing and size. Similar to other studies, it was found that surface micelles form already at low surface pressures and that compression results in a closer micelle packing rather than in a

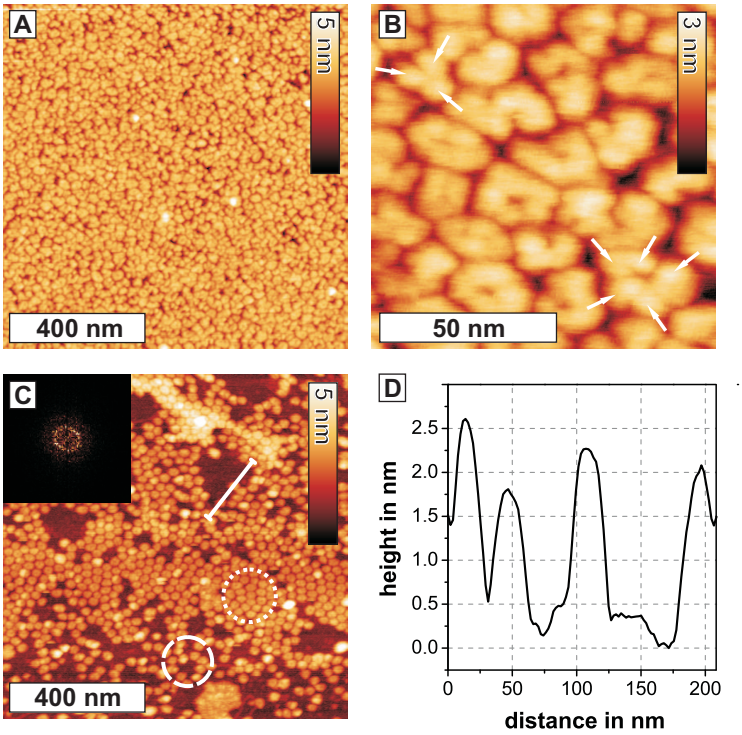

Figure 3.6: (A) SFM topographic image of an F12H12 monolayer transferred at 2 mN/m. (B) Zoom-in of the topographic image. Different micelle shapes and individual substructures marked by white arrows are visible. (C) SFM topographic image of an F12H12 monolayer deposited by direct evaporation of the subphase without compression. The image shows closely packed micelles (dotted circle) as well as disordered regions (dashed circle). The inset in the upper left corner shows an Fast Fourier Transformation (FFT) spectrum of the region in the dotted circle confirming the hexagonal packing. (D) Line plot at the location marked in image C. The plot shows the dimensions of one individual surface micelle (height $\approx$ 2.2 nm, diameter $\approx$ 23 nm).

change of micelle morphology [76]. A noteworthy feature at these surface pressures is the presence of higher three-dimensional agreggates in the dense layer of surface micelles (Figure 3.7 A), which have not been previously reported in literature. Up to collapse, these aggregates are virtually monodisperse (diameter ca. 40 nm; thickness 4.3 nm with respect to the substrate). At 10 mN/m, close to the monolayer collapse, additional larger aggregates appear as flat islands on top of the micelle carpet, which are apparently three-dimensional layered structures associated with the monolayer collapse (Figure 3.7 B). Similar aggregates have been reported for F8H20 diblocks, at high surface pressures, after collapse of the monolayer [75].

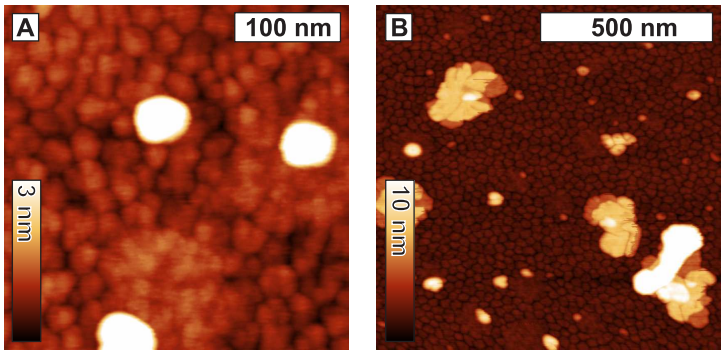

Figure 3.7: SFM topography images of F12H12 films (A) transferred at $\pi = 5$ mN/m, showing the micelle carpet and larger three-dimensional aggregates. (B) transferred at $\pi = 10$ mN/m. The flat islands on top of the micelle carpet are probably associated to the monolayer collapse.

Additionally, KPFM measurements were employed to investigate the orientation of the SFA molecules. In several regions distributed throughout the whole F12H12 film, the surface potential measurements (Figure 3.8 C) reveal domains with lower surface potential, which exhibit only a faint contrast in the topographic images and phase images (marked by a green oval in Figure 3.8). These slightly higher domain structures appear denser with less defined micellar boundaries. The corresponding more negative surface potential difference is independent of the aggregates on top of the micelles, and hints at a different structure/organization of the molecules in these regions. Changes in the surface potential properties can have several possible explanations. The presence of included water would lead to slight changes in topographic, viscoelastic and electric properties. A difference in the micellar density or a change in the molecular orientation would also induce modifications of the surface potential, as all three molecules F12H12, F12H20, and F11H1-core-H12 exhibit a strong dipole moment. It is therefore not clear, which of these effects actually causes the morphological and surface potential difference.

Molecular orientation

As already discussed in the introduction, several arrangements of the F12H12 molecules at the air/water interface are conceivable (Figure 3.1). From the experimental data obtained so far, some of them can already be excluded. In order to do so, the dimensions of the F12H12 molecule are estimated: A stretched F12H12 molecule in all-trans conformation is according to the molecular structure model of Lo Nostro et al. $d(\mathrm{FnHm}) = (0.13 \cdot \mathrm{n})$ nm + $(0.1265 \cdot \mathrm{m})$ nm + 0.258 nm = 3.3 nm long with n = m = 12 [77]. The surface area of one F12H12 molecule was found to be approx.

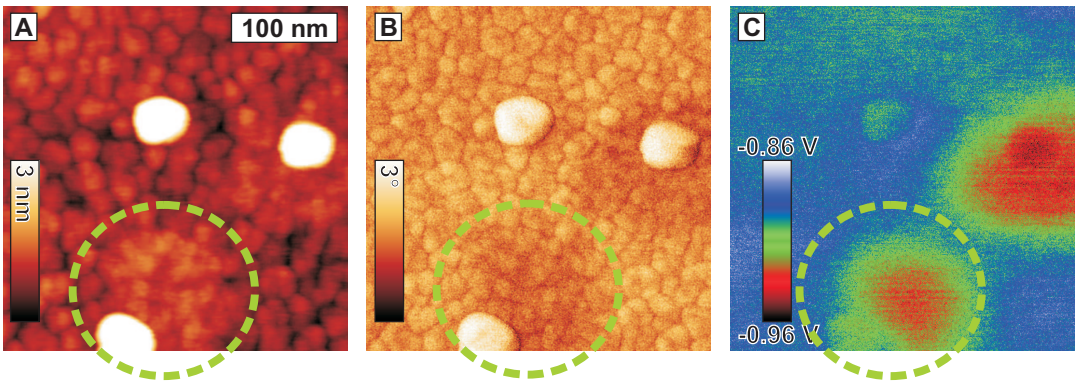

Figure 3.8: SFM images of an F12H12 film transferred at 5 mN/m. (A) Topographic image showing the micelle carpet and larger three-dimensional aggregates. (B) Corresponding phase image showing a slight phase contrast (0.5°) for the domains. (C) Corresponding Kelvin potential image of the same region with domains of lower surface potential, while the three-dimensional aggregates do not show a significant surface potential difference.

33 Å^2 from the isotherm measurements. This value is consistent with the space requirement of a fluorocarbon chain, which lies between 27 and 30 Å^2 [62]. A flat lying F12H12 molecule (Figure 3.1 A), as proposed by Semenov et al. [67] would form a thin film with a thickness of 6.2 Å, if ones considers a circular surface area of 30 Å^2 for a F12H12 molecule. SFM measurements have shown, that the micelle film is 2.1 ± 0.2 nm thick, which is considerably thicker. The majority of the F12H12 molecules thus does not lie flat on the substrate. It can nevertheless not be excluded that some substrate areas are covered by flat lying molecules. The formation of a F12H12 multilayer with the molecules standing upright at the air/water interface (Figure 3.1 B) can also be excluded, because one single F12H12 molecule is theoretically 3.3 nm long. A double layer, with the molecules either arranged in defined layers, or with the molecules interdigitating, would be considerably thicker than 3.3 nm, while the film thickness determined by SFM is even thinner. Also, a calculation considering that each spread molecule occupies a surface area of 30 Å^2 and the amount of molecules spread can be used to obtain the area, which a film of upright standing molecules would occupy at the air/water interface. The result is consistent with the absolute area, at which the surface pressure rises from the isotherm data, leading to the conclusion that the F12H12 molecules have to be standing upright at the air/water interface (Figure 3.1 C-E). The mismatch between theoretically obtained length of a F12H12 molecule and practical film thickness can be explained by considering, that the F12H12 molecules do not necessarily stand vertically in a 90° angle to the air/water or substrate interface, but can be tilted, which reduces the thickness of the film. Also, the existence of flat lying molecules next to the

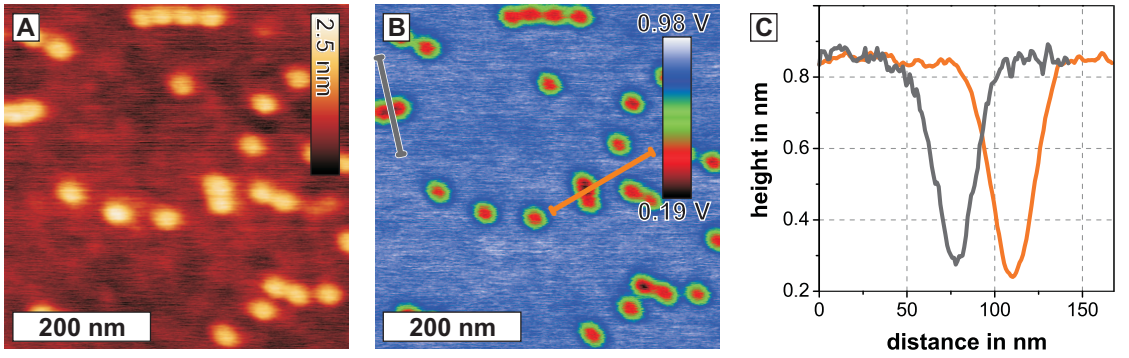

Figure 3.9: SFM images of individual surface micelles at the edge of an F12H12 film without compression. (A) Topography image, (B) corresponding Kelvin potential image, (C) line plot at the locations marked in image (B). The plot shows the surface potential difference between the substrate and the individual surface micelles.

surface micelles would influence the SFM height measurements and let the micelles appear thinner, than they actually are. It is thus reasonable to conclude that the molecules are oriented in an upright position. Considering a monolayer structure with vertically oriented molecules, three different packing models can be proposed (Figure 3.1 C-E). The fluorocarbon chains are a priori expected to orient towards the air (Figure 3.1 C), rather than towards the aqueous phase, because of their larger hydrophobicity and higher affinity for gases compared to hydrocarbon chains. If the fluorocarbon block faces air, this will result in a lower surface energy, which is energetically favorable. An orientation with the fluorocarbon blocks facing water, as proposed in model D (Figure 3.1 D) is hence rather unlikely. Also, Maaloum et al. found by X-ray reflectivity measurements of F8H16 that the hydrocarbon block faces water [68]. However, molecular dynamics simulations of F12H18 molecules support the existence of antiparallel molecular packing (Figure 3.1 E) [78], which was also proposed for F8H18 films based on X-ray reflectivity data [79]. As can be seen by these conflicting observations, it remains a matter of discussion whether or not an antiparallel orientation of the SFA molecules is possible or even preferred. Due to the basic incompatibility of hydrocarbon and fluorocarbon blocks, a parallel alignment of the molecules appears more reasonable.

KPFM was applied as a tool, to investigate the molecular orientation of the SFAs. In the SFAs the major contributions to the effective dipole are the molecular fragment dipoles of the CF_3 group and the central CF_2-CH_2 bond [62,80]. El Abed et al. [79] and Broniatowski et al. [71] investigated the macroscopic surface potential of FnHm molecules directly at the air/water interface. Both attributed a negative surface potential to the fluorinated part of the respective molecules being oriented towards air. KPFM studies on molecules with fluorocarbon and hydrocarbon moieties have been

employed by Chi et al. [81], Sugimura et al. [82], Alexander et al. [80] and Magonov et al. [83], who interpreted differences in surface potential in terms of -CF_2-CH_2- dipole orientation. For SFAs at the air/water interface a surface potential difference of -0.8 V has been proposed corresponding to a vertical molecular orientation with the fluorinated part of the molecules facing air (or for transferred layers -0.6 to -0.7 V relative to a Si wafer surface) [80, 84]. In our experiments it was possible to perform KPFM measurements on individual surface micelles prepared by solvent evaporation (Figure 3.9). Aim was to directly compare surface potential differences between silicon substrate and F12H12 micelles on our sample with those obtained by Magonov et al. following their experimental procedure [84]. At the film edge single surface micelles were found. The surface potential difference between silicon substrate and micelles was determined to be -0.6 V, which is close to the -0.8 V proposed by Magonov et al. [80, 82, 84]. In accordance, for our sample a similar orientation can be concluded, with the F-blocks of the F12H12 molecules oriented towards air (Figure 3.1 C). The divergence between the two values can be explained by taking the size of the investigated structures into account. The size of the surface micelles in our experiment (35.2 ± 7.1 nm diameter) is of the same order of magnitude as the lateral resolution of KPFM (ca. 30 nm), while the measurements from Magonov et al. were performed on structures prepared by spin-coating with a diameter of ca. 1 µm. When measuring structures at the limit of lateral resolution, as in our case, the cantilever will not only detect the surface potential of the pure F12H12 micelle, but also a contribution from the Si-wafer, which decreases the finally determined surface potential difference. Furthermore, the assumed presence of flat lying molecules on the substrate surface between the micelles has to be considered, which would also influence the reference signal from the substrate and additionally alter the determined micelle height. As a consequence, it can be concluded that the F12H12 molecules inside the micelle carpet are oriented vertically with their fluorocarbon moiety facing air. This is in good agreement with literature data [62]: the molecular orientation is similar to the one confirmed by X-ray reflectivity measurements for F8H16 monolayers [68] which present the same lateral organization with hexagonal arrays of circular surface micelles. Also, neutron reflectivity measurements of F12H12 directly at the air/water interface have supported the theory, that the molecule is standing upright with the fluorocarbon moiety facing air [85].

As shown in Figure 3.8, several domains with a more negative surface potential with respect to the micelle carpet have been observed. It appears, that the surface micelles are packed more densely in these domains, which is also supported by the slightly increased height in the topographic images and the reduced intramicellar contrast. Such a denser packing could induce a more vertical orientation of the molecular axis and thus of the associated molecular dipole -CF_2-CH_2-, which results in a more negative surface potential. A second possibility is the existence of domains consisting of molecules with a different orientation (molecules upside down or in an alternating

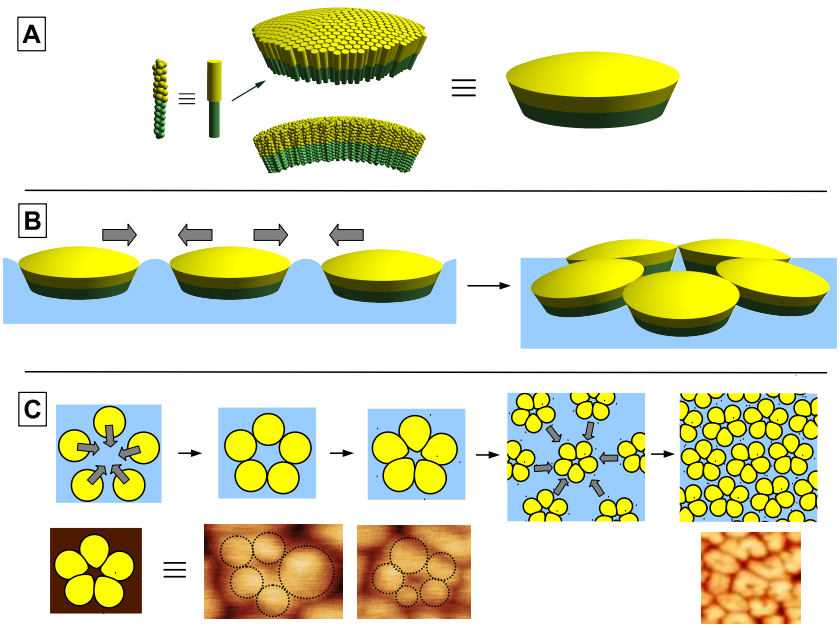

Figure 3.10: Model proposed for the hierarchical formation of the surface micelles. (A) Self-assembly of the amphiphobic F12H12 molecules in parallel orientation with the F-block pointing up to the air into curved primary aggregates with ca. 10 nm diameter. (B) Secondary assembly (side view) of the primary aggregates into clusters of the surface micelles driven by capillary forces. (C) Surface micelle aggregation (top view) with slight deformation of the primary aggregates and comparison to the SFM image details.

packing), but this orientation is expected to lead to a smaller surface potential difference. The most probable scenario is a denser packing of the monolayer, but at the current state it cannot be distinguished between these possibilities with the SFM and KPFM data. The parallel orientation of the F12H12 molecules is apparently driven by phase separation between the F- and H-blocks. Considering this molecular orientation, a simple model for the surface micelle formation can be proposed as a hypothesis (Figure 3.10).

The basic idea is that the F12H12 molecules assemble to form muffin-like structures (Figure 3.10 A). This shape is generated by the volume mismatch between the thick fluorocarbon and the thin hydrocarbon moieties, which results in an isotropic packing strain. The molecules aggregate into a curved monolayer which is counteracted by the planar water surface. The increasing packing strain caused by the layer curvature and the planarizing water surface tension, as well as electrostatic interactions (unfavorable orientation of the dipoles), limit the size of the primary aggregates. These primary aggregates, corresponding to the substructures observed in SFM, assemble to bigger clusters (spirals, circular, or elongated surface micelles)

containing on five to six subunits (spirals, circular, or elongated surface micelles, also discussed in the literature) due to attractive capillary forces (Figure 3.10 C) [86–88]. As the primary aggregates have inclined walls (due to the packing strain/layer curvature), optimal contact between aggregates is enabled by aggregate tilting toward neighboring aggregates and the cluster center. This tilting minimizes contact with surrounding aggregates outside the cluster and explains the appearance of the surface micelles instead of a simple extended hexagonal packing of the primary aggregates (Figure 3.10 B). Slight deformation in the contact regions between the primary aggregates can occur, due to the mobility of the F12H12 molecule and the flexibility of the aggregates. This model is in accordance with other molecular assembly models proposed in literature [23, 67, 68]. Both, the micelles and their arrangements are stabilized by a balance of factors that minimize the system free energy: electrostatic interactions due to dipole moments of fluorocarbons, interfacial tension, and hydrophobic interactions [67].

3.2.2 F12H20

The F12H20 molecule is an asymmetric molecule with an elongated hydrocarbon chain with respect to F12H12. This should, according to literature [22], lead to the formation of elongated micelles. Klein et al. performed rheological measurements of the F12H12 and F12H20 molecules at the air/water interface and came to the conclusion, that F12H20 structures are stronger interlocked than F12H12 structures. This would be the case, if F12H20 formed elongated micelles at the air/water interface. In order to investigate this theory, F12H20 monolayers were transferred onto solid substrates and investigated by SFM (Figure 3.11).

The SFM images show regions with closely packed circular surface micelles (Figure 3.11 A) next to elongated, worm-like micelles (Figure 3.11 B). The circular micelles form a hexagonal pattern. Compared to F12H12, the micelles are slightly larger (ca. 50 nm diameter, 3.3 ± 0.3 nm thickness), but no fine structure is discernible. The enhanced micelle diameter and thickness with respect to F12H12 are probably caused by the longer molecule. F12H20 is according to the structural model 4.4 nm long, which is considerably longer than 3.3 nm for F12H12. Each surface micelle appears to be in very close contact with all neighboring micelles, inducing hexagonal deformation, as can be seen in the Fast Fourier Transfer (FFT) image in Figure 3.11 A in the inset. A high-resolution SFM image of an F12H20 film transferred at 2 mN/m, shown in Figure 3.12, also demonstrates well the coexistence of hexagonal micelles and elongated structures in a more interlocked two-dimensional system, but it does not show any fine structure within the individual micelles.

The corresponding KPFM image (Figure 3.12 C) does not show any contrast within the dense surface micelle film. The substrate is visible because of holes in the

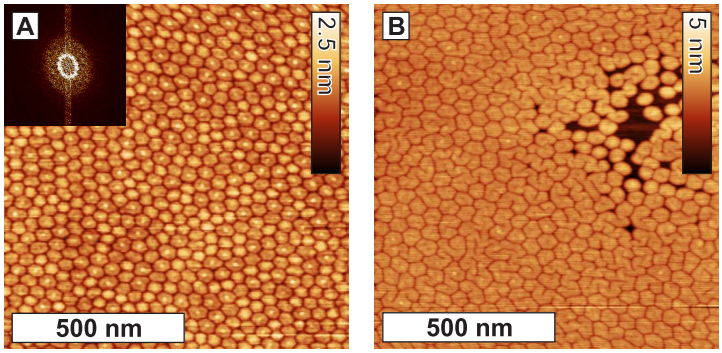

Figure 3.11: SFM images of an F12H20 monolayer transferred at 2 mN/m. (A) Topography of a densely packed, partially hexagonally organized monolayer. Inset: FFT of the topography image, showing the hexagonal packing. (B) Topographic image of a different region showing hexagonal as well as more elongated surface micelles.

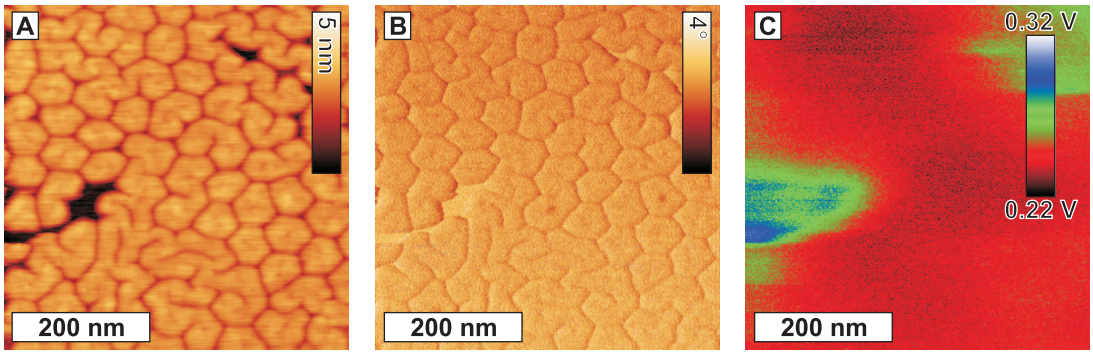

Figure 3.12: Higher-resolution SFM and KPFM images of an F12H20 monolayer transferred at 2 mN/m. (A) Topographic, (B) phase, and (C) Kelvin probe images.

monolayer. The orientation and packing structure of F12H20 molecules is considered to be similar to that of F12H12. This assumption is based on literature data, the analogous behavior in isotherms, and the similar micellar organization imaged by SFM. Structural subunits within the surface micelles are however not discernible.

3.2.3 F11H1-core-H12

The F11H1-core-H12 molecule exhibits a new feature, the insertion of an aromatic core into the SFA molecule. The micellar structure was investigated and compared to F12H12 in order to identify the influence of the aromatic core on the shape of the self-assembly. Films of the F11H1-core-H12 molecules were transferred via surface

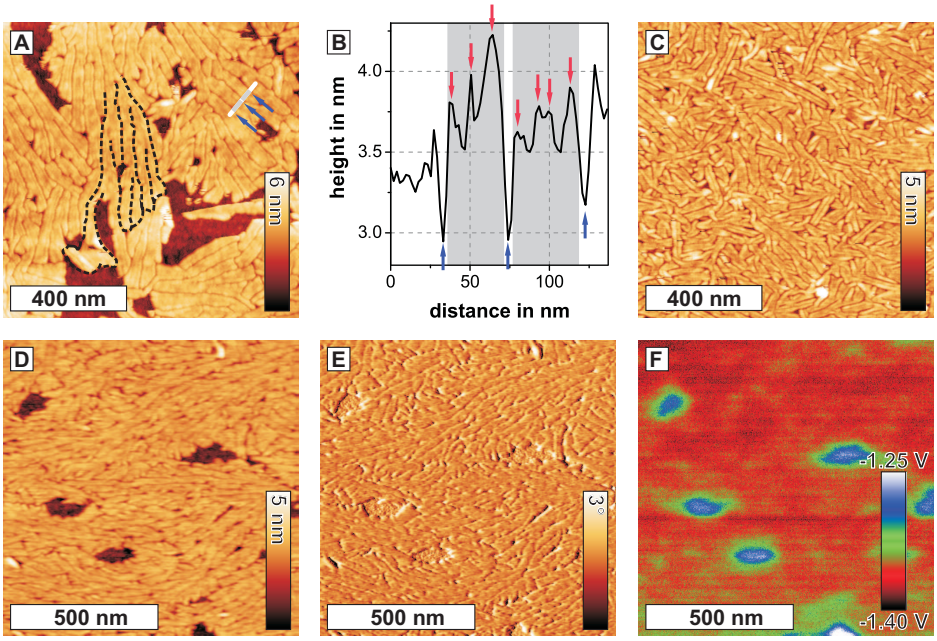

Figure 3.13: SFM images of F11H1-core-H12 films. (A) Topographic image of an F11H1-core-H12 film transferred at 2 mN/m. (B) Line plot at the location marked in image A. Blue arrows mark the edges between neighboring micelles, and red arrows mark substructures inside each micelle. (C) Topographic image of an F11H1-core-H12 film prepared by direct evaporation of the subphase at a nominal surface pressure of 0 mN/m. (D)-(F) SFM images of an F11H1-core-H12 film transferred at 5 mN/m: (D) topographic, (E) phase, and (F) Kelvin potential images.

lowering and investigated employing SFM. SFM images obtained for an F11H1-core-H12 monolayer transferred at 2 mN/m are presented in Figure 3.13. A different type of surface micelles is observed, consisting of straight ribbons with a length of up to 400 nm (Figure 3.13 A and D). The micelle height was determined to be 2.3 ± 0.4 nm and the average width ranged from 30-40 nm, which is similar to the thickness and diameter of the circular micelles formed by the F12H12 molecules. As for F12H12 and F12H20, the micelles appear closely packed even at low surface pressures. Striations of ca. 10 nm width are visible within the ribbons parallel to their longitudinal axis (Figure 3.13 B), again reminiscent of the substructure dimension in the surface micelles of F12H12. The micelles themselves exhibit a fan-like structure with micelles spreading and branching from an initial branching point, which will further be denoted as dendritic growth.

The surface micelles also formed a dense layer and retained their shape, when the film was not purposely compressed but produced by direct evaporation (Section 3.4, Figure 3.13 C). A comparison between Figure 3.13 A and C shows, that both films

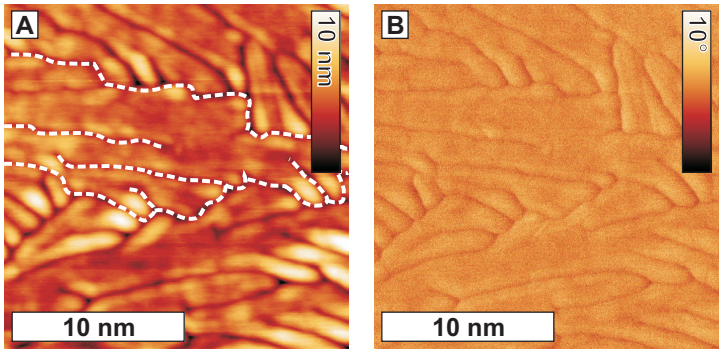

Figure 3.14: SFM images of a F11H1-core-H12 film prepared by direct evaporation. (A) Topography image. Dashed white lines mark an dendritic elongated surface micelle. (B) Phase image.

are closely packed, but the micelles are shorter in Figure 3.13 C. Dendritic growth of the micelles can be observed for both preparation techniques as shown in Figure 3.13 A (exemplarily marked by black dashed lines) and in the zoom-in in Figure 3.14 (marked by white dashed lines), but the effect is less pronounced for samples prepared by solvent evaporation (Figure 3.13 C).

Molecular orientation

As also done for F12H12, neutron reflectivity measurements were employed at the air/water interface to discriminate between the different molecular orientations of F11H1-core-H12 [85]. It appeared that only a structural model consisting of molecules with mixed/alternating orientation as illustrated in Figure 3.15 B and C could lead to acceptable fitting results [85]. A clear distinction between these two models was not possible with the fit. This is, where KPFM comes into play: The formation of distinct domains, as proposed in Figure 3.15 B, can clearly be distinguished from a film with homogeneous molecule distribution, if the formed domains are bigger than the limits of KPFM resolution.

First of all, the thickness of the surface micelles was determined to be 2.3 ± 0.4 nm from SFM measurements. The length of a F11H1-core-H12 molecule can be estimated to be 3.9 nm. Similar to the observations for F12H12, the surface micelle film of F11H1-core-H12 is thinner than expected for an upright standing molecule, but a tilting of the molecules can cause the formation of a thinner film. Also, SFM imaging can have an impact on the height determination, especially since F11H1-core-H12 forms a very soft film. As the height of 2.3 ± 0.4 nm is too thick for molecules lying flat at the air/water interface or on the substrate, it is reasonable to conclude

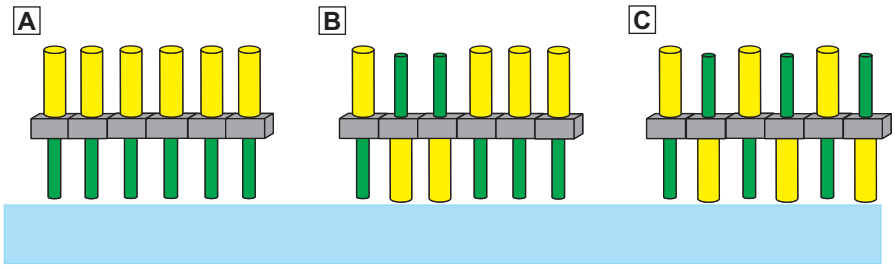

Figure 3.15: Models for the orientation of F11H1-core-H12: (A) Parallel orientation of the fluorocarbon and hydrocarbon blocks, (B) random and (C) alternating chain packing.

that the F11H1-core-H12 molecules are oriented vertically, but tilted. So far, the SFM results were in accordance with the models obtained from neutron reflectivity. KPFM images of the samples do not display any inhomogeneities within the micelle carpet (Figure 3.13 F), but do show a potential difference between sample and substrate. The molecules are therefore either all oriented in a parallel manner (Figure 3.15), as proposed for F12H12, or in an antiparallel manner not forming distinct domains. Domains with a diameter bigger than 30 nm are detectable with KPFM, smaller domains are beyond the lateral resolution of the measurement technique. As a consequence, the results from KPFM measurements do not give a clear indication to which of the orientations can actually be found in the micelles. From the fitting results of the neutron reflectivity data the molecular orientation appears to be different from that of the F12H12 molecule as a consequence of the central aromatic core (PhBr2). As a consequence, the following model for the organization and orientation of F11H1-core-H12 was proposed and published [85]. However, differential scanning calorimetry and wide angle X-ray scattering experiments conducted by the group of George Floudas on F11H1-core-H12 in bulk (unpublished data) revealed that the formation of a phase with alternating fluorocarbon and hydrocarbon blocks is not possible, due to the nano phase separation of the incompatible blocks, which is in contrast to the results from neutron scattering. Accordingly, the orientation of the F11H1-core-H12 molecules at the air/water interface remains a matter of discussion and could not be elucidated by KPFM measurements.

A considerable difference between the F12H12 and the F11H1-core-H12 aggregates was the shape of the surface micelles. The F11H1-core-H12 self-assembled into ribbons which were about 10 times larger than the average diameter of the circular micelles observed for F12H12 monolayers. The aromatic core induces a structural as well as a dipole asymmetry in the molecule, compared to the rotational symmetry of the F12H12 along the molecular main axis. This asymmetry induces a strong packing anisotropy. While the antiparallel orientation of the molecules is suggested

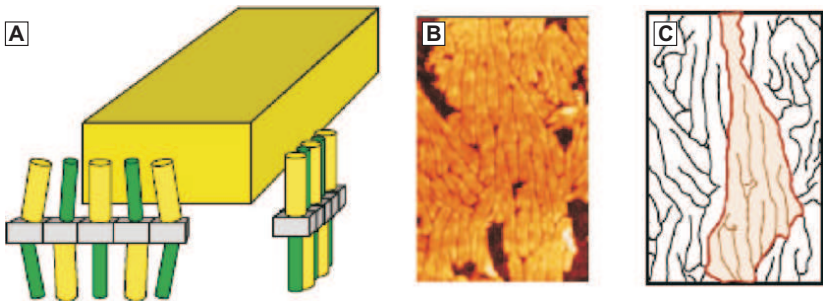

Figure 3.16: (A) Model proposed for the hierarchical packing structure of the F11H1-core-H12 molecules into a ribbon element (yellow-green block). (B) SFM image with observed dendritic ribbon structure. (C) Line illustration of a single dendritic domain with a fingering of the ribbons.

by the fitting of the neutron reflectivity data, such packing would not induce a strain buildup by a volumetric mismatch between F- and H-blocks. Extended monolayer domains would be expected for this molecule type, ignoring the anisotropic core structure. Since well defined surface micelles exist, obviously, a different mechanism limiting the layer extension due to the presence of the aromatic core in the layer must be present, which leads to a packing structure with elongated micelles. These form either in the direction of the phenyl ring face or edge. The packing structure model in Fig.3.16 may be proposed as a hypothesis. The aromatic core has about the same thickness as the alkyl chain, so no distortion but rather a stabilization of the alkyl packing is expected along the stacking direction of the cores, which is assumed to be the long axis of the elongated surface micelle. Moreover, the core is much broader than the cross section of the alkyl chain; thus along the direction of edge-on stacking a strong packing mismatch is expected to limit the width of the surface micelle along the short axis.

3.2.4 bis-F11H1-core-H12

The bis-F11H1-core-H12 is another molecule of the SFA family with an extended core system of two phenyl moieties coupled via an ethinyl bridge and two fluorocarbon and hydrocarbon moieties, respectively (Figure 3.17A). Since the F11H1-core-H12 molecule has proven to form exceptional new structures, which feature a directionality, it is of major interest, whether this effect can be enhanced upon extension of the aromatic core. Preliminary experiments with these bis-F11H1-core-H12 molecules at the air/water interface and transferred onto solid substrates have been performed. The bis-F11H1-core-H12 molecules were spread at the air/water interface and compressed to a surface pressure of 32 mN/m, which is below the collapse pressure of

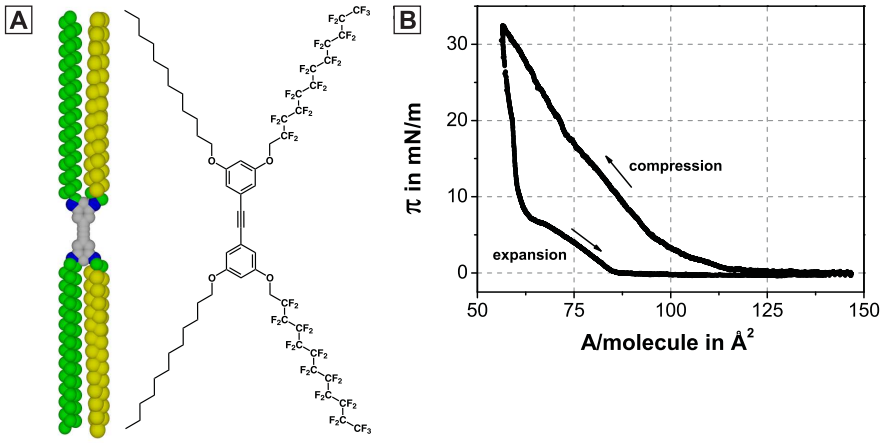

Figure 3.17: (A) Model and molecular structure of bis-F11H1-core-H12. (B) Isotherm of bis-F12H12 spread from hexane.

the monolayer. Immediately after reaching 32 mN/m, the monolayer was expanded to reach zero surface pressure (Figure 3.17 B). Upon compression, the surface pressure starts rising at A_0 = 110-120 Å^2, which is significantly bigger than the alues obtained for the other SFA molecules discussed in this Chapter. The area increase is reasonable, because the number of moieties is doubled and the molecule therefore requires more space. The surface pressure rises as long as the barriers are compressed. Upon expansion, the surface pressure drops immediately and at a steeper slope as during compression. The expansion isotherm exhibits a kink at π = 7.5 mN/m, at which the slope of the isotherm changes again. A similar kink could be found for F12H12, F12H20 and F11H1-core-H12 upon expansion of the monolayers after the collapse pressure was reached [74]. The compression and expansion isotherms exhibit a strong hysteresis, which is in contrast to the results obtained for the other SFM molecules: The area per molecule at a given surface pressure π = 2 mN/m decreases from A_{comp} = 105 Å^2 to A_{exp} = 80 Å^2. The surface area at zero surface pressure is significantly smaller after the film has been compressed. The compression of the molecules is therefore likely to be irreversible, meaning that aggregates formed during compression stay aggregated even after expansion of the barriers. The shift is also an indication for a partial collapse of the bis-F11H1-core-H12 monolayer before the actual collapse pressure is reached. This hypothesis is emphasized by the fact, that a similar isothermal behavior could be observed for F12H12, F12H20 and F11H1-core-H12 after collapse of the monolayer.

The morphology of the bis-F11H1-core-H12 monolayers was investigated employing SFM. Samples were prepared by transfer of bis-F11H1-core-H12 molecules onto Si substrates using the surface lowering technique (Figure 3.18). The images show fiber like surface micelles with defects revealing the substrate as well as higher three-

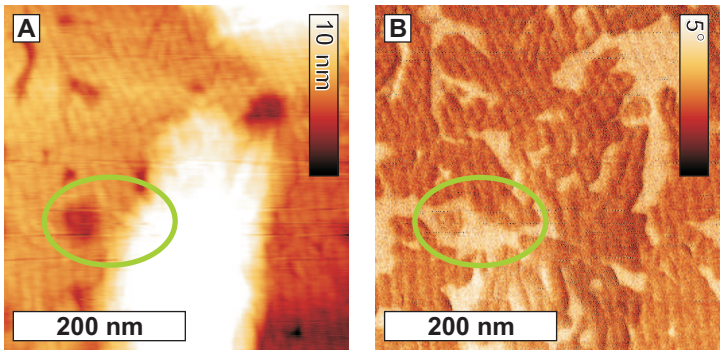

Figure 3.18: SFM images of a bis-F11H1-core-H12 film transferred at $\pi = 2$ mN/m. (A) and (C) topography, (B) and (D) phase images.

dimensional aggregates. The long micellar structures are ordered regularly (Figure 3.18 A). Most of the micelles are oriented with their longitudinal axis running from top to bottom of the image. Measurements at other positions showed surface micelles with arbitrarily oriented longitudinal axis. The ordering of the fiber-like structures is thus a local effect. The width of such a fiber was determined to be 16.1 ± 3.0 nm, by measuring the distance between two height maxima of neighboring fibers. Determination of the height gave 2.4 ± 0.4 nm, which is consistent with values for F11H1-core-H12. The agreement between both values is consistent with similarities in the chemical structure and indicates that the core-extended molecules are oriented in an upright standing position, as proposed for F11H1-core-H12. The bis-F11H1-core-H12 surface micelles are narrower than the elongated surface micelles from F11H1-core-H12. Further, the characteristic dendritic growth of F11H1-core-H12 cannot be observed for bis-F11H1-core-H12 micelles. These are individually separated and randomly arranged on the substrate. The differences in structure are probably caused by the extended core: A second phenyl moiety enhances the effect of directionality, which was already found for one phenyl core. Additionally, the geometry of the bis-F11H1-core-H12 molecules with four instead of two fluorocarbon and hydrocarbon moieties influences the interaction between neighboring molecules. The three-dimensional aggregates, which can already be found at low surface pressures (film transfer at $\pi = 2$ mN/m), are probably a product of the aggregation and early collapse, which have already been suspected from the isotherm data. The aggregates feature the fiber-like micelles, meaning that the basic film structure is not disturbed by the three-dimensional aggregation. A comparison between topography and phase images shows, that the light contrast observed in the phase image (green oval in Figure 3.18 B) cannot be directly related to a topographic feature in the height image (green oval in Figure 3.18 B). On the contrary, the phase contrast can be observed on the higher three-dimensional aggregates as well as on the surface

micelles. The slightly darker region within the light phase contrast image can be correlated to a hole in the micelle carpet and thus probably shows the substrate. The origin of the phase contrast other than from the substrate, as well as how the bis-F11H1-core-H12 molecules are oriented and assembled are not clear from the experiments so far.

3.3 Conclusions

The original two-dimensional structure of non-classical amphiphobic molecules with symmetric F- and H-block lengths was studied by SFM, coupled with KPFM measurements and confirmed by neutron reflectivity measurements [85]. As reported in the literature for asymmetric block lengths and shown here for F12H20, both molecules with symmetric chain length (F12H12 and its core extended analogue F11H1- core-H12) form surface micelles when spread at the air/water interface. The symmetry does not appear to play a crucial role as the F12H12 molecules were found to behave like other asymmetric derivatives, e.g., F12H20. With the molecular main axis perpendicular to the air/water interface and the F-block pointing towards the air, F12H12 molecules self-organize into 30 nm circular surface micelles, composed of circular 10 nm substructures size-controlled by free-energy minimization. Analogous micellar organization was found for F12H20 molecules, but with a more close packed self-assembly, which induces the coexistence of hexagonally deformed micelles with interlocked extended ones. Conversely, the phenyl ring insertion induces dramatic structural changes with respect to the probable molecule orientation and the resulting micelle shape, consisting of branched elongated structures, but which again feature a 10 nm striation substructure (which appears to be a more general structure motif). The introduction of a second phenyl ring into the core of the molecules even enhances this effect of directionality, as preliminary experiments have shown. The extended core leads to the formation of fiber-like micelles rather than branched ones. These results illustrate how chemical modifications can be used to tailor the hierarchical self-assembly of such semifluorinated alkanes to extend their possible applications for driving supramolecular assembly.

3.4 Experimental details

Isotherms and film transfer

Surface pressure versus molecular area (π-A) isotherms were recorded using two different Langmuir troughs made of hydrophobic Teflon, equipped with two movable

hydrophilic polyoxymethylene barriers: KSV Minitrough 4 for ISR 400 (KSV Instruments Ltd., Finland) and Langmuir-Trough RK1 (Riegler and Kirstein GmbH, Potsdam, Germany). Temperature was regulated to 20.0°C and equilibration time of 5 min after spreading was used for solvent evaporation. Molecules were spread from hexane solutions ($c = 1$ mg/mL). The monolayers were compressed up to the desired surface pressure (compression speed 5 mm/min and 25 mm/min for compression-expansion cycles) and transferred onto plasma-cleaned (10 min Ar plasma) Si wafers. The Si substrates were positioned on a custom made sample holder with an inclination of 6° to the air/water interface in the aqueous subphase before spreading. The monolayer was transferred by removal of the subphase from the trough with a peristaltic pump (Minipuls 3, Abimed, Gilson Inc., United States) with a pump rate of approx. 10 mL/min, thereby lowering the monolayer onto the wafer [36]. Monolayers without compression for SFM imaging were prepared by direct evaporation (overnight) of one drop (submonolayer coverage) of the amphiphobe solution ($c = 1$ mg/mL) spread on an aqueous film on a freshly cleaned wafer.

SFM measurements

The transferred films were analyzed with a scanning force microscope (Dimension 3100, Veeco Instruments, United States, and MFP-3D, Asylum Research, United States) in tapping mode, equipped with sharpened, Al backside coated Si cantilevers (Olympus OMCL-AC240TS, nominal tip radius < 7 nm, resonance frequency 50 - 90 kHz, spring constant 0.7 - 3.8 N/m). The cantilevers were put on a glass coverslip with the tip side facing air and were Ar plasma cleaned (Plasma Cleaner/Sterilizer PDC-002, 200 W, Harrick Scientific Corp., United States) for 30 s at a pressure of approximately 1.6 mbar. For KPFM measurements the chip was electrically connected to the chip holder using conductive Ag paste (Fluka, for electron microscopy). An AC bias of 2000 mV was applied to the tip during the second scan in lift mode while the sample remained grounded. The KPFM images were flattened using median line correction. SFM and KPFM measurements were performed under ambient conditions (room temperature, air). Imaging of all samples was performed at the lowest possible tapping forces characterized by the ratio of free amplitude/amplitude set point [49] of 0.96 and a peak offset of -3%. The free amplitude was determined to be the amplitude of the cantilever at peak maximum before approaching the surface. Even then I observed in some cases that material was dislocated or removed by the tip during the measurements, in particular in the case of F11H1-core-H12 films. The generated ”holes” in the surface micelle layer were used to estimate the layer thickness. The SFM topographic images were flattened and analyzed using Gwyddion Software (www.gwyddion.net). Measurements following the protocol of Magonov et al. [84] were performed using the Agilent 5500 (Agilent Technologies,Chandler, USA) and a Pt coated cantilever (Olympus, OMCL-AC240TM-BL, nominal tip ra-

dius < 25 nm, resonance frequency 45 - 95 kHz, spring constant 0.5 - 4.4 N/m) was used.

4 Properties of amphiphilic DNA films at the air/water interface and after film transfer

Deoxyribonucleic acid (DNA) molecules are particularly promising candidates for the design of new materials and macromolecular assemblies [89]. The highly specific binding through Watson-Crick base-pairing facilitates convenient creation of defined assemblies by molecular recognition. One strategy is to induce defined conformational changes by DNA hybridization to realize complex molecular machines in liquids [90, 91]. A popular example is the design of molecular tweezers, which can be actuated by DNA hybridization, as reported by Yurke et al. [92]. With the increasing requirements and complexity of structures in nanotechnology hybrids being composed of nucleic acids and other building blocks have moved into reserach focus [93]. One class of such DNA hybrid materials are amphiphilic molecules like DNA block copolymers [94,95] and oligonucleotides modified with small hydrophobic moieties [96, 97]. The partial hydrophobicity of the DNA hybrid materials induces micro phase separation in aqueous solution leading to the formation of self-assembled aggregates like micelles and vesicles [94, 98, 99]. The micelle shape is tunable by hybridization with tailored complementary DNA sequences [100]. Besides in micelle morphologies such DNA amphiphiles were introduced into vesicle membranes composed of phospholipids. In this regard, the surface of liposomes could be easily functionalized by hybridization [101]. More sophisticated functions mediated by the DNA motif and specific base pairing of complementary sequences were vesicle aggregation and fusion [102–105]. In a similar manner DNA with lipid tails was doped in supported phospholipid bilayers allowing selective tethering of liposomes, enzymes, drugs or fluorescent probes and therewith the fabrication of highly functional surfaces [106]. Moreover, the use of hydrophobic moieties allows the organization of DNA at the air/water interface. Langmuir monolayers composed of single nucleosides functionalized with a lipid moiety have been investigated intensely [107–109]. Many of these studies focused on the interaction between the single nucleoside and its complementary base. However, this interaction is rather unspecific in comparison to the hybridization of complementary DNA oligomers. The use of molecules with longer DNA sequences is hence an important progress for molecular recognition experiments. Recently, Caseli et al. reported the use of DNA blockcopolymers contain-

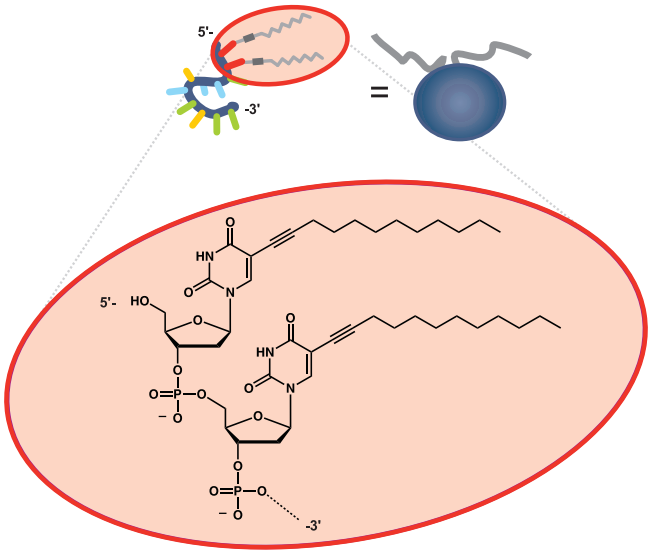

Figure 4.1: Schematic diagram and chemical structure of the dU11. The DNA sequence is 5'-UUT GGC GTC TT-3'. The U represents the modified uracil base deoxyribonucleotide 5-5-(dodec-1-ynyl)uracil.

ing a poly(butadiene) block adsorbing to the air/water interface with the intention to study their interaction with cell membranes [110]. However, the preparation of pristine monolayers of amphiphilic DNA has so far not been realized, although these films can provide a platform for the design of a directed molecular machine driven by DNA hybridization. Also, the transfer of these films onto substrates can be of use for the preparation of functional thin films accessible for further modification by DNA hybridization. An amphiphilic DNA molecule (dU11) [111], which consists of a single stranded DNA (ssDNA) 11mer containing two hydrophobically modified 5-(dodec-1-ynyl)uracil nucleobases at the terminal 5'-end of the DNA sequence, was investigated (Figure 4.1). Hereby, the alkyl chains of the dU11 act as arm floats for the DNA. The air/water interface was used as confinement for the self-assembling process of dU11 in order to prepare functional thin films for a subsequent transfer process onto a solid. The dU11 molecules were synthesized and purified by xxx and xxx and have been provided within the framework of a cooperation with xxx from xxx.

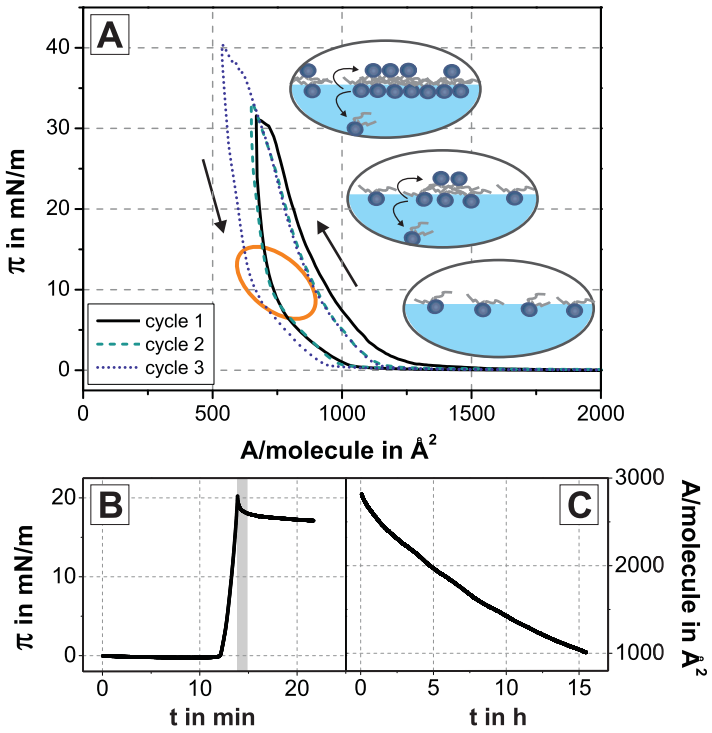

Figure 4.2: (A) π-A isotherms of one dU11 monolayer showing the first (black), second (turquoise) and third (purple) compression-expansion cycle. Arrows indicate direction of the barrier movement. Kinks are indicated by an oval in the isotherm. The schemes outline possible structures formed at the air/water interface at increasing pressure (from bottom to top). (B) Surface pressure decrease of a dU11 film at the air/water interface at constant surface area A = 320 Å^2. The grey bar marks the first minute after stopping the barriers. (C) Decrease of area per molecule of a dU11 film at the air/water interface at constant surface pressure π = 0.2 mN/m.

4.1 Film stability at the air/water interface

In order to investigate the stability of the dU11 molecules at the air/water interface π-A isotherms were recorded as compression-expansion cycles (Figure 4.2). The isotherms showed a continuous increase of the surface pressure upon compression at A/molecule $\leq$ 1300 Å^2. A weakly pronounced kink at π = 7 mN/m was observed upon expansion (marked by an oval in Figure 4.2A). Furthermore, no phase transitions or plateaus were found. Such isotherms indicate liquid like phase behavior and were also measured for the lipid dilauroylphosphatidylcholine (DLPC), which exhibits the same alkyl chain length as dU11 [112]. However, upon measuring π-A isotherms, the DLPC molecules were found to start interacting with each other at an area per molecule of 120 Å^2 while the dU11 molecules start to interact at a much

larger area per molecule of 1300 Å^2. The reason for this difference is attributed to the higher spatial occupancy of the DNA head group ($M_W(dU11 - headgroup) = 3289$ g/mol, $M_W(dU11) = 3629$ g/mol) [113] compared to that of phosphatidylcholine group ($M_W(PC) = 239$ g/mol). It was found that all isotherms exhibited a strong hysteresis between surface pressures measured during compression and expansion. Upon compression the surface pressure started increasing at an area per molecule of 1300 Å^2. Upon expansion the surface pressure was always lower compared to the compression at the same area and reached zero surface pressure at an area per molecule of 1100 Å^2. When increasing the maximum surface pressure from 32 mN/m in cycle 1 and 2 to 40 mN/m in cycle 3 this hysteresis became more pronounced: The expansion regime was shifted by 68 Å^2 for cycle 3 with respect to the expansion regime of cycle 1 and 2 for $\pi = 10$ mN/m. It is in addition noteworthy that the expansion regime of cycle 2 was widely congruent with the expansion regime of the cycle 1 and the compression regime of the cycle 3 was widely congruent with the compression of cycle 2. However the compression regimes of cycle 2 and 3 were shifted from 1300 Å^2 to 1100 Å^2 with respect to cycle 1. The monolayer structure and morphology depended on the history of the monolayer, meaning that after the first compression the molecules at the air/water interface did not reach the initial state again but remained partially aggregated, which is the reason for the observed shift. As phospholipids [114] and other surfactants [115] containing a double hydrocarbon chain behaved in a similar way, this effect can be associated to an aggregation of the hydrophobic moieties of neighboring dU11 molecules at the air/water interface, despite the voluminous DNA head group. Rodríguez Patino et al. reported for the lipid dipalmitoylphosphatidylcholine (DPPC) that the memory effect was more pronounced after the first isotherm than for the successive ones [114], similar to my observation. They attributed this effect to changes in monolayer morphology at the microscopic level due to self-association of the DPPC molecules after the first compression of the monolayer. Both effects, hysteresis and isotherm shifts, have been observed by Niño et al. [116] for the lipid dioleoylphosphatidylcholine (DOPC) at surface pressures close to the collapse pressure. Niño et al. attributed both effects to relaxation phenomena inside the film at the air/water interface. Typical relaxation phenomena include molecular loss, the formation of three-dimensional structures at the collapse point and molecular reorganization at the air/water interface, meaning the formation of double or multilayers. Unlike Niño et al. [116], I have observed the existence of hysteresis and shifts in the isotherms even before a clear signal of the collapse pressure was reached. This can be taken as an indication, that the dU11 monolayer as such is not fully stable at the air/water interface. Possible scenarios in this context are either the loss of molecules into the subphase or a reorganization at the air/water interface into a multilayer structure as illustrated in Figure 4.2 A.

To further investigate the stability of the dU11 molecules at the air/water interface three more experiments were performed: (i) A dU11 film was compressed up to a

surface pressure π of 20 mN/m and then the molecular area was kept constant by stopping the barriers (Figure 4.2 B). I measured a pressure decrease of 10% within the first minute after stopping the barriers. The decrease after 5 min corresponded to 14%. Upon stopping the barriers at a higher surface pressure of 40 mN/m, I measured an area per molecule decrease of 20% after 1 min. Thus a higher surface pressure results in a more pronounced surface pressure drop. (ii) A dU11 film was compressed to a surface pressure of only 0.2 mN/m, which was then held constant by adjusting the area per molecule with the barriers (Figure 4.2 C). In this experiment the area per molecule decreased by 3% over a period of 10 minutes. Petrov et al. [117] reported a similar behavior for docosyl ethyl ether molecular layers at the air/water interface applying a constant surface pressure of 25 mN/m. In their experiments a decrease in area per molecule of 17% was observed over a time period of 10 minutes. Petrov and co-workers found that the decrease in surface pressure corresponded to the formation of multilayers at the air/water interface even before the collapse pressure was reached, which was proven on the Langmuir trough by Brewster angle microscopy imaging [117]. In analogy it is also possible for the dU11 molecule to form multilayers at the air/water interface, even at low surface pressures. (iii) In my experiments I could never exceed a maximum surface pressure of 40 mN/m irrespective of the amount of molecules spread onto the air/water interface. Furthermore, a clear maximum pressure upon which the dU11 molecular layers collapse, could not be observed. Therefore a certain collapse pressure cannot be defined from the isotherms [118]. Thus, a successive collapse of the molecular layers upon compression and the formation of multilayers at the air/water interface are likely.

In conclusion, from isotherm measurements it is clear that the dU11 interfacial films are semi-stable. Relaxation of the interfacial films can be realized by two processes: the dissolution of molecules from the air/water interface and the formation of multilayers at the air/water interface. From the results so far it is unclear, which of the effects is dominant. Therefore I performed SFM measurements of films transferred onto solid substrates, in order to investigate them in terms of aggregate formation.

4.2 Film transfer

Transferring a dU11 film from the air/water interface onto a silicon substrate via LB film transfer was possible at a slow transfer rate of 0.1 mm/min. SFM imaging of a dU11 film revealed a layered structure of the dU11 film (Figure 4.3 A and B). In the first scan (Figure 4.3 A) the substrate (area 0) and two different dU11 layers (1 and 2) with different heights are visible. Both layers are flat and homogeneous, no aggregates can be found. The first layer (layer 1) is 1.6 $\pm$ 0.1 nm thick, while the second and upper layer (layer 2) is with respect to the substrate (area 0) 3.5

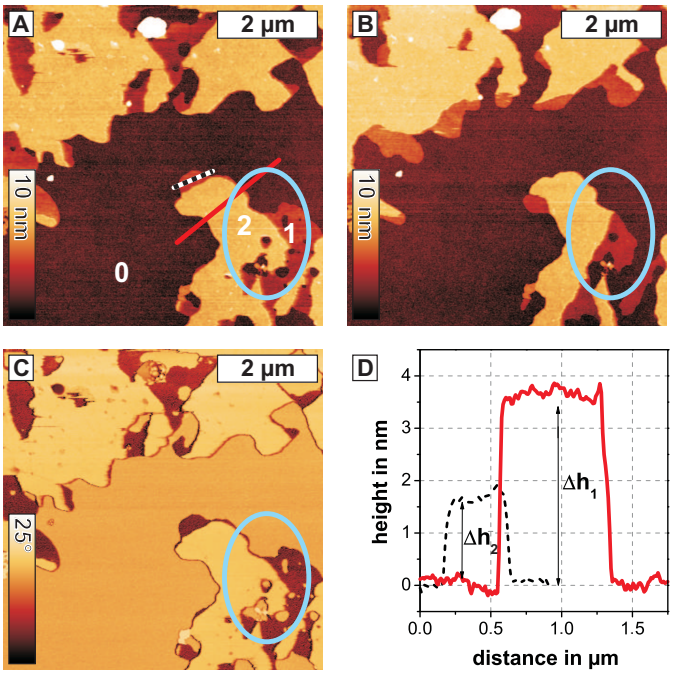

Figure 4.3: SFM images of an LB film transferred with $\pi = 5$ mN/m. (A) Height image of the first scan showing the substrate and a film with two different layers (layer 1 and 2). Red and dashed lines mark the position of the line plots displayed in D. (B) Height image of the second scan at the same position. Ovals mark the same region after the first and second scan. The topography between both scans changed, showing that the tip removed material from the sample upon scanning. (C) Phase contrast image corresponding to A. (D) Line plots mediated over 10 pixels at the positions marked in A to compare the thickness of layer 1 and 2.

$\pm$ 0.1 nm thick. Thicknesses have been determined by fitting the median height difference between substrate and film via a profile using Gwyddion Software (Figure 4.3 D). In addition, the simultaneously recorded phase contrast image exhibited a distinguishable phase contrast between each layer (Figure 4.3 C). In order to interpret the SFM data the sizes of the dU11 components were estimated: The radius of gyration $R_g(11mer)$ of a ssDNA 11mer in solution is $R_g(11mer) = 0.8$ nm [118]. The alkyl chains are not rigid. Therefore they probably lie flat on top of the more voluminous ssDNA coil when deposited on a flat substrate (Figure 4.4). Thus, the diameter of the alkyl chain contributes to the thickness of the film. It corresponds to $d_{alkyl} = 0.4$ nm [119]. The estimated length of one stretched dU11 alkyl chain is $l_{alkyl} = 1.6$ nm, allowing an interaction between alkyl chains of neighboring dU11 molecules even if not fully stretched. In this case 2 nm $(2 \cdot R_g + d_{alkyl})$ thick wet films are expected. However, the films investigated with SFM were dry. During the drying

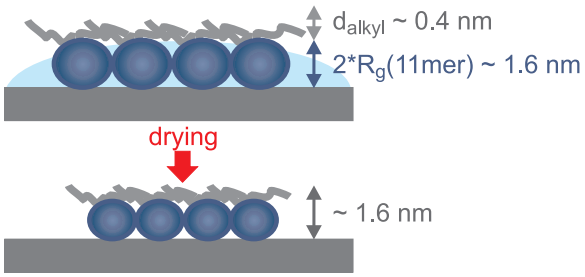

Figure 4.4: Sketch of the size estimation for the dU11 molecule in liquid and after drying.

process strong capillary forces tend to press the film onto the substrate which may reduce the film thickness to 1.6 nm. In addition, the first layer was determined to be half as thick as the second one, indicating that the second, thicker layer actually consisted of two stacked monolayers, each being approximately 1.6 nm thick. It can be assumed that the dU11 molecules inside layer 1 are oriented with the hydrophilic DNA moiety facing the hydrophilic substrate, while the hydrophobic alkyl chains face air. This is the typical orientation when transferring an amphiphilic monolayer onto a hydrophilic substrate via LB technique. Molecules in layer 2 would then arrange inversely with the alkyl chains facing layer 1 and the DNA moiety facing air. Comparison of height and phase image (Figure 4.3 A and C) shows that layer 1 and layer 2 exhibited a significant difference in the measured phase contrast. This indicates that both layers exhibited different interactions with the SFM tip and therefore the exposure of different interfaces to the tip [47]. For my system this is only possible when the hydrophilic or hydrophobic moieties of the dU11 molecule are exposed to the SFM tip, respectively. The latter finding from step heights and phase contrast can only be achieved by tail-to-tail alignment of the molecules in the different layers. Thus, the phase contrast originates from different dU11 orientations resulting in differing interfaces to air. In particular, for layer 2 DNA exposed to the air interface was obtained. About 32% of the substrate were covered by the film as shown in Figure 4.3 A.

Additionally it was found that by scanning with the SFM tip parts of the dU11 film were removed, as can be seen by comparison of the blue oval in Figure 4.3 A and B. In particular, material was removed from individual layers exposing the layer underneath, which then resulted in a different phase contrast. Further SFM measurements at larger scan sizes and at the same position did not reveal any material that was deposited at the edges of previous scans. It can therefore be excluded that the material was displaced to the edges of the scan area by the scanning process. Garnaes et al. observed a similar effect, he was able to write patterns with his SFM tip into LB films from behenic acid upon application of a force of 70 nN in contact mode [120]. When scanning with low forces, he was able to image the

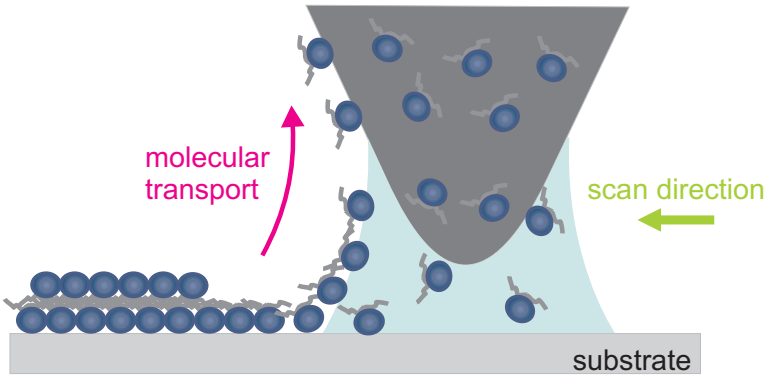

Figure 4.5: Sketch illustrating the inverse dip-pen nanolithography step.

film, without modifying it. In contrast to these findings, the dU11 film was removed upon imaging with the lowest possible force in tapping mode characterized by the ratio of free amplitude/amplitude set point (Section 2.4). Before scanning, the SFM cantilevers were cleaned in a plasma cleaner, which results in a hydrophilic surface of the SFM tips. As a consequence, the thin water film, which forms on samples investigated under ambient conditions, can form a water meniscus between tip and sample. The material on the sample can then be transported along the meniscus to accumulate on the SFM tip. This is the inverse effect of classical dip-pen nanolithography. Jaschke et al. found already in 1995 that material could be deposited from a doped cantilever tip onto the substrate by subsequent scanning in contact mode [121]. The name *dip-pen nanolithography* was later on introduced by Piner et al. [122].

The principle of inverse dip-pen nanolithography is illustrated in Figure 4.5. The major difference between the removal of dU11 films discussed here and the removal of behenic acid reported by Garnaes et al. [120] is that dU11 was imaged in tapping mode. Also, the experiments on material deposition reported in literature were conducted in contact mode [121, 122]. In case of dU11 it was however possible to remove a considerable amount of material although tip and sample were not in permanent contact. Accordingly, the material transport had too be fast because tip and sample were only shortly in contact. The molecular transport rate was estimated by the following considerations: The number of molecules N, which have been removed by scanning, can be deduced as follows:

$$N = \frac{A_r}{A_{dU11}} = 151\,288 \tag{4.1}$$

A_r is the film area, which has been removed between the first (Figure 4.3 A) and second scan (Figure 4.3 B). By scanning, overall 3.2 μm^2 of the dU11 film have been removed. A_{dU11} is the area per molecule of a dU11 molecule at a surface pressure of 5 mN/m and can be deduced from the dU11 isotherm data. It was assigned to be 2116 $Å^2$. The SFM image is composed of 512 scan lines, each of which is scanned twice for the recording of one image. Thus, the SFM tip has scanned 1024 lines between the first and second image (Figure 4.3 A and B). $N_{line} = N/1024 = 148$ molecules have been removed per scan line. The scan speed v of the SFM was $v = 3.5$ μm/s, the length of one scan line $l = 5$ μm and the time per scan line t is thus:

$$t = \frac{l}{v} = 1.4 \text{ s} \tag{4.2}$$

Accordingly, on average $N_{line}/t = 103 \text{ s}^{-1}$ molecules have been removed per second. With a 70 kHz cantilever, which has been used for imaging, this corresponds to an average of 0.001 molecules adhering to the tip per tip-sample contact. Piner et al. reported that he was able to produce a film covering a circular area with a diameter of 0.66 μm by touching the sample with the doped cantilever for 2 min. This corresponds to molecular transport rate of 14 166 1-octadecanethiol (ODT) molecules per second with $A_{ODT} = 20$ $Å^2$ [123]. The molecular transport rate reported by Piner in contact mode is 137 times higher than for the tapping mode measurements of dU11. It is nevertheless remarkable that a considerable amount of molecules can be removed in tapping mode, although the tip-sample contact time is very short as compared to contact mode measurements.

One approach to prevent the removal of the material would be to image with a hydrophobized SFM tip to avoid the formation of a water meniscus between tip and sample. But, as a consequence, a strong adhesion between the hydrophobic tip and the hydrophobic moieties of the dU11 molecules across the thin water film can found. The origin of the strong and often long-range attraction between hydrophobic surfaces has been the focus of a substantial body of work, yet currently there is no single theory that can comprehend all of the experimental results [124]. It is however clear, that long-range attractions (distance between the hydrophobic surfaces bigger that 200 Å) between physisorbed hydrophobic surfactant surfaces like LB films arise from molecular rearrangement of the surfactant films into bilayer islands [125]. As these results from Meyer et al. show that the hydrophobic interaction between tip and sample can have a significant impact on the structure of the LB film, imaging with a hydrophobic tip may also induce considerable changes in the film structure. Imaging in vacuum is thus the easiest approach to prevent removal of the film upon scanning, because in vacuum no water film will form on the sample.

But how is SFM imaging possible, if parts of the sample are removed by scanning with the SFM tip? All images shown and interpreted were gathered within the first

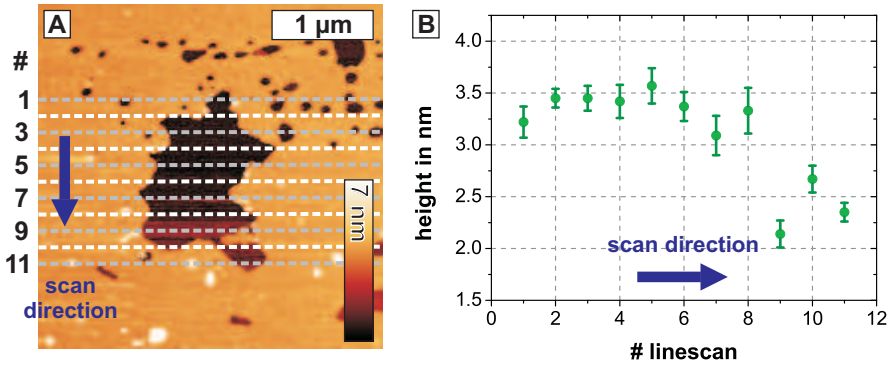

Figure 4.6: (A) SFM height image of a dU11 film transferred at $\pi = 30$ mN/m. The lines indicate the position of the line scans, from which the film thickness of was determined. The blue arrow indicated the scan direction from top to bottom of the image. (B) Plot of film thickness versus the position of the line scan.

2 scans obtained with a fresh SFM tip. If the cantilever was used longer than that, images became blurry and stripy, probably because the removed material accumulated on the tip. The SFM image in Figure 4.6 A shows the first scan with a new hydrophilic tip on a freshly prepared dU11 film. In the middle of the image, a hole in the film exposing the substrate is visible. In order to demonstrate the interaction between tip and sample material, the image was investigated in terms of the film thickness in dependence of the distance covered by the SFM tip while scanning. This was achieved by measuring line scans (width of 3 pixels each) distributed over the hole in the film to determine the thickness of the film relative to the substrate. The scan direction of the SFM image was from top to bottom and the line scans were numbered accordingly. The positions of the line scans is marked in the SFM image (Figure 4.6 A), and the determined film thickness is plotted in Figure 4.6 B. The plot demonstrates, that the determined film thickness is subject to position of the line scan and thus to the distance covered by the SFM tip. The longer the SFM tip has already scanned the surface, the thinner appears the film in the topography image. An actual thinning of film is rather unlikely, which is why it is more reasonable that part of the molecules, which have been collected by the tip, were deposited on the substrate, thus modifying the film thickness by classical dip-pen nanolithography. It is therefore important to note for the interpretation of the SFM images that repeated scanning can alter the images, not only by removing individual layers but also by depositing the collected molecules at the substrate. The procedure of analyzing only the first two images obtained with one SFM tip is therefore not only important for the subjective image quality but also for the quality and reproducibility of the height data. It can nevertheless not be completely excluded, that the determination of film thicknesses is influenced by deposition of material on the substrate.

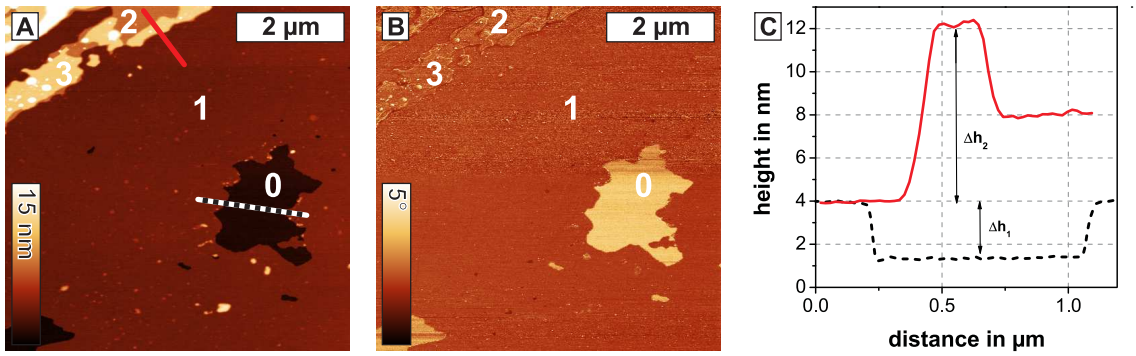

Figure 4.7: SFM images of a LB-film transferred at $\pi = 30$ mN/m. (A) Topography image showing the substrate and covered by a multilayered film. Red and dashed lines mark the position of the line plots displayed in C. (B) Corresponding phase image showing a phase contrast between substrate and layer 1 of the film, but not between layer 1 and layer 2. (C) Line plots at the positions marked in image A mediated over 10 pixels.

Furthermore, I investigated the structure of a film transferred at a higher surface pressure of $\pi = 30$ mN/m (Figure 4.7). In the topography image (Figure 4.7 A) again different layers (labeled with numbers 0, 1, 2, 3) were found. The film, which has been labeled as layer 1, covered most part of the substrate. A hole in the film exposed area 0 underneath, corresponding to the substrate (Figure 4.7 B). Layer 1 is 2.6 ± 0.2 nm thick (Figure 4.7 C, dotted line), which is thinner than the thickness for a dU11 bilayer as derived from films transferred at lower pressures (3.5 ± 0.1 nm, Figure 4.3) [126, 127]. There are a second and third layer visible in the upper left corner of the topography image (Figure 4.7 A). The thickness of layer 2 with respect to layer 1 is 3.8 ± 0.2 nm. The thickness of layer 3 with respect to layer 2 is 4.0 ± 0.1 nm. Both values are close to the estimated thickness of one dU11 bilayer. Furthermore the phase contrast image supports this interpretation as I did not observe a significant phase contrast between layer 1, 2 and 3, which means that all three layers expose the same dU11 moiety to the SFM tip. From this I conclude that I image heights of three individual dU11 bilayers vertically stacked one after another on the substrate. The variations in film thickness, especially for layer 1, can originate from the deposition of collected sample material onto the substrate, as has been discussed above. Also, a reduction of the film thickness due to hard tapping during SFM imaging is a possible artifact effecting the film thickness determination. However, this effect is constant over the complete SFM image and thus cannot selectively alter the thickness of layer 1 without effecting the other layers.

Additionally, dU11 films were transferred via surface lowering technique to investigate the influence of the transfer technique onto the morphology of the dU11 film.

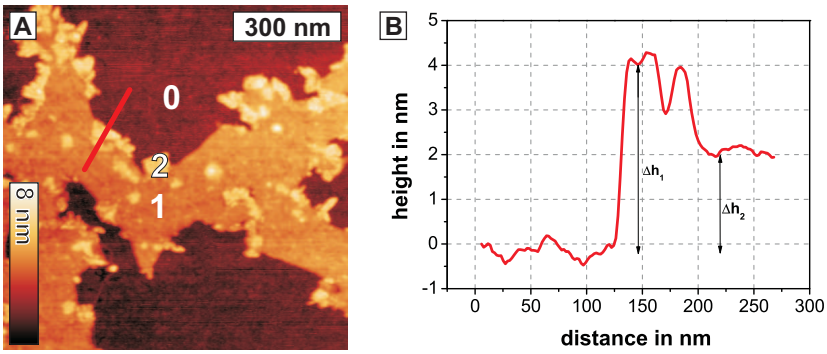

Figure 4.8: (A) SFM height image of a dU11 film transferred transferred via surface lowering at a surface pressure of $\pi = 3$ mN/m. The red line marks the position of the line plot displayed in B. (B) Line plot mediated over 10 pixels at the positions marked in A to compare the thickness of layer 1 and 2.

Aim was to exclude that the multilayer formation is a byproduct of the transfer technique. Films transferred via surface lowering at surface pressures of $\pi = 3$ mN/m and $\pi = 5$ mN/m both exhibited dU11 mono- and bilayers (Figure 4.8). Layer 1 is 1.9 nm thick while layer 2 is twice as thick with 4 nm height. This can be taken as a confirmation that the multilayer formation is not significantly influenced by the transfer technique.

Then the film formation was investigated on a larger scale in dependence of the applied surface pressure from 2 mN/m to 30 mN/m (Figure 4.9). At a low surface pressure of $\pi = 2$ mN/m the dU11 molecules formed a network. Additionally, the beginning of the formation of a more compact film is visible in the marked area (Figure 4.9 A, blue oval). Upon increasing the surface pressure to $\pi = 5$ mN/m a film with a coverage of approximately 77% formed (Figure 4.9 B). A further surface pressure increase to $\pi = 10$ mN/m lead to an increase of the surface coverage to 90% (Figure 4.9 D). At a surface pressure of $\pi = 30$ mN/m I found a surface coverage of 95% (Figure 4.9 E). The average film thickness of all films shown in Figure 4.9 is 3.2 $\pm$ 0.2 nm, which matches the thickness estimated for a dU11 bilayer. In conclusion, this series of experiments shows that the dU11 molecule starts to form a bilayer film at a surface pressure of $\pi = 2$ mN/m, the formation of multiple bilayers can be found at π 30 mN/m and the surface coverage increases upon increasing the surface pressure (Figure 4.9 C).

From the experimental results, the following model is proposed for the assembly of dU11 molecules on the substrate: The first dU11 layer aligns with the hydrophilic DNA head facing the hydrophilic substrate (Figure 4.10). The molecules in layer 2 are aligned inversely. Upon imaging each of the layers individually, a phase contrast can be found between them. Then the origin of the phase contrast is the varying

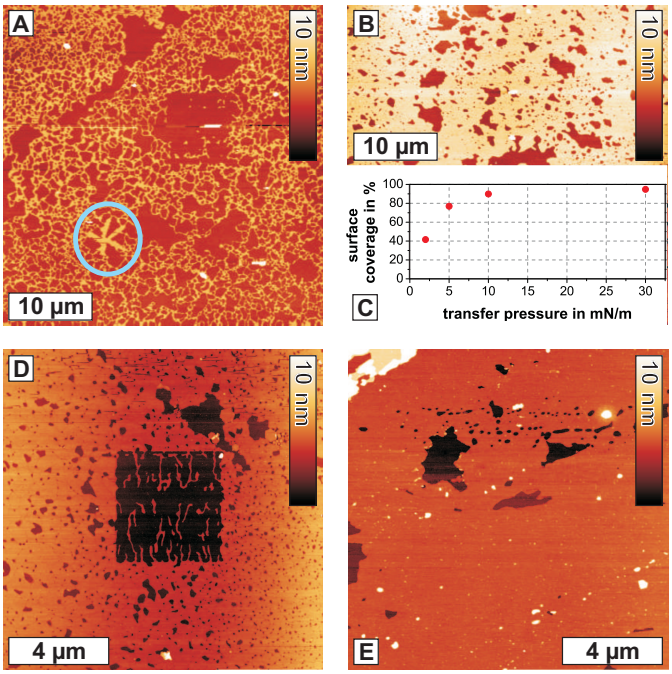

Figure 4.9: SFM topography images of films transferred at surface pressures of 2, 5, 10 and 30 mN/m. (A) $\pi = 2$ mN/m. The image shows a dU11 network on the substrate. The circle marks an area, where the formation of a compact film is denoted. (B) $\pi = 5$ mN/m. (D) $\pi = 10$ mN/m. The square hole in the middle of the image marks the area scanned in the preceding measurement. It is visible, because upon scanning parts of the film have been removed. The missing material is not piling up at the edges of the previous scan area but is rather collected by the SFM tip. The pre scanned areas have been excluded from the surface coverage determination. (E) $\pi = 30$ mN/m. Multilayers have formed in the left upper corner of the image. (C) Surface coverage versus transfer pressure plot. Surface coverage increases upon increasing transfer pressure.

interaction between tip and hydrophilic or hydrophobic moiety of the dU11 molecule, respectively. Additionally, layer 1 and layer 2 are equally thick in the SFM height image. Stacking of a second bilayer on top of the first one (layer 1 + layer 2) leads only to a change in the measured height but not in the SFM phase contrast. In this model, the orientation of the hydrophilic DNA moiety towards air is proposed. This orientation is rather unconventional, but it is nevertheless reasonable when considering that ssDNA molecules exhibit a significant surface activity when diluted in a buffer solution [128]. The adsorption process is in this case probably governed by the nucleic acid bases, because Caseli et al. found that adsorption kinetics of DNA blockcopolymers were subject to the DNA sequence [110].

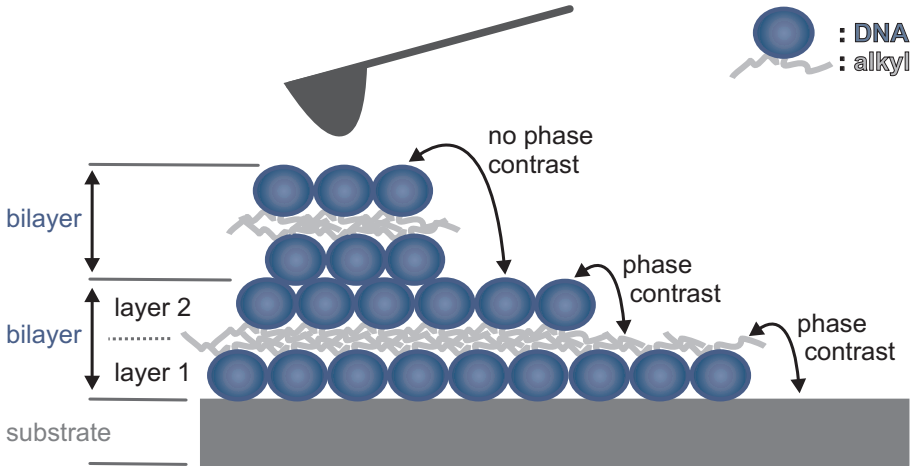

Figure 4.10: Model proposed for the bilayer formation on the substrate and the according phase contrast in SFM phase images. The phase contrast between a dU11 mono- and bilayer is caused by the altered orientation of the molecules. The hydrophobic tails of the molecules are facing air in the first monolayer, the molecules in the second layer are oriented oppositely.

4.3 Conclusion

The dU11 molecules form semi-stable films at the air/water interface: Upon film compression the molecules exhibit relaxation phenomena like dissolution of dU11 molecules into the subphase but also reorganization into multiple layers at the air/water interface. Langmuir-Blodgett and surface lowering film transfer as well as SFM investigation of the interfacial films elucidated, that the formation of multiple layers at the air/water interface is one of the major relaxation mechanism for films made from this molecule. Presumably, the rearrangement of the molecules into bi- and multiple bilayers happens already at the air/water interface and is one of the reasons for the measured semi stability of the dU11 films. The multilayer formation enables us to fabricate hydrophilic samples covered with dU11 molecules exposing at maximum 95% of ss DNA to the air interface which might then be accessible for further chemical reactions or DNA base-pairing . Upon SFM imaging single dU11 layers can be removed individually in an analogous manner of inverse dip-pen nanolithography. This enables patterning of DNA amphiphile films into desired regions of DNA or alkyl chains facing towards the air.

4.4 Experimental details

Materials

The dU11 molecule was synthesized and purified as reported previously by Anaya et al. [111]. The ssDNA 11mer sequence was designed to be non-self-complementary: 5'-UUTGGCGTCTT-3' with 2 alkyl modified uracil bases at the 5' end of the DNA sequence. Spreading solutions (c = 1.4 µmol/L) were prepared in dichloromethane (Chromasolv, Merck). Water was purified to a resistance of 18.2 MΩ/cm using a Milli-Q filtration system (Millipore) and additionally distilled before use. The amphiphilic molecules were dissolved in Milli-Q water and the DNA concentration was determined by measuring a UV/Vis absorption spectrum of the solution. The absorption at $\lambda = 260$ nm was used to determine the ssDNA concentration by applying Lambert Beers law. The respective molar extiction coefficient was calculated according to the DNA sequence ($\epsilon(dU11) = 103327$ L/(mol · cm)).

Monolayer preparation

500 µL of the respective solution in dichloromethane were spread onto the Milli-Q subphase with a microliter syringe. The spread layer was left for solvent evaporation for 15 min prior to each measurement.

Monolayer isotherms and monolayer transfer

Surface pressure versus molecular area (π-A) isotherms were recorded on a Langmuir-Trough RK1 (Riegler und Kirstein GmbH, Potsdam Germany) equipped with a subphase exchanging system, which is attached to a peristaltic pump (Minipuls 3, Abimed, Gilson Inc, United States). The surface pressure $\pi = \gamma_0 - \gamma$, was measured using a Wilhelmy plate (filter paper); here, γ_0 is the surface tension of the pure subphase and γ is the surface tension at a certain amount of dU11. The subphase and room temperature were regulated to 20°C. Surface pressure was calibrated using arachidic acid as a reference. Isotherms were recorded at a compression speed of 6.7 cm/min. Compression - expansion cycles were recorded leaving the monolayer to equilibrate for 15 minutes before recompression. Monolayers were transferred onto silicon wafers (both sides polished) by Langmuir-Blodgett (LB) film transfer [7]. The silicon wafers were treated in an Ar-Plasma (Plasma Cleaner/Sterilizer PDC-002, 200W, Harrick Scientific Corp., United States) for 10 minutes. They were stored and transported in Milli-Q water. For Langmuir-Blodgett (LB) film transfer the wafer was immersed vertically into the water subphase before the film was prepared

at the interface. The barriers were compressed to the designated surface pressure π and the films were transferred onto the substrate by pulling the substrate out of the subphase at a transfer speed of 0.1 mm/min while the surface pressure was kept constant. For film transfer via surface lowering [36] a hydrophilic silicon wafer was immersed into the subphase before spreading the dU11 at the interface. The sample was hydrophilized as explained before and placed on a custom-made sample holder at an inclination of 6° relative to the air-water interface. Then, the dU11 solution was spread, left for solvent evaporation and compressed up to the designated surface pressure. The barriers were stopped and the subphase was pumped out of the Langmuir trough with a peristaltic pump (Minipuls 3, Abimed, Gilson Inc., United States) at a pump rate of approximately 10 mL/min, thereby lowering the interfacial film onto the wafer.

SFM measurements

The transferred films were investigated using a scanning force microscope (Veeco Dimension 3100, Veeco Digital Instruments, United States) in tapping mode equipped with sharpened, Al backside-coated Si cantilevers (Olympus OMCL-AC 240TS, nominal tip radius < 10 nm, resonance frequency: 50 - 90 kHz, spring constant: 0.7-3.8 N/m). Prior to the SFM measurements, the cantilevers were cleaned by placing them on a glass cover slip with the tip side facing an Ar-plasma (Plasma Cleaner/Sterilizer PDC-002, 200W, Harrick Scientific Corp., United States) for 30 s at a pressure of 1.6 mbar. SFM images were flattened and analysed using Gwyddion Software (www.gwyddion.net). The surface coverage was determined by masking the covered regions and counting the according pixels in the SFM topography image using Gwyddion software. The ratio of the number of pixels displaying the covered area divided by the total number of pixels in the image was taken to be the surface coverage.

5 DNA hybrid materials for molecular recognition at the air/water interface

The formation of monomolecular films from lipophilic nucleosids and the binding of complementary nucleic acids via molecular recognition have been subject to research for several years [107–109]. The investigations have been restricted to molecules with head groups consisting of one single nucleic acid. Caseli et al. made first attempts to broaden the spectrum and investigated amphiphilic blockcopolymers with head groups consisting of oligonucleotides (ssDNA 12mer) [110]. He found that these DNA blockcopolymers adsorbed readily to the air/water interface to form Gibbs monolayers and that they could be inserted into existing lipid monolayers at the air/water interface by adsorption from the subphase. The selective formation of pure monolayers from amphiphilic oligonucleotides at the air/water interface has so far not been realized, although such systems provide a platform for more specific molecular recognition. The longer ssDNA sequence available for binding allows highly specific interaction through base pairing of not only one but a dozen of nucleotides. By preparation of a monolayer consisting of only the amphiphilic nucleotide, the use of a matrix molecule becomes redundant. This is an advantage, because unspecific side reactions between the complementary DNA sequence for molecular recognition and the matrix molecules can be eliminated. The establishment of a pure DNA hybrid material film at the air/water interface would therefore improve and simplify molecular recognition experiments. In this context, two promising candidates for the realization of pure ssDNA hybrid material monolayers at the air/water interface will be introduced in this thesis. One of these is the dU11 molecule, which has already been introduced in Chapter 4. A second candidate is the ssDNA-poly(propyleneoxide) blockcopolymer (DNA-*b*-PPO), which can be synthesized via solid phase synthesis [129]. The hydrophobicity of the PPO moiety enables the anchoring of the hydrophilic ssDNA to the air/water interface. The molecular weight of the PPO moiety is variable. All experiments discussed in this Chapter were performed with PPO with a molecular weight of 6800 g/mol. The ssDNA moiety was an 11mer with a non-self-complementary ssDNA sequence (5'-TTC TAT AGA AA-3') (Figure 5.1). In this Chapter, the characteristics of DNA-*b*-PPO films at the air/water interface will be discussed. Furthermore, the influence of the experimental conditions on the

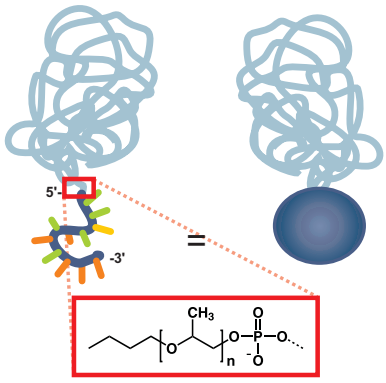

Figure 5.1: Schematic diagram and chemical structure of the DNA-*b*-PPO. The DNA sequence is 5'-TTC TAT AGA AA-3'.

interfacial films of either DNA hybrid material in terms of conducting molecular recognition experiments will be issued. The material was synthesized and purified by xxx and xxx and has been provided within the framework of a cooperation with xxx from the univesity of xxx.

5.1 DNA-*b*-PPO at the air/water interface

The general characterization of DNA-*b*-PPO blockcopolymer Langmuir monolayers is a crucial step to be able to pursue further experiments aiming at molecular recognition or other applications. In order to do so, monomolecular films were prepared by dissolving the DNA-*b*-PPO in dichloromethane and spreading this solution onto the air/water interface. The monolayer was compressed after solvent evaporation and the isotherms measured. This experiment was repeated under nominally equal conditions, resulting in different isotherms (Figure 5.2).

The isotherms do not show a characteristic area per molecule A_0, at which the surface pressure starts rising (Figure 5.2). A_0 ranges from 2000 to 5500 Å^2. Also the isotherm shape and slope is not consistent for all experiments. How can this effect be explained? The area per molecule A_0 can be calculated from the interfacial area available between the barriers divided by the amount of molecules spread onto the interface. The calculation is based on the assumption that concentration and volume of the spreading solution are known and that all spread molecules form an ideal monomolecular film at the air/water interface. A discrepancy between the nominal and the actual amount of molecules spread can cause a variation of the A_0 value. All experiments were performed under identical conditions, a variation of the

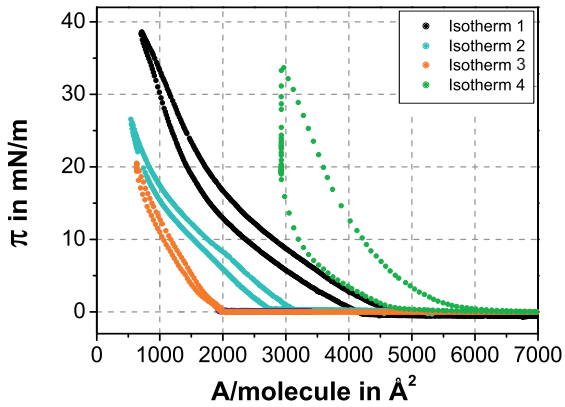

Figure 5.2: Isotherms of DNA-*b*-PPO blockcopolymers spread on MilliQ water repeated under nominally equal conditions.

experimental procedure as cause of the different isotherm shapes is therefore rather unlikely.

Two scenarios give reasonable explanations for the variation of A_0 and the isotherm shape: (i) The molecules do not form an ideal monolayer at the air/water interface but three-dimensional aggregates, as has already been observed for dU11 (Chapter 4). The nominal and actual number of molecules assembled directly at the interface deviate in this case and can thus cause variations of A_0. Additionally, these aggregates can exhibit compressibility different from that of a thin monolayer and can thus cause changes in the isotherm shape. (ii) The actual space requirement of the molecules at the air/water interface varies, e.g. due to variation of electrostatic repulsion between the molecules. In order to investigate the occurance and influence of both effects onto the isotherm shape and area per molecule, the following experiments were performed.

5.1.1 Aggregate formation

The DNA blockcopolymers can aggregate at the air/water interface or in the spreading solution and the A_0 value would alter accordingly. BAM was used as a tool to visualize the DNA-*b*-PPO films at the air/water interface in order to investigate their homogeneity (Figure 5.3). A homogeneous monomolecular film consisting of one monomolecular layer exhibiting only one phase would exhibit one shade of grey without any features in the BAM image. Images of DNA-*b*-PPO taken before compression of the molecules at the air/water interface show a grey backround (yellow arrows) with several lighter features (light green arrows in Figure 5.3 A). These lighter features correspond to three-dimensional structures swimming at the interface. It is

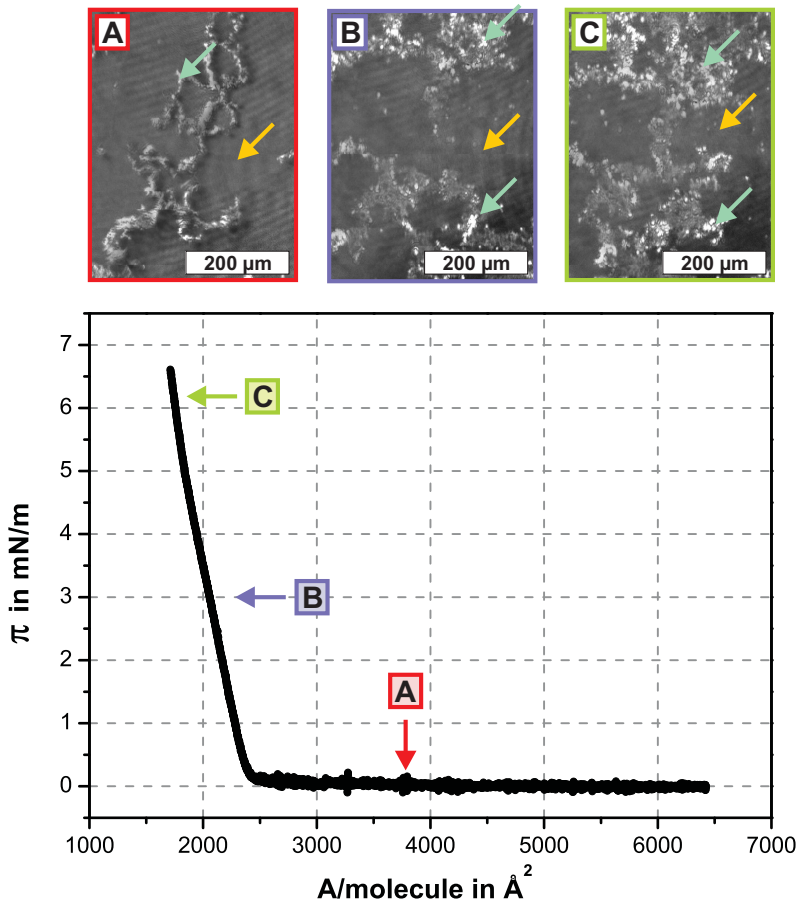

Figure 5.3: BAM images taken before and during compression of DNA-*b*-PPO molecules (M_W= 6800 g/mol) at the air/water interface. (A) $\pi = 0.0$ mN/m, (B) $\pi = 3.0$ mN/m, (C) $\pi = 6.2$ mN/m.

therefore clear that the initial formation of these three-dimensional structures was not a consequence of film compression. Hence the structure formation can either be an artifact from the spreading process or the structures already existed in the spreading solution. A possible reason for aggregation in the spreading solution is the bad solubility of the ssDNA 11mer in dichloromethane (DCM). The concentration of the solution was therefore chosen to be very low (c = 0.25 µmol/L). Nevertheless, any remainder of water in the sample, like condensing water from the atmosphere when the sample was removed from the freezer, will prevent the molecules to dissolve in DCM. Also, the remainder of salt in sample from the purification process of DNA-*b*-PPO enhances the formation of aggregates in the spreading solution, because the salt will not dissolve in DCM and instead accumulate with the DNA moieties. Compression of the DNA-*b*-PPO molecules at the interface results in closer packing

of the aggregates (Figure 5.3 B and C), suggesting that the aggregate morphology is not significantly altered by compression. The isotherm measured simultaneously to BAM imaging is consistent with the isotherms shown earlier (Figure 5.2), which shows that the formation of aggregates is a common phenomenon for DNA-*b*-PPO molecules in bulk solution and at the air/water interface. One approach to prevent aggregate formation could be to use more diluted spreading solutions. This can hardly be realized in practice, because the handling of solutions with even lower concentrations is afflicted with deviations of the actual concentration from the nominal concentration, which again results in variations of A_0.

5.1.2 Molecular volume

A change in the DNA-*b*-PPO molecular volume at the air/water interface also influences the space requirement of the respective molecule at the air/water interface. The interaction of the phosphate backbone contained in the ssDNA head group with cationic ions can influence the shape of the DNA-*b*-PPO molecules and their space requirement at the interface, because of electrostatic interactions. Expected is that positively charged ions in the subphase shield the negative charges of the phosphate backbone from each other, leading to a less pronounced repulsion between phosphate groups and thus reducing the volume and space requirement of the ssDNA head group. A characteristic measure of this effect is the *Debye length* λ_D, the decay length of the electric potential, which is defined as

$$\lambda_D = \sqrt{\frac{\epsilon_{H_2O} \cdot \epsilon_0 \cdot k_B \cdot T}{e^2} \cdot \frac{1}{\sum c_i \cdot z_i^2}} \tag{5.1}$$

With ϵ_{H_2O} the permittivity of water and ϵ_0 the vacuum permittivity, k_B the Boltzman constant, T the temperature, e the elementary charge, c_i the concentration of the ith ion and z_i the corresponding valency. λ_D decreases with increasing ion concentration, as is shown in Figure 5.4. The idea was hence to investigate the influence of salt in the subphase onto the volume of the DNA head group by exchanging the MilliQ subphase with solutions containing salt, namely NaCl, $MgCl_2$ and $BaCl_2$, with concentrations ranging from 0 - 100 mM. NaCl and $MgCl_2$ were chosen because of their relevance in biology, especially in the hybridization process of DNA. $BaCl_2$ was chosen as a weaker ion for comparison with $MgCl_2$. In the experiments the salt concentration of the subphase was increased successively up to 100 mM and afterwards exchanged with pure MilliQ water to test for reversibility by employing the subphase exchange system of the Langmuir trough. Isotherms were recorded after each subphase exchange as shown exemplarily for DNA-*b*-PPO

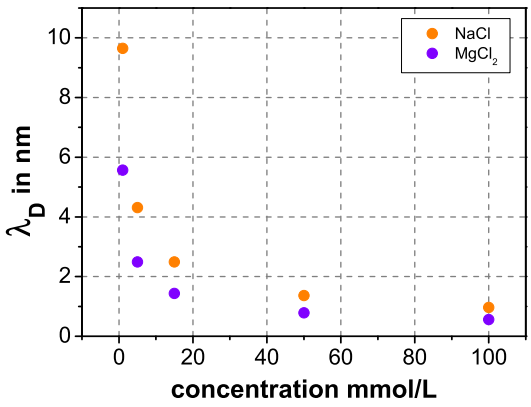

Figure 5.4: Debye length for monovalent and divalent ions according to equation 5.1.

and NaCl in Figure 5.5 A. The experiments with $MgCl_2$ and $BaCl_2$ showed similar results. A comparison of the isotherms measured on pure MilliQ water and on 1 mM NaCl solution shows that the isotherm is shifted towards higher area per molecule values for the salty subphase. This effect was not expected. Also, the higher the NaCl concentration, the larger is the area per molecule A_0. The exchange of the 100 mM NaCl solution back to pure MilliQ water does not result in an decrease of the area per molecule, the effect is therefore not reversible. It is remarkable, that the isotherms for NaCl concentrations higher than 5 mM do not show a baseline with $\pi = 0$ mN/m, because the area of the molecules at the interface exceeded the area of the trough. It was not possible to expand the barriers any further which resulted in an increased surface pressure π even before the barriers were moved. It was therefore not possible to quantify the size increase for concentrations higher than 5 mM NaCl, because then the area available for expansion of the DNA-*b*-PPO molecules was limited. As a next step, this experiment was repeated with $MgCl_2$ and $BaCl_2$ solutions of identical concentrations. In order to compare the results obtained for the different salt solutions, two values are defined: Mg^{2+} and Ba^{2+} are bivalent ions, whereas Na^{+} is monovalent. In order to compare the changes in the area per molecule due to electrostatic interactions between the phosphate backbone of ssDNA and ions, the ionic strength I of the subphase solutions was calculated.

$$I = \frac{1}{2} \cdot \sum_i c_i \cdot z_i^2 \tag{5.2}$$

c_i is, as mentioned above, the concentration of the ith ion and z_i the corresponding valency. $I(NaCl) = c(NaCl)$ applies for monovalent ions, while for bivalent ions like $MgCl_2$ with $z(Mg^{2+}) = 2$ and $z(Cl^-) = -1$ the ionic strength is:

$$I(MgCl_2) = \frac{1}{2} \cdot (z^2(Mg^{2+}) \cdot c(Mg^{2+}) + z^2(Cl^-) \cdot c(Cl^-)) \tag{5.3}$$

When considering that $c(Mg^{2+}) = c(MgCl_2)$ and $c(Cl^-) = 2 \cdot c(MgCl_2)$ the equasion can be modified to:

$$I(MgCl_2) = \frac{1}{2}(\cdot 2^2 \cdot c(MgCl_2) + (-1)^2 \cdot 2c(MgCl_2)) \tag{5.4}$$

$$I(MgCl_2) = 3 \cdot c(MgCl_2) \tag{5.5}$$

Since the A_0 value is not easily determined reproducibly for isotherms with different slopes and features like phase transitions, the area per molecule at a surface pressure of $\pi = 2$ mN/m, A_2, was chosen to compare the area per molecule values of different isotherms. Also, as mentioned earlier, the initial area per molecule on MilliQ water is not reproducible for DNA-*b*-PPO films, therefore all values plotted in Figure 5.5 B are relative to A_2^0 determined on pure MilliQ water. For comparison A_2/A_2^0 was plotted versus the ionic strength I of the subphase solution. The results for all three ions show an identical tendency: The relative area per molecule A_2/A_2^0 increases with increasing ionic strength of the subphase up to $I = 45$ mM. For NaCl A_2/A_2^0 increases further with each concentration increase, but seems to approach a plateau. This plateau probably originates from the limited area available for the molecules to expand, which has been discussed before. In contrast, A_2/A_2^0 of $MgCl_2$ and $BaCl_2$ reaches a maximum at $I = 45$ mM and decreases for higher ionic strengths. The addition of ions was expected to shield the negative charges from each other and thus to reduce the repulsion between neighboring head groups. This effect can be observed for $MgCl_2$ and $BaCl_2$ at ionic strengths higher than $I = 45$ mM. The first increase of the area per molecule upon addition of salt was however not expected and indicates, that a second effect besides the shielding of Coulomb interactions between charges by addition of ions has to be considered.

Wu et al. and Gong et al. observed a comparable effect for surface grafted poly(acrylic acid) (PAA) brushes [130, 131]. The thickness of the PAA film in differently concentrated salt solutions was investigated by ellipsometry and it was found that the

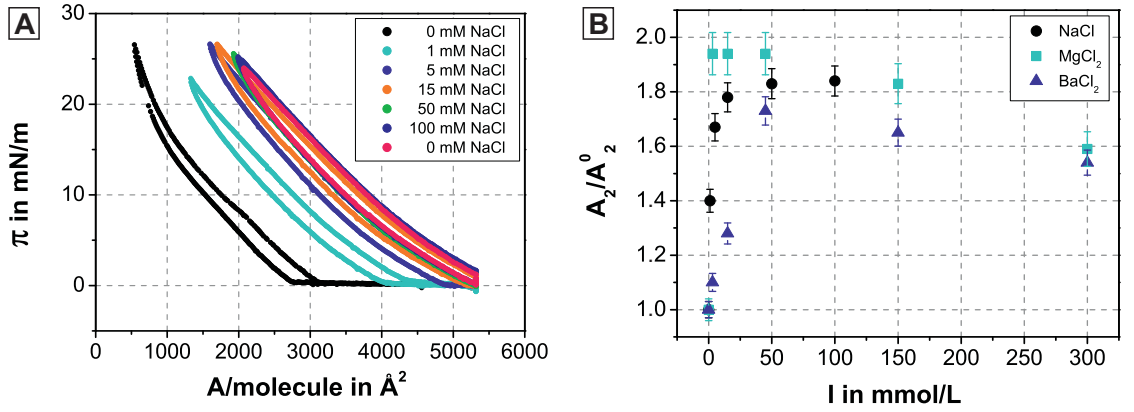

Figure 5.5: (A) Isotherms recorded before and after subphase exchange with NaCl solution of increasing concentration. (B) Relative area per molecule A_2/A_2^0 increase versus ionic strength I of the subphase.

thickness of the PAA film first increased upon increasing the salt concentration in solution and then dropped after having reached a maximum. The trend of the PAA film thickness is similar to that observed for the molecular volume of DNA-*b*-PPO in dependence of the salt concentration. Both systems are comparable, because in each case a negatively charged polyelectrolyte molecule was investigated, which was tethered to an interface and could thus not freely move in the bulk solution. The main difference between both systems is however, that the DNA-*b*-PPO molecules were able to move freely along the air/water interface while the PPA brushes were fixed at a certain point of the substrate. As a consequence, a change in the polyelectrolyte volume would be visible in the isotherms for DNA-*b*-PPO. In contrast, the PAA brushes could not move and thus any volume increase would result in an increase of the film thickness, because the available space for each brush is limited by the neighboring brushes. If the laterally available space for each brush is occupied, but the brushes still swell due to an external trigger like the ionic strength, the brushes will stretch to release stress. Changes in the molecular area for DNA-*b*-PPO as measured in isotherms and the thickness of PAA films thus have the same origin and can be compared. Also, PAA and DNA-*b*-PPO are both considered as weak polyelectrolyte brushes, meaning that the degree of dissociation of the acid groups is not fixed and varies with the pH of the solution.

Wu and Gong et al. explain the phenomenon of the first thickness increase and the later thickness decrease upon increase of the ionic strength by the interplay between two opposing effects. The degree of dissociation of the acid groups in PAA was shown to be dependent on the ionic strength of the solution. At low ion concentrations only few dissociated acid groups can be found, which results in a repulsion between the acid groups and as a result the molecules stretch and the film becomes thicker. Upon

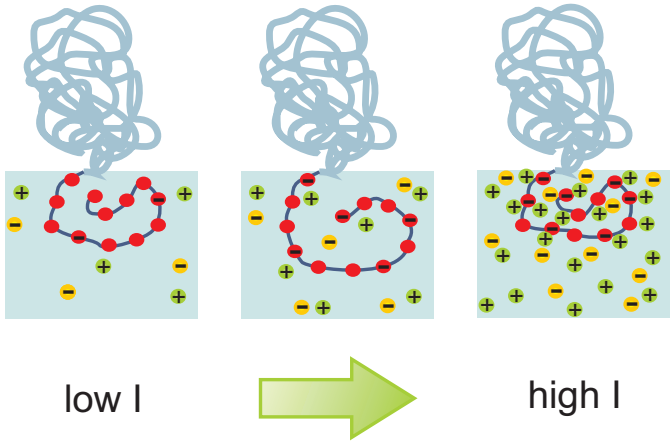

Figure 5.6: Schematic representation of the volume changes upon increase of the solution ionic strength. The red spheres demonstrate the undissociated phosphate groups while the red spheres with a negative sign correspond to dissociated phosphate groups. The green spheres represent positively charged ions from the dissolved salt and dissociation, the yellow spheres represent negatively charged counterions.

further increase of the ion concentration in solution the degree of dissociation increases, but not all generated charges can be compensated by the counterions, which then again results in an even stronger repulsion between the charged groups and thus in a thicker film. Upon further increase of the ion concentration, more negative charges of the backbone can be compensated and the repulsion is less pronounced, which results in shrinking of the PAA film. If all charges are compensated by the counterions from solution, the polyelectrolyte brush will behave like a neutral brush and the repulsion between the charged groups will be at its minimum resulting in a thin film. The theory can be transferred to the DNA-*b*-PPO molecules. The degree of dissociation and the according repulsion between charged groups is counteracted by the increase of ionic strength in the solutions which results in shielding of the negative charges. The repulsion between the undissociated acid groups is dominant at low concentrations and results in a volume increase of the ssDNA moiety of the DNA-*b*-PPO molecule, while the shielding of the Coulomb interactions between the dissociated groups becomes more dominant at higher ionic strengths and results in a reduction of the ssDNA moiety volume. The basic principle is illustrated in Figure 5.6. It is also noteworthy that not only intramolecular electrostatic interactions of the polyelectrolyte chains but also intermolecular interactions have to be taken into account. The effect of the actual volume change within the polyelectrolyte chain is probably rather small and is further enhanced by similar electrostatic interactions between neighboring polyelectrolyte chains. A stronger repulsion between neighboring molecules will trigger the increase the effective area per molecule extracted from

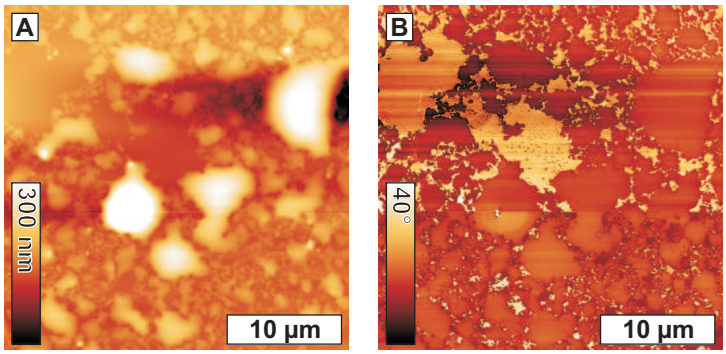

Figure 5.7: SFM images of a typical DNA-b-PPO film with aggregates- (A) Topography image. (B) Phase image.

isotherm measurements. This repulsion is governed by the effective charge of the polyelectrolyte and the dielectric constant of the surrounding medium.

Mg^{2+} and Ba^{2+} ions cause a similar effect on the DNA-*b*-PPO molecules. The A_2/A_2^0 increase is more pronounced for Mg^{2+} than for Ba^{2+}, although both ions are equally charged. Mg^{2+} is known to stabilize dsDNA helices, as has been demonstrated by the increase in helix melting temperature upon addition of Mg^{2+} [132], and to assist in DNA hybridization. Mg^{2+} binds exclusively to the phosphate groups in the DNA backbone and forms a chelate complex. This binding can stabilize and induce conformational changes of the DNA, e.g. in order to trigger enzyme binding [133]. The natural preference of DNA for Mg^{2+} might be the reason for the observation of a stronger effect. The relative area increase for Ba^{2+} is even smaller than for Na^+ pointing to a weaker interaction with the phosphate groups. This weaker interaction can be explained when considering Pearsons *hard and soft acids and bases* (HSAB) principle [134]. Na^+ and Mg^{2+} are considered as hard Lewis acids, while Ba^{2+} is a soft Lewis acid. The phosphate group is a hard Lewis base, meaning that it interacts more strongly with the hard acids than with soft ones. The irreversibility of the isotherm expansion upon rinsing with MilliQ water is probably caused by the electrostatic interactions between the phosphate backbone of the DNA molecules and ions. The ions cannot simply be rinsed away because they are attracted by the oppositely charged DNA.

5.2 Film transfer of DNA-*b*-PPO

LB films of DNA-*b*-PPO at the air/water interface were transferred to investigate the film structure. The basic idea was that not all molecules spread at the interface are aggregated into clusters so that a monolayer is present between the aggregates, which

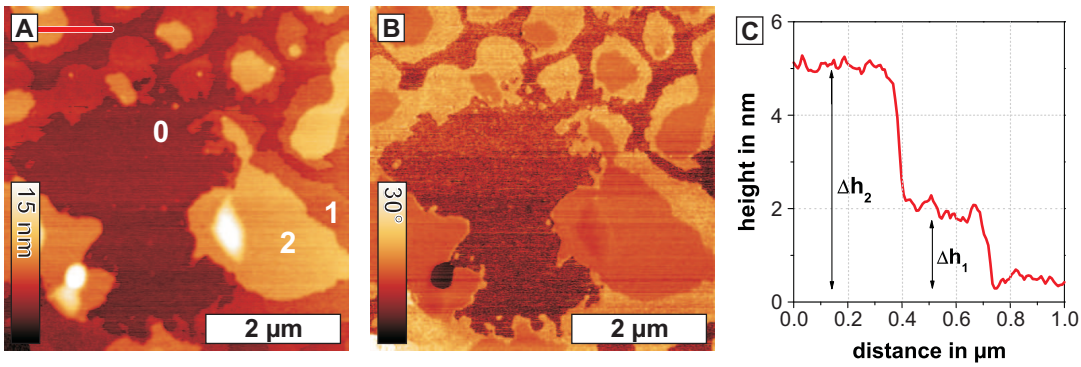

Figure 5.8: SFM images of DNA-*b*-PPO (M_W = 6800 g/mol) films transferred onto hydrophilic Si substrates via LB film transfer at a surface pressure of 30 mN/m. (A) SFM topography image. The red line marks the positions of the line plot in (C). (B) SFM phase image. (C) Line plot at the positions marked in image A averaged over 10 pixels.

have been imaged with BAM (Section 5.1.1) and can be investigated employing SFM. Figure 5.7 shows a typical SFM image of a DNA-*b*-PPO film. The image shows aggregates of varying sizes. Their height ranges from 20–600 nm. Nevertheless, it was also possible to locate sample areas, which exhibit less aggregates and allow for the identification of a monomolecular film in between them.

Figure 5.8 shows an SFM image of such a region. The substrate (area 0) and two layers, layer 1 and 2 are visible. These layers exhibit a phase contrast. The thickness of layer 1 was estimated to be $\Delta\, h_1 = 1.8 \pm 0.2$ nm and that of layer 2 to be $\Delta\, h_2 = 5.0 \pm 0.3$ nm. The phase contrast difference of layer 1 and 2 can be attributed to differences in material properties, like soft- or stickiness of the material. The dimensions of the DNA-*b*-PPO molecule are estimated to be $R_g(11mer) = 0.8$ nm [118] and $R_g(PPO) = 2.0$ nm [135]. When transferred onto a substrate this yields a theoretical film thickness of 5.6 nm ($2 \cdot R_g(11mer) + 2 \cdot R_g(PPO)$). Considering that the film consists of the pure DNA-*b*-PPO blockcopolymer, a different arrangement of the molecules provides a reasonable explanation for the phase contrast. From the film thicknesses, which have been determined, a model can be proposed (Figure 5.9): The thinner layer 1 corresponds to DNA-*b*-PPO molecules lying flat on the substrate, while layer 2 corresponds to molecules erected perpendicular or at an angle to the substrate, corresponding well with the theoretical film thickness of 5.6 nm.

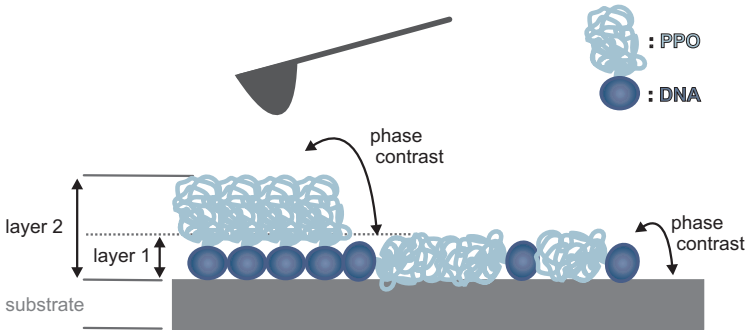

Figure 5.9: Model proposed for the different layers on the substrate and the according phase contrast in SFM phase images. The phase contrast between layer 1 and layer 2 is caused by variation of the molecular orientation. The molecules in layer 1 lie flat on the surface, while the molecules in layer 2 stand upright in the substrate with their hydrophobic moieties facing air.

5.2.1 Effect of ionic strength on dU11

Experiments similar to those with DNA-*b*-PPO have been performed with a dU11 monolayer (Chapter 4) for comparison. The dU11 molecules occupy less space at the air/water interface and the film can thus expand more freely. It is therefore interesting to compare the behavior of both molecules upon exposure to salt in the subphase. Both molecules consist of a hydrophilic ssDNA 11mer head group, which is immersed in the subphase, only the hydrophobic tail is different. The dU11 molecules were spread onto a pure water subphase, an isotherm was recorded and the subphase was subsequently exchanged with NaCl solutions with concentrations varying from 0-100 mM (Figure 5.10 A). The effect on the isotherms is similar to the effect observed for the DNA-*b*-PPO molecules: The A_0 value increases with increasing salt content of the subphase. As also observed for DNA-*b*-PPO, the effect is not reversible upon rinsing with MilliQ water (Section 5.1.2). This is a clear indication for the interaction between the ions and the ssDNA head groups of both molecules, DNA-*b*-PPO and dU11. The head groups are immersed in the subphase and sensitive towards the ionic strength of the surrounding medium. A comparison of the relative A_2/A_2^0 values for dU11 and DNA-*b*-PPO at similar ionic strengths shows that A_2/A_2^0 does not move towards a plateau for dU11, as observed for DNA-*b*-PPO (Figure 5.10B). In contrast to the experiments with DNA-*b*-PPO, the expansion of the dU11 film was not hindered by the trough barriers, because the dU11 molecules in general occupy less space at the air/water interface. Hence, the plateau observed for the NaCl measurements of DNA-*b*-PPO is likely to be an experimental artifact, indicating that without restriction the molecule behaves similar to dU11.

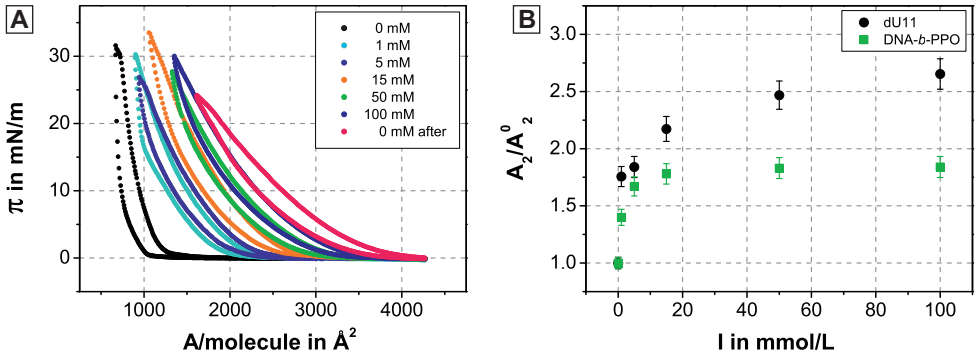

Figure 5.10: (A) Isotherms recorded before and after subphase exchange with NaCl solution of increasing concentration. (B) Relative area per molecule A_2/A_2^0 increase versus ionic strength I of the NaCl subphase plotted for DNA-*b*-PPO and dU11 for comparison.

Furthermore, LB films were transferred from the salty subphase to determine the film thickness and structure under these conditions. This is of interest, because the DNA hybrid molecules dU11 and DNA-*b*-PPO are potential candidates to perform molecular recognition experiments at the air/water interface. DNA hybridization is assisted by salt and usually performed in buffer solution, the influence of salt on the film morphology is therefore interesting. The transferred films were investigated with SFM (Figure 5.11). As can be seen from the topography image, the substrate is completely covered with a dU11 film at $\pi = 30$ mN/m (Figure 5.11 A). The small square in the middle of the topography and phase images shows the substrate (layer 0). The film in this area was removed by scanning with the SFM tip (see also Section 4.2). Besides the film covering the substrate (layer 1), some islands positioned on top of layer 1 can be found (layer 2). A comparison between topography and phase image shows that the substrate and layer 1 exhibit a phase contrast of 5° (Figure 5.11 B). Between layer 1 and layer 2, no phase contrast can be found. The thickness of layer 1 and 2 was determined using mediated topography profiles (Figure 5.11 C). The thickness of layer 1 is $\Delta h_1 = 2.8 \pm 0.2$ nm, which corresponds to the thickness of a bilayer determined in Chapter 4. The addition of salt did thus not significantly render the thickness of a dU11 bilayer. Accordingly, the variation of A_0 in the isotherms can probably be attributed to repulsive interactions between the molecules at the interface rather than to real volume changes. Then again, the film is in a dry state when investigated with SFM, the influence of the drying process on a potential volume change due to interaction with salt is not clear. An increased repulsion between the molecules at the air/water interface should result in a molecular density decrease. A variation of the molecule density could not be observed in the measurements, probably because the molecules were compressed for the film transfer. The thickness of layer 2 was determined to be $\Delta h_2 = 4.4 \pm 0.2$

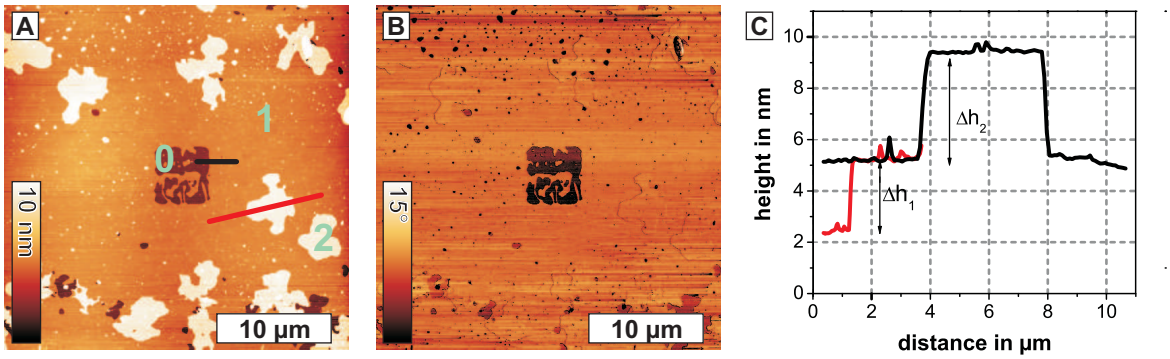

Figure 5.11: LB film of dU11 transferred from a 15 mM NaCl solution at a surface pressure of 30 mN/m. (A) Topography, (B) phase image and (C) profiles as designated in A.

nm. The film thickness and identical phase contrast indicate, that layer 2 is a second dU11 bilayer stacked on the first one. As has been observed before, the second bilayer above the first one is usually thicker, than the one in contact with the substrate. The same phenomenon can be observed here. Reasons can be repulsive interactions between layer 1 and layer 2 or measurement artifacts from scanning with the SFM tip, which are discussed in detail in Chapter 4. Conclusively, the salt in the subphase does not alter the film morphology significantly, although it influences the isotherm measurements heavily.

5.3 Molecular recognition at the air/water interface

Both DNA hybrid materials presented in this Chapter theoretically offer the possibility to perform molecular recognition experiments at the air/water interface. One part of this thesis was to investigate their practical potential for the performance of this kind of experiment. The basic idea was to prepare a stable ssDNA monolayer, which was anchored to the air/water interface and accessible by molecules from the subphase, e.g. complementary ssDNA (cDNA). Aim was to detect the DNA hybridization at the air/water interface by changes in the isotherm shape and area per molecule. In order to do so, several practical aspects had to be investigated: On the one hand, hybridization of the complementary DNA strands under conditions sim-

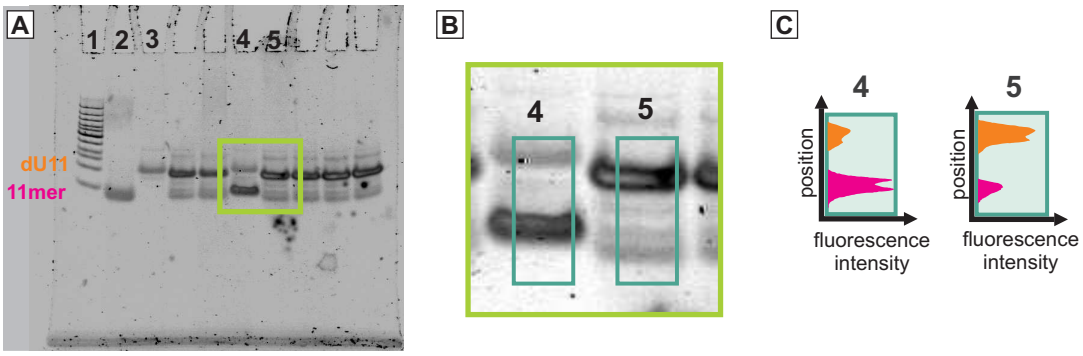

Figure 5.12: (A) 20% polyacrylamide gel stained with ethidium bromide and imaged in UV transillumination at $\lambda = 260$ nm. Lane 1: Standard low molecular weight ladder. Lane 2: cDNA 11mer. Lane 3: dU11. Lane 4: dU11 + noncomplementary DNA. Lane 5: dU11 + complementary DNA. The image was inverted for better contrast. (B) Zoom in into the area marked by the green box in A. (C) Fluorescence intensity vs. position plots for the areas marked in lane 4 and 5 of B. The orange peak corresponds to the fluorescence intensity of dU11, the pink peak to the fluorescence intensity of the DNA 11mer.

ilar to those in the Langmuir film balance had to be ensured and investigated. On the other hand, control experiments had to be performed to confirm that isotherms are only altered by molecular recognition between complementary DNA strands and not by unspecific interactions between components of the system.

In order to investigate the hybridization of the dU11 molecule with its complementary DNA, PAGE experiments were performed. A common procedure to conduct DNA hybridization is to heat the sample containing both cDNA strands to 80 °C and cool it down very slowly afterwards. This procedure gives a high yield of ds-DNA. The subphase of the Langmuir trough cannot be heated up as high as 80°C, because evaporation of the subphase would interfere with the surface tension measurements and may also influence the structure of the film spread at the air/water interface. Thus, hybridization experiments at the air/water interface have to be conducted under more gentle conditions, preferably without heating. In order to investigate whether dU11 hybridizes under gentle conditions, which can be applied to the trough, dU11 samples with cDNA and noncomplementary DNA (ncDNA) were prepared in 0.5× TAE buffer with NaCl and $MgCl_2$ ($c_{NaCl} = 100$ mM, $c_{MgCl_2} = 60$ mM), heated up to 40 °C and were left for cooling at room temperature. Both samples were then investigated in terms of PAGE in order to study the hybridization of the DNA strands. Since PAGE is a relative method, a standard with DNA strands of known lengths was added in lane 1 and pure samples of cDNA and dU11 were added in lanes 2 and 3 as references. The dU11 samples with ncDNA and cDNA,

respectively, were added to lanes 4 and 5. After application of a voltage of 130 V for 60 min, the gel was immersed in a diluted ethidium bromide solution for staining and afterwards imaged by UV transillumation at $\lambda = 260$ nm. The corresponding image can be found in Figure 5.12 A. The samples in lane 4 and 5 both exhibit two bands, which means that two different molecule species can be found in each sample. These have migrated as far as the reference bands of the ssDNA 11mer in lane 2 and the dU11 molecules in lane 3. This means that the upper band in lane 4 and 5 contains dU11 molecules, while the lower band contains the ssDNA 11mer, both complementary (lane 4) and noncomplementary (lane 5). In gel electrophoresis with classical DNA molecules without hyrdophobic moieties, hybridization would be accompanied by the appearance of a third band, because the molecular weight of the molecules changes upon hybridization. The dU11 molecule is a DNA hybrid material and its migration through the gel is influenced by the large hydrophobic moieties and by aggregation of the molecules into micelles. It is thus possible that the new species, which has formed after hybridization, the double stranded dU11 molecule, does not migrate significantly less than the single stranded dU11 molecule. Hence, no new band can be found in the gel. Another approach, to interpret the gel is to investigate the fluorescence intensity of the individual bands, as this is a measure for the amount of DNA contained in the band after staining with ethidium bromide. A zoom of the respective bands in lane 4 and 5 can be found in Figure 5.12 B. The green rectangles mark the areas of the lanes, of which the fluorescence intensity was determined. Figure 5.12 C shows the fluorescence intensity within each band plotted against the position in the band. This analysis was performed with ImageJ image processing software. The ratio of the intensities can be calculated and gives information about the amount of DNA molecules contained in each band. A comparison of both spectra (Figure 5.12 C) shows, that this ratio varies significantly for lane 4 and 5, although the initial DNA concentration in the samples was similar. Lane 4, containing the dU11 + ncDNA sample, exhibits a ratio of 28:72 dU11:ncDNA. Lane 5, containing the dU11 + cDNA sample, exhibits a ratio of 73:27 dU11:cDNA. Thus, lane 5 contains significantly more DNA in the first band, the dU11 band, than in the second one, the ssDNA 11mer band. This is in contrast to the sample with the ncDNA, which displays an inverse ratio. Under the precondition that both samples initially contained identical concentrations of dU11 and the respective ssDNA 11mer and that the same amount of sample solution was added to the gel, it can be concluded that hybridization of dU11 was partially successful for the sample in lane 5. From these results it can be expected, that dU11 molecules at the air/water interface will hybridize with their complementary DNA, yielding qualitative amounts of double stranded dU11 at the air/water interface.

The second practical precondition for the performance and detection of molecular recognition experiments in a Langmuir trough is that the cDNA is not surface active. Otherwise changes in the isotherm cannot distinctly be attributed to the

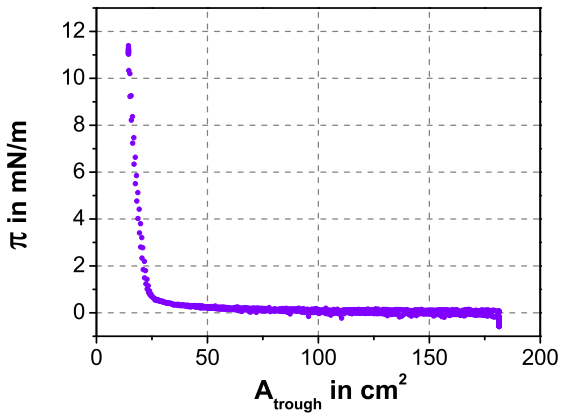

Figure 5.13: Isotherm obtained after adsorption of complementary ssDNA from bulk solution to the air/water interface

DNA hybridization but can also stem from simple DNA adsorption to the interface. Frommer et al. already investigated the adsorption of ssDNA and dsDNA to the air/water interface in 1968 and found that both species are surface active in salt solution [128]. They also found, that the change in surface pressure π never exceeded 0.2 mN/m, which can be considered negligible in isotherm experiments. In contrast to Frommer et al. I found in experiments with ssDNA that the molecules adsorbed readily to the air/water interface and accordingly generated changes in surface pressure. Figure 5.13 shows an isotherm obtained after adsorption of cDNA from buffer solution. The cDNA molecules, which have adsorbed to the air/water interface can even be compressed up to a surface pressure of 12 mN/m, which is very high and can thus not be neglected in molecular recognition experiments. Molecular recognition by DNA hybridization at the air/water interface can therefore not explicitly be detect by isotherm measurements, because the adsorption of ssDNA molecules to the air/water interface significantly alters the isotherms.

5.4 Conclusion

Pure DNA-*b*-PPO films can be prepared at the air/water interface and transferred via LB technique onto solid substrates. Isotherms, BAM and SFM experiments have shown, that the DNA-*b*-PPO molecules form films, which do not only consist of monomolecular layers of flat lying and upright standing molecules, but also of bigger three-dimensional aggregates. It was also found, that the nominal volume of the ssDNA head group is subject to the ionic strength of the subphase. The relative

area per molecule A_2/A_2^0 increases upon increase of the ionic strength and reaches a maximum at $I = 45$ mM for Mg^{2+} and Ba^{2+} in order to decrease upon further I increase. A similar effect was observed by Gong et al. [131] for the film thickness of grafted poly(acrylic acid) brushes upon variation of the ionic strength of the bulk solution. Gong et al. have investigated the thickness of the brush films as a function of not only the ionic strength but also of the grafting density. This can be achieved more easily in our system by simply compressing the film at the air/water interface. For the dU11 molecule, a similar behavior was observed. Furthermore, experiments were performed to investigate the potential to perform molecular recognition experiments with DNA hybrid materials at the air/water interface. It was shown, that the hybridization under experimental conditions applicable in the Langmuir trough can be conducted. Experiments investigating the adsorption behavior of ssDNA revealed, that this molecule adsorbs readily to the air/water interface and thus interferes with the detection of DNA hybridization at the air/water interface. The system is thus not suitable for the sensing of molecular recognition experiments at the air/water interface.

5.5 Experimental details

Materials

The DNA-*b*-PPO molecules were synthesized and purified by xxx and xxx as reported elsewhere [129]. The molecular weight of the PPO was $M_W(PPO) = 6800$ g/mol. The single stranded DNA 11mer sequence was designed to be non-self-complementary: 5'-TTC TAT AGA AA-3'. Water for dissolution and subphase was purified to a resistance of 18.2 MΩ/cm using a Milli-Q filtration system (Millipore) and additionally distilled before use. The concentration of the amphiphilic molecules was determined by UV/Vis adsorption spectra measured in aqueous solution. The solutions were aliquoted accordingly, frozen in liquid nitrogen, lyophilized and stored at -7°C. Samples were removed from the freezer for temperature accumulation before preparation of spreading solutions (c = 0.25 µmol/L) in dichloromethane (Chromasolv, Merck).

Monolayer preparation

500 µL of the respective solution in dichloromethane were spread onto the Milli-Q subphase with a microliter syringe. The spread layer was left for solvent evaporation for 15 min prior to each measurement.

Monolayer isotherms and monolayer transfer

Experimental details for the isotherm measurements and film transfer are similar to those introduced in Section 4.4. Experiments with varying salt concentrations in the subphase were performed by employing the subphase exchange system with a peristaltic pump (Minipuls 3, Abimed, Gilson Inc., United States) at a pump rate of 4 mL/min. The subphase volume was approx. 110 mL, accordingly at least 250 mL of the new subphase solution were pumped through the trough in order to reduce effects from dilution by the previous solution.

SFM measurements

The procedure for SFM imaging was similar to that introduced in Section 4.4.

BAM measurements

For the BAM measurements, V = 3250 µL of the DNA-*b*-PPO solution in dichloromethane (c = 0.25 µmol/L) were spread on a MilliQ water subphase. The Brewster angle microscope employed for the measurements in this thesis is a EP3 from Nanofilm (Göttingen), which is mounted on a Langmuir trough (Nima, type 601 BAM), equipped with a 50 mWlaser with a wavelength of $\lambda = 532$ nm. The lateral resolution of the images is 2 µm, the image size is 500 × 400 µmwith a 10× objective from Nikon. After evaporation of the solvent, BAM imaging was started at a Brewster angle of $\theta = 52.98°$. The monolayer was compressed at a compression speed of $V_{comp} = 20$ cm^2/min. Isotherm data and BAM images were taken simultaneously during compression of the film.

PAGE

For the PAGE experiments, precast polyacrylamid gels with 20% cross-linking (Novex 20% TBE Gel, Invitrogen) were used. The gel was immersed in so called 1× TBE or TRIS/borate/EDTA buffer. TRIS stands for 2-Amino-2-hydroxymethylpropane-1,3-diol, borate for boric acid and EDTA for ethylenediaminetetraacetate. The corresponding concentrations of a 1× TBE buffer are 89 mM TRIS, 89 mM Borate and 2 mM EDTA, the corresponding pH = 8.3±0.2. The samples for PAGE were prepared in 0.5× TAE buffer, here the A stands for acetate. The corresponding concentrations of a 0.5× TAE buffer are 20 mM TRIS, 10 mM acetate and 0.5 mM EDTA. dU11 and the corresponding DNA 11mer (cDNA or ncDNA) in a ratio of 1:1 as well as salt (100 mM NaCl and 60 mM $MgCl_2$) were mixed and left for hybridization at 40°C for 2 h. Afterwards, the samples were mixed with 2 µL of a glycerol/MilliQ = 1:1 mixture and 1 µL of loading dye (Fermentas, 6× DNA loading buffer) for PAGE, and MilliQ water was added to yield a total volume of 5 µL and a dU11 and cDNA/ncDNA concentration of 16 µM. The control samples containing either dU11 or cDNA/ncDNA were prepared in a similar way. The gel was loaded with all samples and the reference ladder and a voltage of 130 V was applied for 1h. The blotting was performed in a XCell surelock Mini-Cell (Invitrogen) in 1× TBE buffer. For staining, the gel was removed from the cell and immersed in a diluted ethidium bromide solution (100 mL 1× TBE buffer and 15 µL ethidium bromide) for 15 min. Afterwards, the gel was imaged in UV transillumination at $\lambda = 260$ nm to vizualize the bands.

6 SFM as a tool to investigate the structure of polyglycerol ester foams

A foam is a dispersion of gas in a liquid or solid medium. However, a bubble produced by shaking a pure liquid ruptures almost immediately. Several effects are responsible for this: The formation of a foam involves a huge increase of surface area, which is always accompanied by an increase in surface energy. However, the state of equilibrium is the state of minimum energy and thus minimum surface area [136]. A foam is therefore never thermodynamically stable, its just a matter of different timescales, until the film around a bubble ruptures. The evaporation of water from the foam film between two bubbles is one main issue causing film rupture [136]. Also, van der Waals attraction between two gas phases separated by a liquid film will lead to rupture of this film. Therefore, the gas will only be able to stay dispersed inside the liquid to form a foam, when the bubble interface is stabilized by addition of a surface active material [137, 138]. This material adsorbs to all available air/water interfaces. Considering one single bubble, two air/water interfaces can be found, one separating the air entrapped inside the bubble from the liquid film and one, separating this liquid film from the surrounding atmosphere. Given that a foam consists of multitude of bubbles, even more air/water interfaces will be available

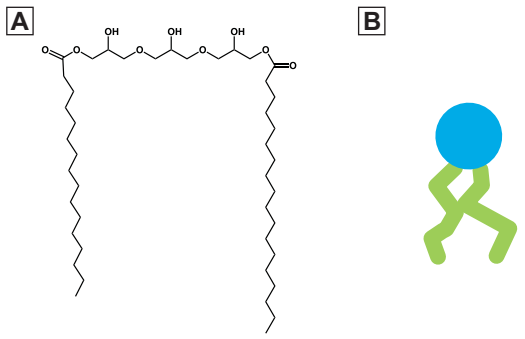

Figure 6.1: (A) Chemical structure of PGE. (B) Schematic representation of a PGE molecule.

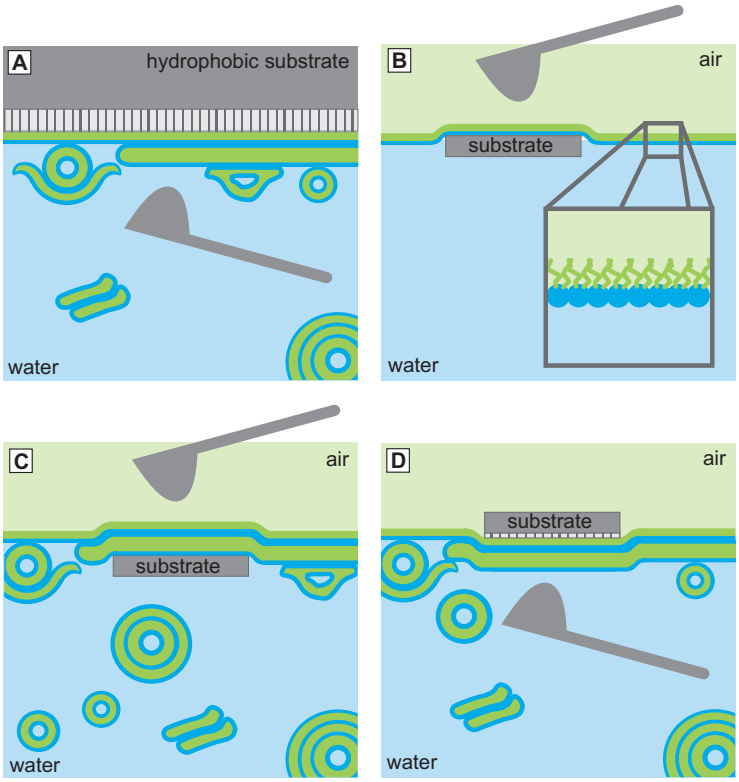

Figure 6.2: Sketches of the different transfer methods used to investigate the PGE structure at the air/water interface. (A) Measurement at the substrate-liquid interface. (B) Langmuir monolayer. (C) Gibbs adsorption layer. (D) Langmuir-Schaefer like transfer.

for surfactant adsorption. A foam can thus be considered as a complex network of interfacial films, which complicates their characterization substantially. Aim of this work was to investigate the potential and limits of SFM as a tool to investigate foams.

Possible candidates for this stabilization of a foam are low molecular weight surfactants [139, 140], enzymes [141–144] or nanoparticles [145–148]. In these three cases, the thermodynamic and dynamic characteristics of the surface active material are different. Thus, the foamability of a solution and the stability of a resulting foam are influenced significantly by the choice of surface active material [149]. The surface active material of interest in this Chapter is a commercially available food-grade polyglycerol ester (PGE), which consists predominantly of a hydrophilic triglycerol head group and an equimolar mixture of hydrophobic hexadecanoic acid and octadecanoic acid(Figure 6.1 A). It is a low molecular weight non-ionic surfactant and has been shown to have extraordinary foaming properties [150]. Due to this behavior it is of relevance for the production of ice cream and other foamed food products. It

is however not understood, why this particular surfactant forms these stable foams. Typical foam characterization methods like e.g. small angle neutron scattering and interfacial rheology [151] have given a general overview about the properties of PGE foams: Electron microscopy and small angle neutron scattering experiments have shown that PGE solutions are composed of multilamellar PGE vesicles as well as of planar lamellar phases [26]. Measurements of the interfacial tension of dilute solutions (0.01 wt %) at room temperature have shown a slow adsorption process of PGE molecules from bulk solution to the air/water interface. Even after an adsorption time of 4 hours no true equilibrium in interfacial tension was reached [27]. At higher concentrations (1 wt %) an equilibrium surface tension of 40 mN/m was reached after 30 minutes [26]. Interfacial rheology measurements on dilute solutions have shown a viscoelastic behavior that was discussed as a possible result of a temporary network formed by hydrophobic interactions of fatty acid chains of the PGE molecules. It was further found, that the interfacial storage modulus of a defined PGE monolayer prepared by spreading was lower than the one measured on adsorbed interfacial films. This is an indication for the adsorption of multiple layers from the bulk solution to the air/water interface [26]. Additionaly, it was found that the pH of the PGE solution substantially influences the surfactant behavior: A reduction of the native pH from pH 7-9[1] to pH 3 leads to an increased foamability of the solution on the one hand [150], but to a reduced bubble stability on the other hand [152]. This effect is yet not well understood. Despite of these results, neither of the above mentioned techniques was able to clarify the molecular structure of PGE foam films nor the adsorption mechanism involved. It is of interest to understand, whether single molecules or complete vesicles adsorb from bulk solution to the air/water interface.

Scanning force microscopy is attractive as a tool to investigate foam films because the resolution is far beyond the limits of optical microscopy (Section 2.4). The development of model systems and new film transfer techniques combined with well-established ones to characterize the complex composition of a PGE foam film was therefore the aim of this project. Several techniques have been applied to fabricate surfactant films (Figure 6.2): Langmuir monolayers were prepared to determine the thickness of a defined monolayer (Figure 6.2 B) and compare these results with films prepared by adsorption of PGE from bulk solution (Figure 6.2 C). Two different film transfer techniques were investigated and compared, namely surface lowering and Langmuir-Schaefer like film transfer (Figure 6.2 D). The adsorption process itself was investigated by mimicking the air/water interface: A hydrophobic highly ordered pyrolytic graphite (HOPG) substrate was immersed into a PGE solution. The adsorption of PGE molecules from bulk solution to the water/HOPG interface was studied by employing SFM measurements in liquid (Figure 6.2 A). The experiments

[1] depending on the PGE concentration in the solution

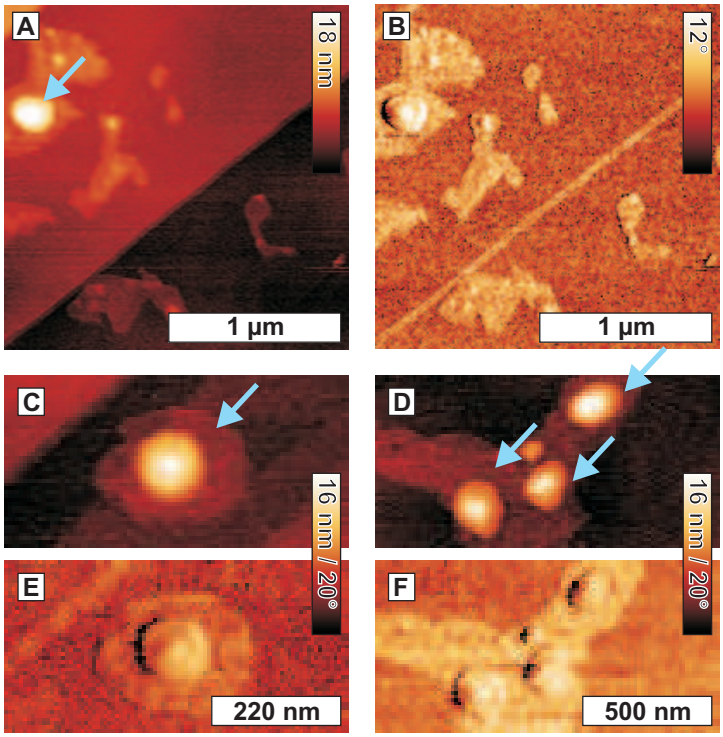

Figure 6.3: PGE adsorption at the solid-liquid interface. SFM height ((A), (C) and (D)) and phase ((B), (E) and (F)) images of PGE molecules adsorbed onto a graphite surface. The images were recorded in an aqueous solution. The blue arrows mark the fried egg like structures.

were conducted together with xxx within the framework of a cooperation with xxx from xxx.

6.1 Adsorption to the interface - measurements in liquid

The adsorption process of PGE molecules from the bulk solution to a hydrophobic surface was investigated employing SFM measurements in liquid (Figure 6.2 A). HOPG was immersed in a 1 wt% PGE solution to mimic the air/water interface of a bubble. In the SFM measurements it was found that PGE adsorbs slowly[2] to the HOPG/water interface (Figure 6.3). Parts of the interface are covered with PGE patches. In most cases these patches contain a second elevated structure, consisting

[2]Measurements were performed after 3-5 days adsorption time.

of a thin outer layer and a raised inner hemisphere recalling a fried egg shape (blue arrows in Figure 6.3 A, C and D). The thickness of the underlying patch is 1.6 nm. This has been determined by fitting the median height difference between substrate and patch over a mediated profile (width of 10 pixels). Small angle neutron scattering experiments have revealed a bilayer thickness of PGE in bulk solutions of 4.9 nm [26]. This value is more than twice as thick as the patch, it seems therefore reasonable that the patch consists of a PGE monolayer with the hydrophobic tail group of the PGE molecule facing the HOPG substrate and the hydrophilic headgroup facing the bulk solution. Fried egg like structures can be found resting on the underlying monolayer patches. The outer area corresponding to the egg white is 5.6 ± 0.9 nm thick, whereas the higher regions in the center, corresponding to the egg yolk, rise up to 12.1 ± 2.2 nm. The egg white is within the error as thick as a PGE bilayer. The spherical shapes resembling the egg yolk are assumed to be adsorbed PGE vesicles. The presence of PGE vesicles in the bulk solution has already been shown [26]. The formation of the fried egg like structures can be explained by considering mono- or multilamellar vesicles, which have adsorbed onto the PGE monolayer, and have either deformed, or partially unfolded (Figure 6.2 A). With these results it is demonstrated that vesicular structures play a role in the adsorption process of PGE onto a hydrophobic surface.

6.2 Films at planar air/water interfaces

In this Section I would like to highlight the importance of the film preparation technique, as this is a key parameter for the structuring of the final film. In order to investigate planar air/water interfacial PGE films, two different layer preparation techniques were employed. Films were prepared either as Langmuir monolayers or as Gibbs adsorption layers. They were then transferred onto hydrophilic silicon substrates employing several transfer techniques. The dried films were investigated by SFM to compare the structure of artificial (Langmuir) monolayers with natural (Gibbs adsorption) layers, which self-assemble at the air/water interface from the bulk solution.

6.2.1 Langmuir monolayers

The goal of the Langmuir monolayer transfer was to determine the thickness of a dry PGE monolayer for comparison with Gibbs adsorption layers, as well as to understand the behavior of a PGE monolayer at different surface pressures (Figure 6.4 B). Langmuir monolayers of PGE were prepared on a Langmuir film balance and transferred via surface lowering at lateral surface pressures of $\pi = 5$ mN/m and $\pi = 50$ mN/m (Figure 6.4). The dried film were investigated by means of

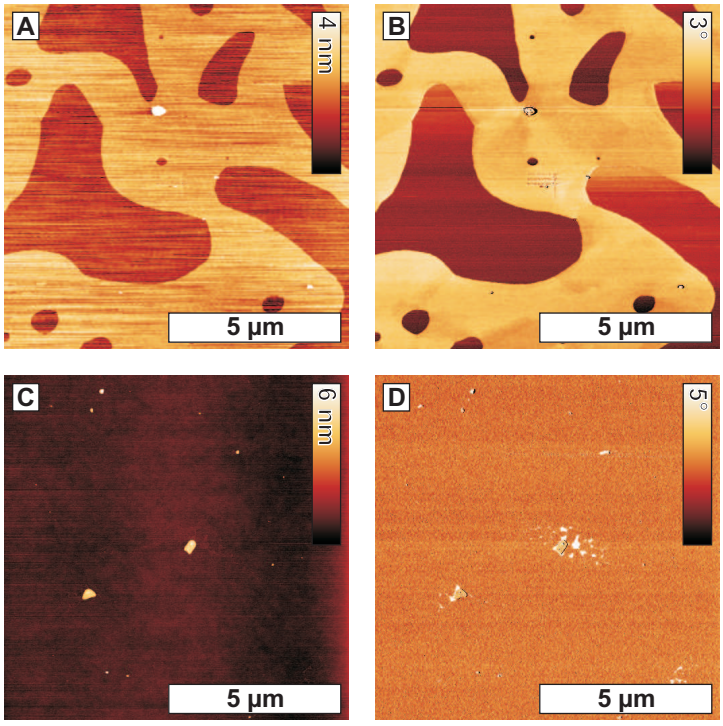

Figure 6.4: SFM height A and phase B image of a Langmuir monolayer transferred at a lateral pressure of $\pi = 5$ mN/m. The images show the Langmuir monolayer with defects on a silicon substrate. SFM height C and phase D image of a Langmuir monolayer transferred at a lateral surface pressure of $\pi = 50$ mN/m. The images show a closely packed PGE layer with few three-dimensional assemblies showing a phase contrast compared to the underlying layer. Areas exhibiting the same phase contrast as these assemblies can also be found in the neighborhood of the elevated structures. This can be taken as an indication for the formation of monolayer collapse products, as they provide a proof that the layer morphology has also changed around the elevated structures.

SFM. Films transferred at low surface pressure ($\pi = 5$ mN/m, Figure 6.4 A and B) revealed a partial coverage of the silicon substrate with a monolayer of PGE molecules. From the SFM measurement I obtained a PGE monolayer thickness of 1.2 ± 0.2 nm. This value was determined statistically from 13 independent thickness measurements. The difference in the monolayer thickness of approx. 0.4 nm between measurements in air and in aqueous solution (Section 6.1) can be attributed to the dehydration of the PGE monolayer during the drying process. Films transferred at a high lateral surface pressure of $\pi = 50$ mN/m (Figure 6.4 C and D) showed a full coverage of the silicon wafer surface. Also some small, elevated structures on top of this homogeneous underlying layer were observed. They can originate from a partial collapse of the PGE film due to the high surface pressure. No detailed information

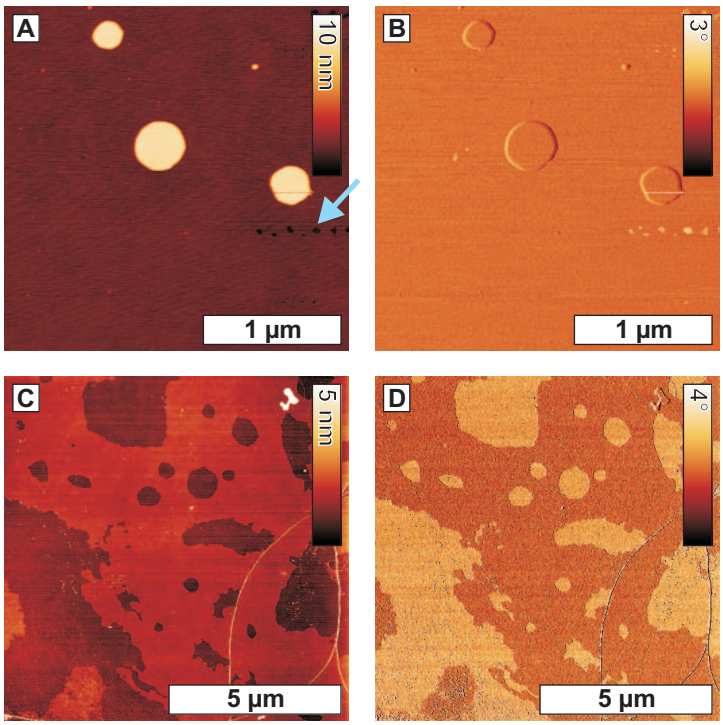

Figure 6.5: Gibbs adsorption layer and control sample. SFM height A) and phase B) image of a Gibbs adsorption layer (16 hrs adsorption time) transferred onto a hydrophilic substrate. The images show a closely packed PGE monolayer with few three-dimensional assemblies on top of the monolayer. SFM height C) and phase D) image of a hydrophilic silicon substrate, which had been immersed into the bulk solution, but where no film transfer had taken place. It becomes clear from this control experiment that molecules adsorb onto the substrate even without film transfer.

about the layer structure or its thickness can be extracted from these experiments at high surface pressure, because the substrate is completely covered by the film. Overall it can be summarized from these studies that an increase in surface pressure increases the surface coverage leading to a homogeneous surface layer with a small number of three-dimensional assemblies on top of this layer.

6.2.2 Gibbs adsorption films

In contrast to the Langmuir monolayer transfer, the goal of the Gibbs adsorption experiments was to investigate, whether multiple layers adsorb at an air/water interface (Figure 6.2 C), as suggested by interfacial rheology experiments [27]. Furthermore lamellar structures present in the bulk solution [26] might also adsorb. Dilute

surfactant solutions (0.01 wt% PGE) were poured into a clean and empty Langmuir trough. The surfactant was left to adsorb from the bulk solution onto the interface for 16 hours. Then the resulting film was transferred onto a hydrophilic substrate by lowering the air/water interface and thus the interfacial film onto the hydrophilic substrate. After the transfer and drying of Gibbs adsorption layers the silicon substrate was completely covered with PGE (Figure 5 A and B). The molecules could be removed upon scanning with the SFM tip (blue arrow) and thus expose the substrate to the tip, which is indicated by the phase contrast. At these holes I determined the film thickness to be 0.9 ± 0.1 nm. This film is thinner than the Langmuir monolayer transferred at $\pi = 5$ mN/m (thickness of 1.2 nm). One possible explanation for this height difference is that the Langmuir monolayer was compressed before transfer, while this monolayer could adsorb freely. Accordingly, the density of the PGE molecules on the substrate and the tilting angle of the molecules differ and lead to varying film thicknesses. Additionally, several elevated spherical structures were found on top of the PGE monolayer. Their thickness was 6.6 ± 1.1 nm, their diameter ranged from 40 - 350 nm. The thickness of the spherical structures corresponds to the estimated thickness of two dried bilayers stacked in top of each other. Two scenarios are possible to explain the formation of these structures: (i) A multilamellar vesicle consisting of exactly two PGE bilayers as a shell adsorbs from the bulk solution onto the monolayer, ruptures and unfolds completely, similar to a typical rupture process proposed for unilamellar phospholipid vesicles [153]. As a result, two bilayers have formed on top of the underlying monolayer. (ii) A vesicle with a shell consisting of one PGE bilayer adsorbed on the substrate and collapsed releasing its content into the bulk solution. Then the vesicle will lie flat on the underlying monolayer like an empty balloon, forming two stacked bilayers. (iii) Upon transferring the film onto the hydrophilic substrate drops of the bulk solution remain on the substrate. Since the bulk solution contains multilamellar vesicles as well as planar lamellar structures, these remain on the substrate after evaporation of the water and will not explicitly be discernible from structures, which have adsorbed to the interface and were transferred afterwards. However, from the drying process of the drops structures of random heights and shapes can be expected: During the gradual drying of the solution drop, which contains self-assembled surfactant structures, these structures are expected to adsorb to the interface of the drop, simply due to the volume reduction. This would create local differences in interfacial tension, which would lead to a non-spherical shape of this partially dried drop. Furthermore, the self-assembled structures are not believed to be distributed homogeneously within the drop. Therefore, upon drying, the areas where the structures finally adhere to the substrate would be elevated, as compared to the remaining area of the dried drop. The spherical structures I found though are round and smooth, which is why it seems more reasonable that these structures originate from collapsed or ruptured vesicles, i.e. scenario (i) or (ii).

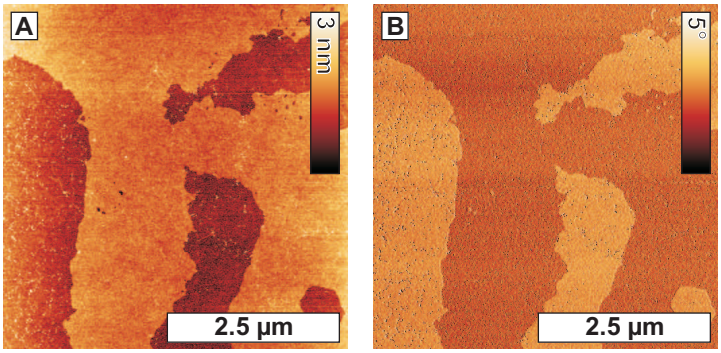

Figure 6.6: Langmuir-Blodgett film transfer: SFM topography (A) and phase (B) image of a Gibbs adsorption film transferred by the Langmuir-Blodgett technique. This film was transferred after an adsorption time of 4 hours.

Identical experiments have been performed transferring films via LB film transfer technique varying the adsorption time between 2 and 13 hours. The dried films were investigated employing SFM (Figure 6.6). The topographic image shows that the substrate is partially covered by a PGE film (Figure 6.6 A). The film thickness was determined to be 0.7 ± 0.1 nm, which corresponds to the film thickness determined for films transferred via surface lowering. Films transferred by both techniques, surface lowering and the LB technique, were shown to be very similar. One major difference is that the elevated spherical objects on top of the monolayer can only be found on films transferred via surface lowering. It seems therefore likely, that these structures originate from the rupture of vesicles during surface lowering or drying of the film. Independent of the transfer method, differences between films transferred from the Langmuir trough after different adsorption times did not yield any conclusive answers as to what changes take place within the film upon letting the surfactant adsorb for longer times. From interfacial rheological experiments it had been expected that longer adsorption times lead to thicker films [138]. This hypothesis could not be confirmed by the conducted SFM experiments.

In the experiments, where the film was transferred either by surface lowering or by the Langmuir-Blodgett technique, the wafer was immersed in the bulk solution during the whole time of the adsorption process of the surfactant onto the air/water interface. Therefore a control experiment was performed on a hydrophilic silicon substrate, which was immersed in the solution during the adsorption process of 16 hours, but the film from the interface was not transferred (Figure 6.5 C and D). In this control experiment I found that PGE molecules readily adsorbed onto the hydrophilic substrate and partially covered the silicon substrate (65%), as seen by the phase contrast image. The thickness of this dried film was determined to be

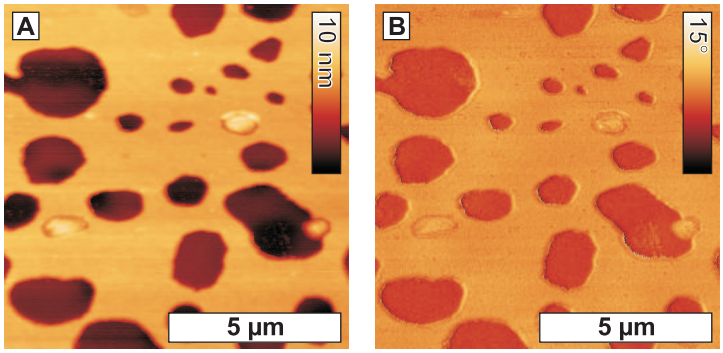

Figure 6.7: SFM topography (A) and phase (B) images of a film transferred by the Langmuir-Schaefer-like technique after an adsorption time of 16 hours.

0.7 ± 0.1 nm. This thickness value is in agreement with thickness measurements from the transferred Gibbs adsorption layers.

6.2.3 Langmuir-Schaefer like transfer

For the Langmuir-Schaefer-like film transfers the silicon wafers used were hydrophobized with octadecyltrichlorosilane prior to their use. For these experiments, 110 ml of a 0.01 wt% PGE solution were poured into the clean Langmuir trough and the surfactant was left to adsorb onto the air/water interface. The adsorption times were varied between 1 and 16 hours. The interfacial film was transferred onto the hydrophobic silicon wafer by gently touching the air/water interface with the silicon wafer and retracting it immediately. The drop of bulk solution retained on the silicon wafer surface was carefully removed using a paper towel. The remaining thin solution film was left to dry with the wafer lying in a horizontal position. This transfer method provides the advantage that the silicon wafer is not immersed in the bulk solution during the adsorption process. The dry films were investigated employing SFM (Figure 6.7). The average film thickness determined from mediated height profiles is 4.3 ± 0.5 nm. This corresponds to the thickness estimated for a dry PGE bilayer. The presence of the holes in the film, as well as the pattern in which they are present cannot be explained. They could be an artifact from the film transfer or the drying process. The formation of a bilayer on the substrate under these transfer and drying conditions is reasonable, because it suggests that the PGE molecules are assembled with the hydrophobic tails facing the hydrophobic silicon wafer and air, while the hydrophilic head groups are facing each other. The existence of a single PGE bilayer at the air/water interface is however unlikely, as this would require the hydrophobic PGE tails to face the water subphase, which is energetically unfavorable. It is therefore more reasonable, that the organization

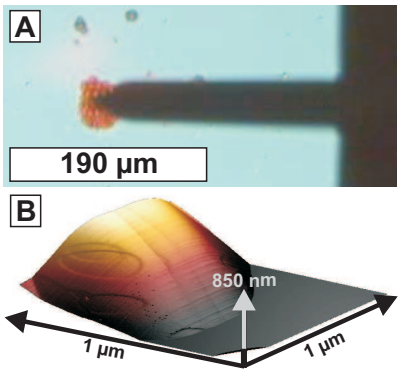

Figure 6.8: Multilamellar aggregates adhering to silicon wafers. (A) Light microscopy image of spherical aggregates visible on samples prepared by surface lowering. (B) Three-dimensional SFM image combining height and phase data measured on one of the spherical aggregates mentioned in A).

of the PGE molecules in the transferred film is not identical with the situation at the air/water interface. There are two possible scenarios for the reorganization: (i) The PGE molecules form a monolayer at the air/water interface. During the drying process a reorganization of the PGE molecules is possible, because part of the PGE bulk solution covers the silicon wafer after the film transfer. Therefore PGE molecules can diffuse from the bulk solution onto the monolayer during the drying process to finally result in a dried PGE bilayer. (ii) It has been shown for lipids, that a Langmuir-Blodgett or Langmuir-Schaefer transfer of a film with the hydrophilic part of the molecules facing air is not possible. The top layer simply rips off when moving the substrate from the bulk solution through the surface, resulting in a film with hydrophobic moieties facing air [27, 38]. This could also be true for a PGE triple layer at the air/water interface resulting in a bilayer on the silicon wafer, with the third layer remaining on the air/water interface of the Langmuir trough.

6.3 Multilamellar aggregates

On the Gibbs adsorption layer samples transferred by surface lowering, I found spherical objects by optical microscopy (Figure 6.8 A). Such aggregates were never found on films transferred by other methods. These structures had either been present at the air/water interface of the Langmuir trough or in the bulk solution, and probably adhered to the wafer during the surface lowering and subsequent drying process. The objects are most likely large vesicles, which are known to be present in the micrometer size range in PGE solutions [154]. An alternative explanation is that the objects are small air bubbles dispersed in the solution and covered with PGE,

as I did not degas the solutions prior to the experiments. The reason for omitting a degassing step was twofold. Preliminary experiments had shown that a standard degassing step is not sufficient to remove those small air bubble contained in 1 wt% PGE solutions. Furthermore, the pouring of 0.01 wt% solutions into the Langmuir trough would have introduced new air bubbles, thereby rendering the degassing step redundant. Nevertheless, in both cases, vesicle or air bubble, a full collapse of the structures would be expected upon drying. The retaining of a three dimensional shape of these objects even in the dried state could be argued to be caused by a small interior volume, which is sparsely effected by the drying process. SFM imaging on the dried objects was possible and revealed a multilamellar structure with step heights of 3 nm, 9 nm, 12 nm and 15 nm, indicating multiple bilayers (Figure 6.8 B). Independent of the nature of these spherical objects, they are of major interest in the current project. In case of the aggregates being vesicles, this experiment would confirm their multilamellar nature [26]. On the other hand, if they were bubbles, the experiment would show that bubbles are indeed covered by more than a single monolayer of PGE. A distinction between vesicles and air bubbles in this dried state seemed not feasible. The spherical object being either a vesicle or an air bubble would in both scenarios be covered with PGE multilayers. A vesicle would be covered with an even number of layers, while the interface of an air bubble would be covered by an uneven number, due to the hydrophilic and hydrophobic medium incorporated inside the structure, respectively. A clear discrimination between either case was not yet possible.

6.4 Conclusion

Different techniques of producing and transferring polyglycerol ester films, were studied by SFM, investigated and compared. From the results of the different measurements it can be concluded that the combination of these techniques is useful to get a better understanding of non-equilibrium surfactant structures at the air/water interface. However all film preparation methods for SFM measurements can be associated with potential artifacts owing to the transfer, drying process or interaction with a solid substrate. In the case of Gibbs adsorption layers an additional inconvenience is given through the presence of very small bubbles, as they cannot easily be distinguished from vesicles, once the film is dried. Nevertheless the combination of all these different film preparation methods allowed us to identify common features in the films and thereby reduce the problem of misinterpretation due to artifacts. SFM measurements in liquid have shown, that PGE vesicles are involved in the adsorption process to a hydrophilic/hydrophobic interface. It is however not known, in which way the hydrophobic graphite substrate influences the adsorption process and the structures formed at the interface, compared to air. All studies have shown,

that the air/water interface is covered with at least one PGE monolayer. Adsorption studies in liquid as well as samples prepared by surface lowering and LS transfer even suggest the formation of multi layers, as has already been proposed from rheologic experiments by Duerr-Auster et al. [27]. The major drawback of the experiments discussed so far is that neither of the films resembles a real foam film. The surfaces investigated were always planar, while a bubble film is curved. Also, in a foam bubble, two interfacial films are present in close proximity stabilizing a thin layer of bulk solution, while here one individual interfacial film was examined. All of these effects may influence the PGE molecule density and organization at the interface.

6.5 Experimental details

Materials

The polyglycerol ester used was the commercially available, food-grade surfactant PGE 55. It was purchased from Danisco (Braband, Denmark) and used without any further purification. It is not a pure substance, but contains predominantly a mixture of esters of di-, tri- and tetraglycerol with the degree of esterification being unknown [26]. The average molecular weight is $M_W(PGE) = 770$ g/mol [127], and the product contains about 1.4 wt% free fatty acids, which are residues from the production process [26]. The water used in all the trials was purified with a Millipore purification unit (Millipore) and had a resistivity of 18.2 MΩ cm. A PGE solution with a concentration of 1 wt% has a native pH of 9 [150]. Two types of solid supports were used to study polyglycerol ester films. For all trials, where films were transferred from the air/water interface onto a wafer, air-dried Si wafers (epitaxial and polished, Siltronic AG) were used. The wafers were rinsed with Milli-Q water and then plasma cleaned (Plasma Cleaner/Sterilizer PDC-002, 200W, Harrick Scientific Corp.) with Ar for 5 min before use. For experiments with hydrophobic wafers, following the cleaning procedure the wafers were placed into a petri dish and a few drops ($\approx$ 0.25 ml) of octadecyltrichlorosilane (ABCR GmbH & Co KG) were added to the petri dish, without being in direct contact with the wafers. The petri dish was covered with a lid and the octadecyltrichlorosilane was left to evaporate and thereby render the wafers hydrophobic over night. For the measurements performed in liquid, HOPG platelets (SPI-2 grade, SPI supplies) were used as substrate.

Solution preparation

The PGE solutions were prepared (adapted from [26]) by weighing the respective amounts of surfactant and Milli-Q water into clean glass flasks. These solutions were

heated to 80°C in a water bath and then kept at this temperature for 10 min. During the whole heating process the solutions were stirred using a magnetic stirrer. The solutions were then quiescently cooled in an ice water bath. Before any experiments the solutions were left to equilibrate at room temperature for at least 12 h, but no longer than 40 h. An appropriate equilibration time after solution preparation and prior to further experiments should be respected, as solutions investigated directly after preparation showed an different behavior compared to older solutions in calorimetric measurements [26]. Also over the course of several weeks, dilute solutions show a phase separation [26], indicating their non-equilibrium state.

Scanning force microscopy

The experiments were performed on a Dimension 3100 (Veeco Digital Instruments) and a Multi Mode (Veeco Digital Instruments) microscope. All SFM images were obtained in tapping mode, resulting in SFM height and phase images. In order to obtain the best topography imaging conditions I used the lowest possible force, which is characterized by a setpoint amplitude very close to the free vibrational amplitude. This helps to reduce artifacts while scanning, with possible artifacts being for example the removal of material, as well as the deformation or rupture of vesicles [155]. The cantilevers used were Olympus Micro Cantilevers AC 240 (Atomic Force F&E GmbH, Germany), which have a nominal resonance frequency of 70 kHz and a spring constant of 2 N/m. Their backside is coated with Al. All SFM images were flattened and analyzed employing Gwyddion Software (www.gwyddion.net).

Planar air/water interfacial films were prepared using a Langmuir trough (Langmuir-Trough RK1, Riegler und Kirstein GmbH) equipped with a subphase exchanging system. Before and after every measurement the trough was cleaned with chloroform, ethanol, and finally with Milli-Q water. Langmuir monolayers were prepared by spreading 20 µL of a solution of PGE in dichloromethane ($c = 1$ mg/mL) onto the clean Milli-Q water subphase using a microliter syringe. The film was left for solvent evaporation for 15 min before measurements were started. For the Gibbs adsorption film trials, 110 mL of a 0.01 wt% PGE solution were poured into the clean trough. The surface pressure was calibrated employing arachidic acid (Sigma Aldrich) as a reference substance. For both Langmuir monolayers and Gibbs adsorption films the surface pressure was recorded over the full course of the experiment. The trough was kept at 20°C during all measurements. The films were transferred from the Langmuir trough onto the substrate by surface lowering. After pouring the solution into the Langmuir trough (or the pure water, in the case of Langmuir monolayers), the wafer was immersed into it and placed onto a custom made sample holder. This sample holder kept the wafer at an inclination of 6°. The surface pressure was set to zero and the surfactant was left to adsorb onto the air/water interface. After different

adsorption times (adsorption times were varied between 1 and 16 h) the surfactant film at the air/water interface was transferred to the wafer by surface lowering. This was achieved by pumping the surfactant bulk solution out of the Langmuir trough employing the subphase exchange system with a speed of approximately 10 mL/min. The inclination of the wafer helps in draining off the water but retaining the surfactant film. The wafer was then left to dry on the sample holder, before it was examined by scanning force microscopy. All SFM pictures were recorded from the part of the wafer being at a higher position on the sample holder to reduce artifacts arising from the drying process. In order to perform SFM measurements in liquid, HOPG platelets were freshly cleaved and then immersed into a 1 wt% PGE solution, where they were left for 3-5 days. Following this adsorption time the platelet was removed from the solution and a drop of Milli-Q water was put onto the wafer to prevent drying of the film at any time. This partial dilution of solution by pure water was necessary to reduce scattering of the laser light, which is required for SFM. To transfer films from bubbles, 1 wt% PGE solutions were poured into a petri dish. Using a disposable glass Pasteur pipette, air was bubbled into the solution. This was done for a few seconds with some of the bubbles immediately coalescing. After the bubbling was stopped the foam films were left to drain for 6 min $\pm$ 1 min. A hydrophobized wafer was then gently brought into contact with the film of a single bubble. After removing the wafer it was left to dry in a horizontal position. This was done with 1 wt% PGE solutions at native pH (pH 9), as well as with solutions, where the pH was adjusted to pH 3 prior to the bubble production.

7 Foam films via bubble film transfer

Due to the model character of the film preparation methods described in Chapter 6, they can only give hints for the understanding of the structural assembly of PGE foams. Therefore, a new method to transfer a true foam film from the skin of a single bubble onto a hydrophobic substrate was developed and will be introduced in the following Chapter. The transfer procedure is based on a method proposed by Benattar et al. for Newton Black films, which are surfactant films thinner than 5 nm [156–158]. He and his coworkers were able to show that a free standing Newton Black film can be transferred onto a hydrophobic substrate by simply touching the film with the substrate. The integrity of the film could be validated by X-ray reflectivity and SFM measurements, which confirmed the transfer of an intact film [157]. The idea was to transfer the foam film of a single bubble in a similar manner by approaching it with a hydrophobic substrate. This allows the investigation of structures present at the air/water interfaces of the foam film and in between. In order to characterize the film quality and to ensure the film integrity, a high speed camera was used to follow the bubble rupture during film transfer. The transferred films were investigated with SFM in order to gain a deeper insight into the interfacial structure of PGE films. Finally, the transfer procedure was applied to other surfactant solutions in order to investigate the general applicability of the bubble transfer. The experiments were conducted within the framework of a cooperation with xxx and xxx from xxx.

7.1 Transfer of PGE bubble films

Single PGE foam bubbles were prepared by sparging air through a 1 wt% PGE solution using a pipette and thereby creating millimeter sized bubbles. The produced bubbles were left to drain for 6 min before the bubble surface was touched with a hydrophobic substrate to transfer the bubble skin (Figure 7.1 E and F). The films were left to drain prior to the transfer in order to minimize the transfer of bulk solution entrapped between the two surface films. A time of 6 min was chosen as the best compromise between achieving a high drainage and the maximum bubble

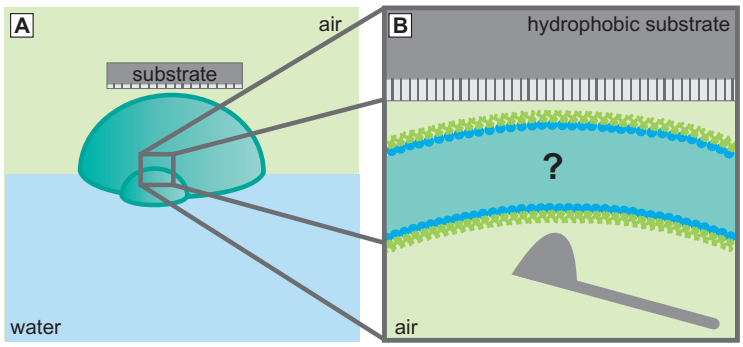

Figure 7.1: (A) Basic concept of the film transfer of a bubble surface onto a hydrophobic substrate. (B) Close-up of the transfer according to transfer method (A). As can be seen in (A), the transferred bubble skin is made up of two air/water interfacial films and the material contained in between them. With the technique applied in the current work to transfer such a bubble skin, the PGE film facing the atmosphere adhered to the substrate and therefore the layer which assembled on the inside of the bubble was investigated by SFM.

stability. As the bubble film production and transfer time are short as compared to the other film preparation procedures, solutions at both native and adjusted pH could be studied. The structure of PGE films at pH 3 is of interest, because it was found that acidic PGE solutions exhibit an increased foamability but a decreased foam stability. An effect of the pH variation on the PGE foam properties was not expected, because PGE itself is a non-ionic surfactant. However, fatty acid soaps from the production process are incroporated in the samples [26], which can be effected by the pH variation [150].

7.2 High speed camera investigation - PGE

In order to investigate the quality of the new established film transfer method from a bubble onto a hydrophobic substrate a high speed camera was used. These experiments were performed with PGE at pH 9 and pH 3 as well as with other detergents, namely SDS and CTAB for comparison. The substrate was continuously lowered towards the bubble, which was produced as described in Section 7.1, until the bubble film adhered to the substrate. This initial adherence was taken as a starting point for further analysis. For the PGE solution at pH 9 the bubble film started to rupture after 34.8 ms (Figure 7.2 B). Initially a small hole was visible in the bubble skin (indicated by the arrow in Figure 7.2 C), which increased in size within 1.3 ms (edges indicated by the dashed arrows in Figure 7.2 D). The bubble rupture continued from this initial point. The bubble film broke away from the substrate

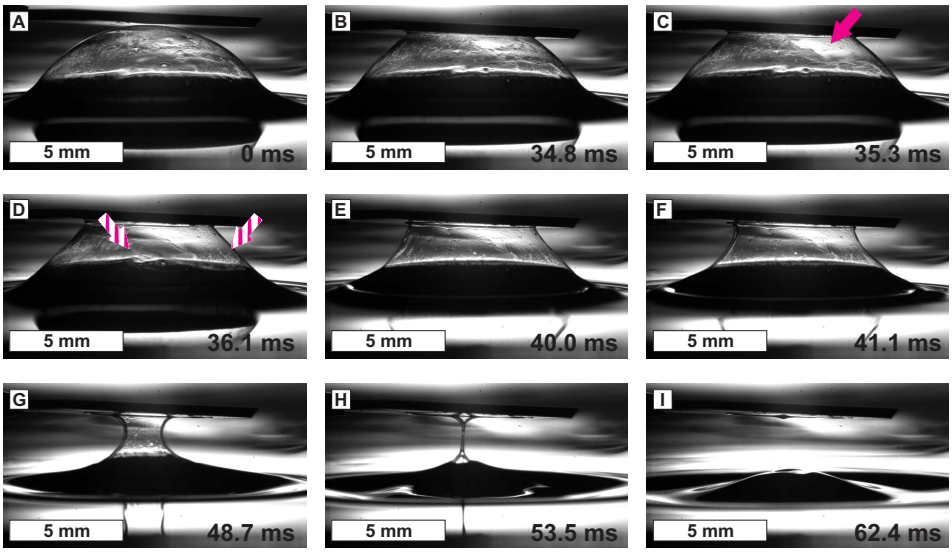

Figure 7.2: Bubble surface transfer at pH 9. Series of images recorded with a high speed camera while transferring a PGE film from a bubble onto a hydrophobic substrate at pH 9. Arrows mark the initial rupture point on the bubble.

along the contact area of bubble and substrate reminiscent of a curtain being ripped off a ceiling. This process advanced without splattering of the film or altering the adsorbed film visibly. The rupture process was finished within 30 ms (Figure 7.2 I). This procedure was found to be characteristic for PGE films at pH 9.

Additional experiments have been performed with PGE solutions at pH 3. Here, the same basic rupture principle was found, but the rupture process at pH 3 took more than 150 ms and was thus 5 times slower than at the native pH (Figure **??**). Moreover the film only ruptured completely after the substrate had been pulled away from the interface. This is a result of the altered film morphology at pH 3. Again, the procedure was found to be characteristic for this kind of solution and bubble.

From these experiments with the high speed camera it can be concluded that the skin of a PGE foam bubble is indeed transferred as a complete film onto hydrophobic substrates, with the films presumably representing the preserved PGE film structure inside the bubble film.

7.3 SFM investigation of bubble films

The films transferred via bubble transfer were left to dry under ambient conditions and afterwards investigated employing SFM. For interpretation of the SFM

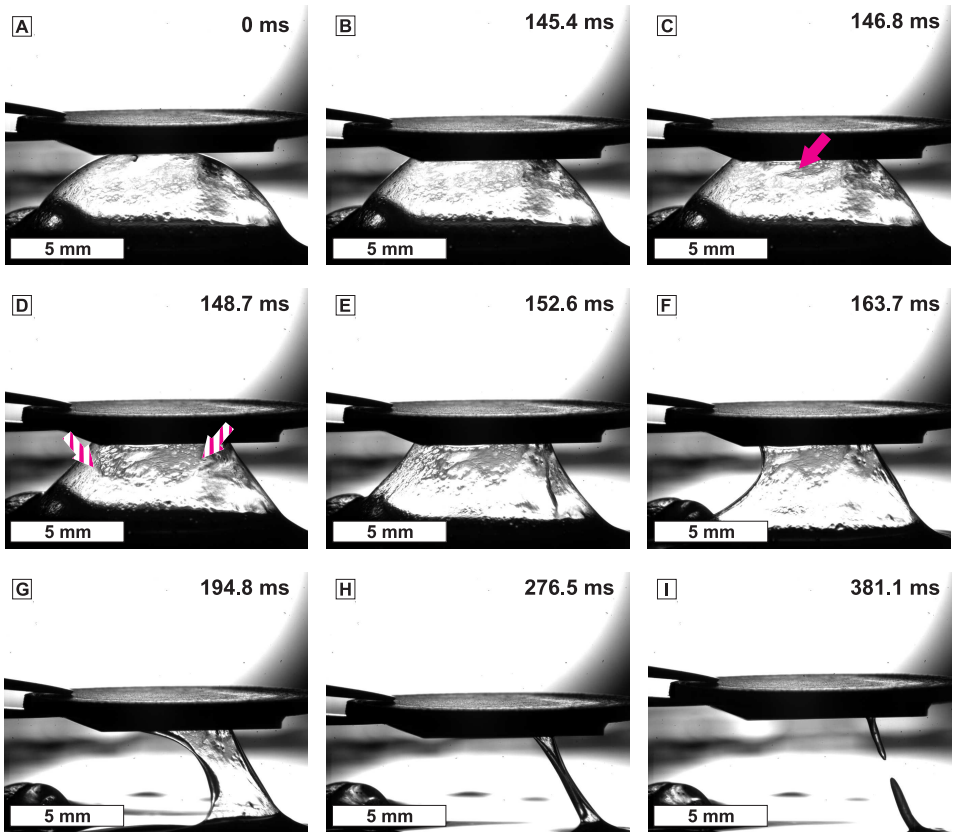

Figure 7.3: Bubble surface transfer at pH 9. Series of images recorded with a high-speed camera while transferring a PGE film from a bubble onto a hydrophobic substrate at pH 3. Arrows mark the initial rupture point on the bubble.

images, it has to be taken into account that this method results in the transfer of molecules situated at both water/air interfaces of the bubble skin (Figure 7.1 B). Furthermore, any material possibly contained in between the two PGE solution/air interfaces (vesicles, lamellar structures) would be present on the substrate as well. Investigating films formed at pH 9 by SFM revealed a network-like structure in the film transferred via the bubble method (Figure 7.4 A and B). The ridges are 25-30 nm high and are surrounded by areas of lower levels. In these lower areas several layers can be found (see arrow in Figure 7.4 A). The average thickness of any given single layer has been determined from mediated profiles to be 4.5 ± 1.7 nm. Statistics over the layer thicknesses revealed that step heights of around 3 nm, 6 nm and 13 nm appear frequently (Figure 7.4 E). In addition I also found positions on the sample without network structuring (Figure 7.4 C and D). Here again different height levels with increments of 3 nm, 6 nm and 13 nm were found. Since I have estimated the thickness of a dried monolayer of PGE molecules by the Langmuir

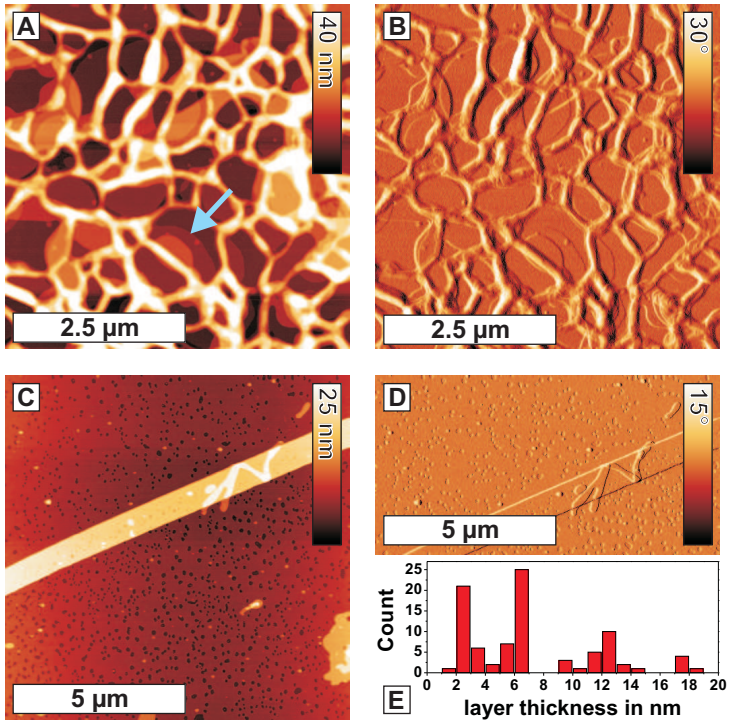

Figure 7.4: SFM height (A) and phase (B) image of a film transferred from a PGE bubble at pH 9. The network-like structure visible in A and B is most likely an artifact introduced by the drying of the film. SFM height (C) and phase (D) image measured at a different position. (E) Statistics over the determined layer thicknesses.

monolayer method to be around 1.2 nm, I attribute the step heights seen here to the formation of bilayers being approximately 3 nm in height. The thicker films originate from stacking of individual bilayers on top of each other. From the general composition of a foam film, at least two monolayers, one from each air/water interface, were expected. Any additional layers hint to the formation of multilayers at the air/water interfaces or to lamellar structures which have been incorporated between the interfacial films from the bulk solution. The network-like structure is most likely caused by drying of the film after its transfer. During the last stages of drying the liquid film becomes instable, because the contact angle of water is significantly above zero due to the hydrophobic parts of PGE and the hydrophobic substrate. Similar dewetting structures have also been observed with thin polymer layers [159–161].

Films that were obtained by bubble transfer at pH 3 showed a much rougher surface with a peak to peak roughness of 38 ± 13 nm (Figure 7.5), compared to 7.6 ± 2.8

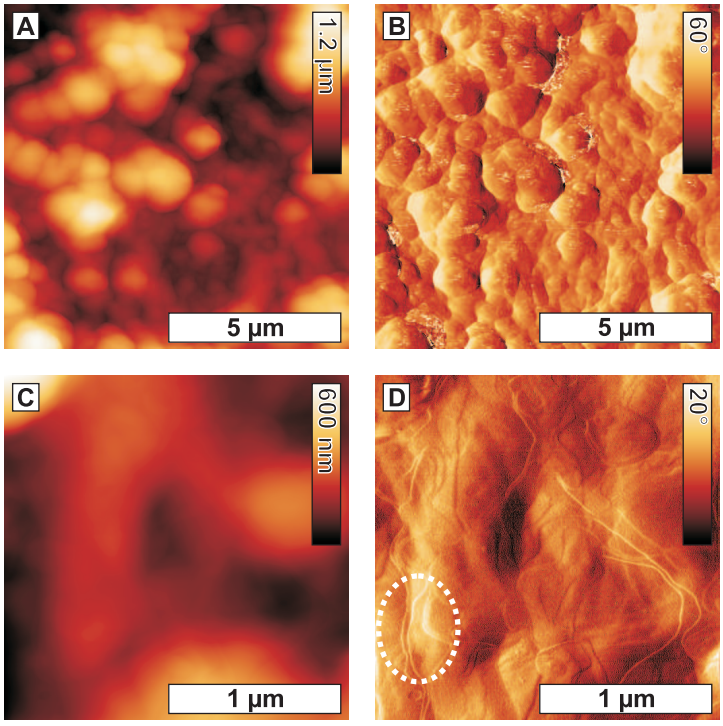

Figure 7.5: SFM height (A) and phase (B) image of a film transferred from a PGE bubble at pH 3. SFM height (C) and phase (D) image measured at a different position. The dashed oval marks clearly visible layers in the phase image.

nm for pH 9 (Figure 7.4). The films at pH 3 consisted of many large spherical objects having diameters ranging from 0.4 µm to 1.4 µm. Duerr-Auster et al. [150] reported that in scanning electron micrographs the vesicles known to be present in PGE bulk solutions were seen to be deformed and partially broken under these acidic conditions. This deformation was suspected to be caused by osmotic stress applied to the vesicles upon addition of the acid for pH modification. Nevertheless the spherical objects present in the films (Figure 7.5) could be such, albeit distorted, vesicles entrapped in the interior of the bubble skin as outlined in Figure 7.1 B. Due to the large height differences it is very difficult to identify individual layers in the topographic images, but the layering is clearly visible from the phase contrast images (see dashed oval in Figure 7.5 D). This would indicate that after the film transfer the interfacial film exposed to air dried onto the underlying vesicles and other structures that had been entrapped in the interior of the film. The average layer thickness of these interfacial multilamellar films was determined to be 4.5 ± 1.6 nm, which is thicker than expected for a dry PGE bilayer, but similar to the average value obtained for films at pH 9. The results from these bubble transfers suggest that the multilayer structuring at the interface, as well as the bilayer thickness of

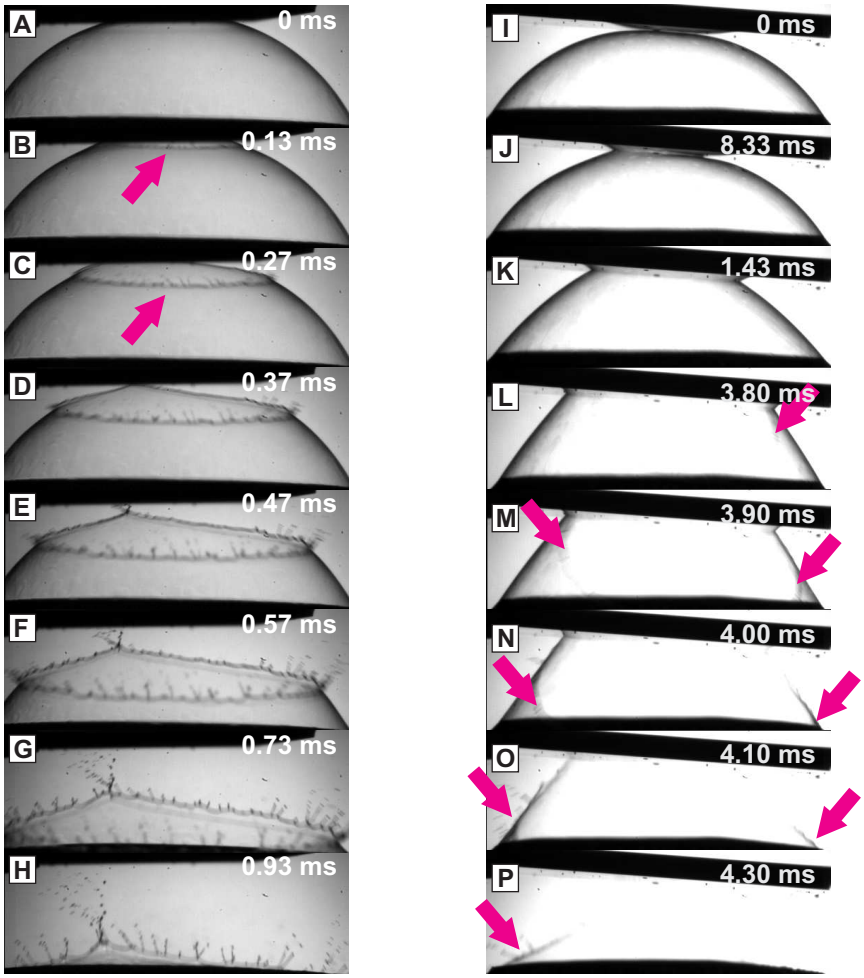

Figure 7.6: Image series from high speed camera recordings of bubble film transfer from SDS (A-H) and CTAB (I-P) bubbles. Pink arrows mark the edges of bubble rupture.

these multilayers, are not significantly dependent on the pH. Furthermore, if the network-like structure seen at pH 9 really was caused by the drying, the absence of this structure at pH 3 could possibly be explained by the increased thickness of the films, which leads to a much slower drying process inhibiting the formation of such a network-like structure.

7.4 High speed camera investigation - other surfactants

In a second set of experiments, the applicability of this kind of bubble film transfer was tested for bubble films in general by investigating other surfactants. The substances of interest were the anionic surfactant sodium dodecyl sulfate (SDS) and the cationic surfactant cetyltrimethylammonium bromide (CTAB)(Figure 7.6). Foam bubbles of both surfactants were prepared independent from each other and the transfer of the bubble film was again investigated with a high speed camera.

The rupture process for both surfactants was very fast compared to the film rupture of PGE at either pH. At a concentration of $c = 32$ mM for SDS the rupture process took only 2 ms (Figure 7.6 A-H). The rupture process for CTAB at a concentration of $c = 4$ mM was even twice as fast and took only 1 ms (Figure 7.6 I-P). For both molecules, the concentration was chosen to equal 4 times the critical micelle concentration (cmc) of the respective surfactant, to give comparable results. In addition to the faster rupture of the SDS and CTAB surfactant films, it was also found that the rupture process was less defined than for PGE. The example of the CTAB bubble rupture (Figure 7.6 I-P) shows that the film rips off the substrate almost simultaneously at any position along the contact line. The solution spatters, which can cause modification of the transferred film. This spattering was not observed for PGE, because PGE solutions are more viscous. The spattering and unpredictable rupture process were also found for SDS. The rupture processes for both CTAB and SDS were not found to be characteristic. Repeated experiments have shown the curtain like rupture along the contact line similar to the PGE film rupture but also other scenarios, like concomitant hole formation in the bubble film at several positions.

7.5 Conclusion

A technique to transfer and investigate complete bubble films was developed and investigated. The proposed approach marks a new method of film preparation for SFM measurements. The main appeal lies in the films being true foam films, where the bubbles have been produced by a simplified foaming process. SFM characterization of PGE films transferred with this method showed thick films, even when considering the fact that they were made up of two air/water interfacial films. Their structure was found to be dependent on the pH of the PGE solution. At both pH values an interfacial structure consisting of multiple PGE layers was seen. These multilayers were superimposed by a network-like structure at pH 9. Even though these network-like structures might be caused by the drying process, it is worthwhile noting that this kind of structures were not detected in any of the other film

preparation and transfer techniques, where the films were dried as well (Chapter 6). An additional point of interest was the role of the vesicles. In both alkaline and acidic conditions they are adsorbing onto the interface, where they unfold and form a multilamellar structure. In addition to this, at pH 3 any remaining vesicles are aggregating into larger assemblies entrapped in the interior of the films. Due to their size these assemblies cannot drain out of the film and are thereby thought to provide a steric stabilization of the foam film. Application of the bubble film transfer technique to other surfactants has shown, that the method is not generally applicable to every surfactant solution. Accordingly, the rupture process of bubble films of new substances needs to be characterized carefully before interpreting the SFM results.

7.6 Experimental details

Solution preparation

PGE solutions were prepared as discussed in Section 6.5. For the experiments performed at pH 3, 1 M HCl (Normapur, VWR) was used for the pH adjustment. SDS and CTAB solution were prepared in MilliQ water by stirring until the solid was dissolved.

Bubble film transfers using a high-speed camera

Bubbles were prepared and films transferred as described before. Videos of the transfer process were recorded using a high speed camera (Photron, Fastcam SA-1, 4-6 $\times$ magnification) with backlighting and a recording rate of 5400 frames per second (fps) at a resolution of 1000 $\times$ 1000 pixels.

Scanning force microscopy

SFM experiments were performed as described in Section 6.5.

8 Concluding remarks and outlook

In my thesis, I could demonstrate that amphiphilic molecules can form a variety of different structures at the air/water interface. The transfer of interfacial films onto substrates and their investigation employing SFM and complementary techniques have proven to be valuable characterization methods in this context. I investigated diverse surface active materials under different aspects, all finally aiming at the elucidation of structures formed at the air/water interface and after film transfer. Furthermore, I proposed models attempting to analyze and explain the driving forces of the structure formation.

Semifluorinated alkanes where found to hierarchically self-assemble into circular surface micelles, which are composed of smaller muffin shaped subunits. Introduction of an aromatic core induces a shape transformation of the surface micelles from circular into elongated ones. This behavior can be attributed to additional molecular interactions like π-stacking induced by the aromatic core. The chemical coupling of two of these modified SFA molecules lead to the formation of even longer fiber-like micelles rather than elongated branched ones. Obviously, the introduction of aromatic cores into the molecules is accompanied by a directionality of the self-assembly. The results demonstrate the major influence of the chemical structure on the morphology of the self-assemblies. From this point of view, it is exceptionally interesting to investigate SFA molecules with new chemical structures in order to identify other structural motifs governing the self-assembling process. As an example, a F11H1-core-H12 molecule with a modified aromatic core is available: The oxygen bridges connecting the aromatic core to the fluorocarbon and hydrocarbon blocks as well as the bromine residues at the aromatic core were removed and thus reduce the intermolecular interactions to three relatively simple components: the fluorocarbon chain, the hydrocarbon chain and the aromatic core without any additional moieties. Differential scanning calorimetry and wide angle X-ray scattering experiments conducted by the group of George Floudas (unpublished data) revealed a significant difference in the phase behavior of both, the F11H1-core-H12 and the new plain core molecules. These results imply that the oxygen and bromine groups have a major influence on the phase behavior and structure formation of the respective molecules. The investigation of the self-assembly morphology of the novel plain core molecules is thus of major interest in order to identify the effect of single functional groups on the structure of the supramolecular assembly. Of further interest

is the temperature dependence of the self-assembly structure, because bulk experiments on semifluorinated alkane molecules have revealed several phase transitions, which may influence the shape of the formed aggregates. The expected findings can be of use for the design of new materials for tailored self-assembling processes. The molecules themselves can find application in the fabrication of nanostructured surfaces or nanofibres. Here the semifluorinated alkanes might find potential application as nanostructured hydrophobic coatings.

The DNA hybrid material dU11 was found to form semi stable films at the air/water interface, which relax by formation of multiple layers stacked on top of each other. When transferred onto solid substrates, these layers can be removed individually by scanning with the SFM tip in tapping mode. This observation is in contrast to the general assumption that SFM is a non-intrusive measurement technique and demonstrates the importance of thorough adjustment of the experimental parameters and critical SFM image interpretation. However, the combination of multilayer formation at the interface on the one hand and directed removal of individual layers on the other hand opens the possibility to engineer the surface by an inverse dip-pen lithography step. This paves a new way for the preparation of functional thin films with tunable local organization of the individual layers. In this specific example, micro- and nanostructured surfaces with the potential to perform molecular recognition experiments can be fabricated. Further processing by hybridization enables to facilitate a multitude of new functionalities like the tethering of lipid vesicles. One possibility to improve the dU11 film stability could be to attach longer hydrophobic tails to the terminal DNA bases, which decrease the solubility of the DNA hybrid material in water. Stable DNA hybrid material films at the air/water interface could be used as platforms for the directed movement of molecular machines like the DNA walker proposed by Shin et al. and Yin et al. in two dimensions along the interface. The second DNA hybrid material DNA-*b*-PPO, which I investigated, was found to form not only monolayers but also aggregates at the air/water interface. I discussed potential reasons for this effect and found that the ionic strength of the subphase has a major influence on the relative head group volume. In my experiments I could also demonstrate the potential to detect molecular changes of molecules at the air/water interface by time-dependent isotherm recording. The Langmuir trough is therefore a versatile and sensitive tool which can be employed to monitor molecular recognition events. Precondition is, that the to be detected component itself is negligibly surface active in order to obtain clear and ambiguous results.

I also investigated foams, which represent complex systems of films from amphiphilic molecules at air/water interfaces. I evaluated several transfer methods and different model systems mimicking real foams in order to characterize the molecular structure of the surfactant PGE at the air/water interface. I found that SFM is a valuable technique for the characterization of these model systems, although artifacts from the different transfer techniques always have to be considered for interpretation of

the results. PGE was found to form multiple surfactant layers at the air/water interface to stabilize the foam. Adsorption experiments additionally indicated the involvement of vesicles in the adsorption process of PGE. In the context of PGE foam film characterization, I developed and investigated a new film transfer method, the so called bubble film transfer. I could show that the skin of a real PGE foam bubble can be intactly transferred onto a substrate and studied employing SFM. My investigations approved, that PGE molecules form more than one molecular layer at the air/water interface, confirming the results obtained from other model systems. The study of bubbles from other surfactants, namely SDS and CTAB, revealed, that the new bubble film transfer cannot ultimately be used for every surfactant bubble, because the rupture process varied significantly with repeated experiments. Nevertheless, SDS and CTAB are surfactants, but they are in contrast to PGE not known for their special foaming and foam stabilization properties. PGE forms exceptionally stable foams and the stabilization mechanism is therefore especially interesting. It is thus likely that other good foaming agents like e.g. the protein β-lactoglobulin can be investigated by employing this technique, because they innately form stable foam bubbles. A potential application of the bubble film transfer is to investigate the influence of the foaming process on the resulting film structures. This influence is often neglected although for example PGE is known to form more stable foams when prepared by dynamically enhanced membrane foaming [162], a membrane based method which produces small foam bubbles, as compared to foams prepared with a rotor/stator mixer [163], where bigger foam bubbles are prepared by shearing of two cylinders. It is not clear, how the molecular structure of the foaming agent at the air/water interface and thus the stability of the foam film is influenced by the different foaming processes. The bubble film transfer opens up new perspectives for the investigation of this phenomenon.

Bibliography

[1] G. G. Roberts. *Langmuir-Blodgett Films.* Contemporary Physics, **25**, no. 2 (1984) 109–128.

[2] O. Oliveira Jr. *Langmuir-Blodgett films-properties and possible applications.* Brazilian Journal of Physics, **22**, no. 2 (1992) 60–69.

[3] B. Franklin. Phil. Trans. R. Soc., **64** (1774) 445.

[4] L. Rayleigh. Proc. Soc., **47** (1890) 364.

[5] A. Pockels. Nature, **43** (1891) 437.

[6] I. Langmuir. *The constitution and fundamental properties of solids and liquids. II Liquids.* Journal of the American Chemical Society, **39**, no. 9 (1917) 1848–1906.

[7] K. B. Blodgett. *Monomolecular Films of Fatty Acids on Glass.* Journal of the American Chemical Society, **56**, no. 2 (1934) 495.

[8] E. K. Rideal and J. H. Schulman. *Reactions with monolayers and their biological analogies.* Nature, **144**, no. 3637 (1939) 100–102.

[9] W. D. Harkins and E. Boyd. *The States of Monolayers.* The Journal of Physical Chemistry, **45**, no. 1 (1941) 20–43.

[10] A. Barraud, C. Rosilio, and A. Ruaudel-Teixier. *Polymerized monomolecular layers: A new class of ultrathin resins for microlithography.* Thin Solid Films, **68**, no. 1 (1980) 91–98.

[11] G. Roberts. *Transducer and other applications of Langmuir-Blodgett films.* Sensors and Actuators, **4**, no. 0 (1983) 131–145.

[12] R. M. Weis and H. M. McConnell. *Two-dimensional chiral crystals of phospholipid.* Nature, **310**, no. 5972 (1984) 47–49.

[13] S. Henon and J. Meunier. *Microscope at the Brewster angle: Direct observation of first-order phase transitions in monolayers.* Review of Scientific Instruments, **62**, no. 4 (1991) 936–939.

[14] C. Helm, H. Möhwald, K. Kjaer, and J. Als-Nielsen. *Phospholipid monolayers between fluid and solid states.* Biophysical Journal, **52**, no. 3 (1987) 381–390.

[15] O. Oliveira Jr. and C. Bonardi. *The Surface Potential of Langmuir Monolayers Revisited.* Langmuir, **13**, no. 22 (1997) 5920–5924.

[16] J. Zasadzinski, R. Viswanathan, L. Madsen, J. Garnaes, and D. Schwartz. *Langmuir-Blodgett films.* Science, **263**, no. 5154 (1994) 1726–1733.

[17] G. M. Whitesides, J. P. Mathias, and C. T. Seto. *Molecular Self-Assembly and Nanochemistry - A Chemical Strategy for the Synthesis of Nanostructures.* Science, **254**, no. 5036 (1991) 1312–1319.

[18] G. M. Whitesides and M. Boncheva. *Beyond molecules: Self-assembly of mesoscopic and macroscopic components.* Proceedings of the National Academy of Sciences of the United States of America, **99**, no. 8 (2002) 4769–4774.

[19] J. N. Israelachvili, D. J. Mitchell, and B. W. Ninham. *Theory of Self-Assembly of Hydrocarbon Amphiphiles into Micelles and Bilayers.* Journal of the Chemical Society. Faraday transactions II, **72** (1976) 1525–1568.

[20] J. N. Israelachvili, D. Mitchell, and B. Ninham. *Theory of Self-Assembly of Lipid Bilayers and Vesicles.* Biochimica Et Biophysica Acta, **470**, no. 2 (1977) 185–201.

[21] N. Gershfeld and K. Tajima. *Energetics of Transition Between Lecithin Monolayers and Bilayers.* Journal of Colloid and Interface Science, **59**, no. 3 (1977) 597–604.

[22] G. Zhang, M. Maaloum, P. Muller, N. Benoit, and M. P. Krafft. *Surface micelles of semifluorinated alkanes in Langmuir-Blodgett monolayers.* Phys. Chem. Chem. Phys., **6**, no. 7 (2004) 1566–1569.

[23] G. Zhang, P. Marie, M. Maaloum, P. Muller, N. Benoit, and M. P. Krafft. *Occurrence, Shape, and Dimensions of Large Surface Hemimicelles Made of Semifluorinated Alkanes. Elongated versus Circular Hemimicelles. Pit- and Tip-Centered Hemimicelles.* J. Am. Chem. Soc., **127**, no. 29 (2005) 10412–10419.

[24] A. E. Abed, M. Faurez, E. Pouzet, and O. Abillon. *Experimental evidence for an original two-dimensional phase structure: An antiparallel semifluorinated monolayer at the air-water interface.* Physical Review E, **65**, no. 5 (2002) 051603.

[25] Z. Huang, A. A. Acero, N. Lei, S. A. Rice, Z. Zhang, and M. L. Schlossman. *Structural studies of semifluorinated hydrocarbon monolayers at the air/water interface.* Journal of the Chemical Society, Faraday Transactions, **92**, no. 4 (1996) 545–552.

[26] N. Duerr-Auster, J. Kohlbrecher, T. Zuercher, R. Gunde, P. Fischer, and E. Windhab. *Microstructure and stability of a lamellar liquid crystalline and*

gel phase formed by a polyglycerol ester mixture in dilute aqueous solution. Langmuir, **23**, no. 26 (2007) 12827–12834.

[27] N. Duerr Auster, R. Gunde, and E. Windhab. *Structure and Mechanical Properties of a Polyglycerol Ester at the Air-Water Surface.* Langmuir, **24**, no. 21 (2008) 12282–12289.

[28] W. Gelbart, A. Ben-Shaul, and D. Roux. *Micelles, Membranes, Microemulsions ans Monolayers.* Springer, New York, **1994**.

[29] D. Evans. *Self-Organization of Amphiphiles.* Langmuir, **4**, no. 1 (1988) 3–12.

[30] C. Tanford. *The Hydrophobic Effect.* Wiley, New York, **1980**.

[31] H. Butt, K. Graf, and M. Kappl. *Physics and Chemistry of Interfaces.* Wiley-VCH, Weinheim, **2006**.

[32] L. Wilhelmy. Annalen der Physik und Chemie, **119** (1863) 177–217.

[33] G. L. Gaines Jr. *On the use of filter paper wilhelmy plates with insoluble monolayers.* Journal of Colloid and Interface Science, **62**, no. 1 (1977) 191–192.

[34] H. Möhwald, C. Böhm, A. Dietrich, and S. Kirstein. *Mesophases in monolayers of fatty acids and phospholipids.* Liquid Crystals, **14**, no. 1 (1993) 265–277.

[35] K. B. Blodgett. *Films Built by Depositing Successive Monomolecular Layers on a Solid Surface.* J. Am. Chem. Soc., **57**, no. 6 (1935) 1007–1022.

[36] N. Vogel, L. De Viguerie, U. Jonas, C. K. Weiss, and K. Landfester. *Wafer-Scale Fabrication of Ordered Binary Colloidal Monolayers with Adjustable Stoichiometries.* Advanced functional materials, **21**, no. 16 (2011) 3064–3073.

[37] I. Langmuir, V. J. Schaefer, and D. M. Wrinch. *Properties of built-up protein films.* Sciences, **85** (1937) 76–80.

[38] G. Gaines. *Insoluble Monolayers at Liquid-Gas Interfaces.* Wiley, New York, **1966**.

[39] R. A. Hann. In G. Roberts (editor), *Langmuir Blodgett Films*, chapter 2. Plenum Press, New York, **1990**.

[40] A. Barraud, J. Leloup, P. Maire, and A. Ruaudel-Teixier. *Microdefect decoration and visualization in Langmuir-Blodgett films.* Thin Solid Films, **133**, no. 1-4 (1985) 133–139.

[41] R. M. Morelis, A. P. Girard-Egrot, and P. R. Coulet. *Dependence of Langmuir-Blodgett film quality on fatty acid monolayer integrity. 1. Nucleation crystal growth avoidance in the monolayer through the optimized compression procedure.* Langmuir, **9**, no. 11 (1993) 3101–3106.

[42] A. P. Girard-Egrot, R. M. Morelis, and P. R. Coulet. *Dependence of Langmuir-Blodgett film quality on fatty acid monolayer integrity. 2. Crucial effect of the removal rate of monolayer during Langmuir-Blodgett film deposition.* Langmuir, **9**, no. 11 (1993) 3107–3110.

[43] R. Steitz, E. Mitchell, and I. Peterson. *Relationships between fatty acid monolayer structure on the subphase and on solid substrates.* Thin Solid Films, **205**, no. 1 (1991) 124–130.

[44] H. Butt and M. Kappl. *Normal capillary forces.* Advances in Colloid and Interface Science, **146**, no. 1-2 (2009) 48–60.

[45] Y. Martin, C. C. Williams, and H. K. Wickramasinghe. *Atomic force microscope - force mapping and profiling on a sub 100 Å scale.* Journal of Applied Physics, **61**, no. 10 (1987) 4723–4729.

[46] Q. Zhong, D. Inniss, K. Kjoller, and V. Elings. *Fractured polymer/silica fiber surface studied by tapping mode atomic force microscopy.* Surface Science Letters, **290**, no. 1-2 (1993) L688–L692.

[47] R. Garcia and R. Parez. *Dynamic atomic force microscopy methods.* Surface Science Reports, **47**, no. 6-8 (2002) 197–301.

[48] S. N. Magonov and N. A. Yerina. *High-Temperature Atomic Force Microscopy of Normal Alkane C60H122 Films on Graphite.* Langmuir, **19**, no. 3 (2003) 500–504.

[49] S. Magonov. *Atomic Force Microscopy in Analysis of Polymers.* In *Encyclopedia of Analytical Chemistry.* John Wiley & Sons, Ltd, **2006**.

[50] M. Nonnenmacher, M. P. O´Boyle, and H. K. Wickramasinghe. *Kelvin probe force microscopy.* Applied Physics Letters, **58**, no. 25 (1991) 2921–2923.

[51] S. Kitamura and M. Iwatsuki. *High-resolution imaging of contact potential difference with ultrahigh vacuum noncontact atomic force microscope.* Applied Physics Letters, **72**, no. 24 (1998) 3154–3156.

[52] R. Berger, H. Butt, M. Retschke, and S. Weber. *Electrical Modes in Scanning Probe Microscopy.* Macromolecular rapid communications, **30**, no. 14 (2009) 1167–1178.

[53] U. Zerweck, C. Loppacher, T. Otto, S. Grafström, and L. M. Eng. *Accuracy and resolution limits of Kelvin probe force microscopy.* Phys. Rev. B, **71** (2005) 125424.

[54] D. Hönig and D. Möbius. *Direct visualization of monolayers at the air-water interface by Brewster angle microscopy.* J. Phys. Chem., **95**, no. 12 (1991) 4590–4592.

[55] K. Winsel, D. Hönig, K. Lunkenheimer, K. Geggel, and C. Witt. *Quantitative Brewster angle microscopy of the surface film of human broncho-alveolar lavage fluid.* European biophysics journal: EBJ, **32**, no. 6 (2003) 544–552.

[56] D. Vollhardt. *Morphology and phase behavior of monolayers.* Advances in Colloid and Interface Science, **64**, no. 0 (1996) 143 – 171.

[57] N. Sunderland and J. McLeish. *Nucleic acid content and concentration in root cells of higher plants.* Experimental Cell Research, **24**, no. 3 (1961) 541–554.

[58] H. Devoe and J. Tinoco, I. *The Stability of Helical Polynucleotides: Base Contributions.* Journal of Molecular Biology, **4** (1962) 500–517.

[59] D. M. Crothers and B. H. Zimm. *Theory of the Melting Transition of Synthetic Polynucleotides: Evaluation of the Stacking Free Energy.* Journal of Molecular Biology, **9** (1964) 1–9.

[60] J. Santa Lucia. *A unified view of polymer, dumbbell, and oligonucleotide DNA nearest-neighbor thermodynamics.* Proceedings of the National Academy of Sciences of the United States of America, **95**, no. 4 (1998) 1460–1465.

[61] G. Gaines. *Suface-Activity of Semifluiorinated Alkanes - F(CF2)M(CH2)NH.* Langmuir, **7**, no. 12 (1991) 3054–3056.

[62] M. P. Krafft and J. G. Riess. *Chemistry, Physical Chemistry, and Uses of Molecular Fluorocarbon-Hydrocarbon Diblocks, Triblocks, and related Compounds - Unique Apolar Components for Self-Assembled Colloid and Interface Engineering.* Chem. Rev., **109**, no. 5 (2009) 1714–1792.

[63] J. G. Riess. *Highly fluorinated amphiphilic molecules and self-assemblies with biomedical potential.* Current opinion in colloid & interface science, **14**, no. 5 (2009) 294–304.

[64] M. Broniatowski and P. Dynarowicz-Latka. *Semifluorinated alkanes - Primitive surfactants of fascinating properties.* Advances in Colloid and Interface Science, **138**, no. 2 (2008) 63–83.

[65] D. Jacquemain, S. G. Wolf, F. Leveiller, M. Lahav, L. Leiserowitz, M. Deutsch, K. Kjaer, and J. Als-Nielsen. *Dynamics of two-dimensional self-aggregation: pressure and pH-induced structural changes in a fluorocarbon amphiphile at liquid-air interfaces. An x-ray synchrotron study.* J. Am. Chem. Soc., **112**, no. 21 (1990) 7724–7736.

[66] S. G. Wolf, M. Deutsch, E. M. Landau, M. Lahav, L. Leiserowitz, K. Kjaer, and J. Als-Nielsen. *A Synchrotron X-ray Study of a Solid-Solid Phase Transition in a Two-Dimensional Crystal.* Science, **242**, no. 4883.

[67] A. N. Semenov, A. Gonzalez-Perez, M. P. Krafft, and J. Legrand. *Theory of Surface Micelles of Semifluorinated Alkanes*. Langmuir, **22**, no. 21 (2006) 8703–8717.

[68] M. Maaloum, P. Muller, and M. P. Krafft. *Monodisperse Surface Micelles of Nonpolar Amphiphiles in Langmuir Monolayers*. Angewandte Chemie International Edition, **41**, no. 22 (2002) 4331–4334.

[69] M. Krafft and M. Goldmann. *Monolayers made from fluorinated amphiphiles*. Current Opinion in Colloid & Interface Science, **8**, no. 3 (2003) 243–250.

[70] M. Broniatowski, I. Sandez Macho, Minones, and P. Dynarowicz-Latkaa. *Langmuir Monolayers Characteristic of (Perfluorodecyl)-Alkanes*. J. Phys. Chem. B, **108**, no. 35 (2004) 13403–13411.

[71] M. Broniatowski, J. Minones Jr., and D.-L. P. *Semifluorinated chains in 2D-(perfluorododecyl)-alkanes at the air/water interface*. Journal of Colloid and Interface Science, **279**, no. 2 (2004) 552–558.

[72] A. El Abed, E. Pouzet, M. Faure, M. Saniere, and O. Abillon. *Air-water interface-induced smectic bilayer*. Physical Review E, **62**, no. 5 (2000) R5895–R5898.

[73] T. Kato, M. Kameyama, M. Ehara, and K.-i. Iimura. *Monodisperse Two-Dimensional Nanometer Size Clusters of Partially Fluorinated Long-Chain Acids*. Langmuir, **14**, no. 7 (1998) 1786–1798.

[74] C. O. Klein, L. d. Viguerie, C. Christopoulou, U. Jonas, C. G. Clark, K. Müllen, and D. Vlassopoulos. *Viscoelasticity of semifluorinated alkanes at the air-water interface*. Soft Matter, **7**, no. 17 (2011) 7737–7746.

[75] C. de Gracia Lux and M. P. Krafft. *Nonpolar gemini amphiphiles Self-Assemble into stacked layers of Nano-Objects*. Chemistry - A European Journal, **16**, no. 38 (2010) 11539–11542.

[76] A. Gonzalez-Perez, C. Contal, and M. P. Krafft. *Experimental evidence for a surface concentration-dependent mechanism of formation of hemimicelles in Langmuir monolayers of semi-fluorinated alkanes*. Soft Matter, **3**, no. 2 (2006) 191–193.

[77] P. Lo Nostro. *Aggregates from semifluorinated n-alkanes: how incompatibility determines self-assembly*. Current Opinion in Colloid & Interface Science, **8**, no. 3 (2003) 223–226.

[78] N. Kim and S. Shin. *Formation of ordered structure in Langmuir monolayers of semifluorinated hydrocarbons: Molecular dynamics simulations*. The Journal of Chemical Physics, **110**, no. 21 (1999) 10239–10242.

[79] A. E. Abed, M.-C. Faure, E. Pouzet, and O. Abillon. *Experimental evidence for an original two-dimensional phase structure: An antiparallel semifluorinated monolayer at the air-water interface.* Phys. Rev. E, **65**.

[80] J. Alexander, S. Magonov, and M. Moeller. *Topography and surface potential in Kelvin force microscopy of perfluoroalkyl alkanes self-assemblies.* J. Vac. Sci. Technol., **27**, no. 2 (2009) 903–911.

[81] L. Chi, S. Jacobi, and H. Fuchs. *Chemical identification of differing amphiphiles in mixed Langmuir-Blodgett films by scanning surface potential microscopy.* Thin solid films, **284** (1996) 403–407.

[82] H. Sugimura, K. Hayashi, N. Saito, N. Nakagiri, and O. Takai. *Surface potential microscopy for organized molecular systems.* Applied Surface Science, **188**, no. 3-4 (2002) 403–410.

[83] S. Magonov, J. Alexander, S. Jeong, and N. Kotov. *High-Resolution Imaging of Molecular and Nanoparticles Assemblies with Kelvin Force Microscopy.* Journal of Nanoscience and Nanotechnology, **10**, no. 11 (2010) 7060–7064.

[84] S. Magonov and J. Alexander. *Single-pass Kelvin force microscopy and dC/dZ measurements in the intermittent contact: applications to polymer materials.* Beilstein Journal of Nanotechnology, **2** (2011) 15–27.

[85] L. de Viguerie, R. Keller, U. Jonas, R. Berger, C. G. Clark, C. O. Klein, T. Geue, K. Mullen, H.-J. Butt, and D. Vlassopoulos. *Effect of the Molecular Structure on the Hierarchical Self-Assembly of Semifluorinated Alkanes at the Air/Water Interface.* Langmuir, **27**, no. 14 (2011) 8776–8786.

[86] P. A. Kralchevsky and K. Nagayama. *Capillary forces between colloidal particles.* Langmuir, **10**, no. 1 (1994) 23–36.

[87] P. A. Kralchevsky and K. Nagayama. *Capillary interactions between particles bound to interfaces, liquid films and biomembranes.* Advances in Colloid and Interface Science, **85** (2000) 145–192.

[88] P. A. Kralchevsky and N. D. Denkov. *Capillary forces and structuring in layers of colloid particles.* Current Opinion in Colloid & Interface Science, **6**, no. 4 (2001) 383–401.

[89] C. M. Niemeyer. *Self-assembled nanostructures based on DNA: towards the development of nanobiotechnology.* Current opinion in chemical biology, **4**, no. 6 (2000) 609–618.

[90] H. Liu and D. Liu. *DNA nanomachines and their functional evolution.* Chemical Communications, , no. 19 (2009) 2625–2636.

[91] J. Bath and A. J. Turberfield. *DNA nanomachines.* Nature Nanotechnology, **2**, no. 5 (2007) 275–284.

[92] B. Yurke, A. Turberfield, A. Mills, F. Simmel, and J. Neumann. *A DNA-fuelled molecular machine made of DNA.* Nature, **406**, no. 6796 (2000) 605–608.

[93] F. A. Aldaye, A. L. Palmer, and H. F. Sleiman. *Assembling materials with DNA as the guide.* Science, **321**, no. 5897 (2008) 1795–1799.

[94] Z. Li, Y. Zhang, P. Fullhart, and C. A. Mirkin. *Reversible and Chemically Programmable Micelle Assembly with DNA Block-Copolymer Amphiphiles.* Nano Letters, **4**, no. 6 (2004) 1055–1058.

[95] M. Kwak and A. Herrmann. *Nucleic Acid/Organic Polymer Hybrid Materials: Synthesis, Superstructures, and Applications.* Angewandte Chemie-International Edition, **49**, no. 46 (2010) 8574–8587.

[96] A. Patwa, A. Gissot, I. Bestel, and P. Barthelemy. *Hybrid lipid oligonucleotide conjugates: synthesis, self-assemblies and biomedical applications.* Chemical Society Reviews, **40**, no. 12 (2011) 5844–5854.

[97] M. Kwak and A. Herrmann. *Nucleic acid amphiphiles: synthesis and self-assembled nanostructures.* Chem. Soc. Rev., **40**, no. 12 (2011) 5745–5755.

[98] M. P. Thompson, M. Chien, T. Ku, A. M. Rush, N. C. Gianneschi, and M. . *Smart lipids for programmable nanomaterials.* Nano letters, **10**, no. 7 (2010) 2690–2693.

[99] N. Cottenye, M. Syga, S. Nosov, A. H. E. Mueller, L. Ploux, and C. Vebert-Nardin. *Biological-like vesicular structures self-assembled from DNA-block copolymers.* Chemical Communications, **48**, no. 20 (2012) 2615–2617.

[100] F. Alemdaroglu and Ding. *Engineering the structural properties of DNA block copolymer micelles by molecular recogntition.* Angewandte Chemie (International ed. in English), **46**, no. 7 (2007) 1172–1175.

[101] A. Kurz, A. Bunge, A. Windeck, M. Rost, W. Flasche, A. Arbuzova, D. Strohbach, S. Mueller, J. Liebscher, D. Huster, and A. Herrmann. *Lipid-anchored oligonucleotides for stable double-helix formation in distinct membrane domains.* Angewandte Chemie-International Edition, **45**, no. 27 (2006) 4440–4444.

[102] M. Hadorn and P. E. Hotz. *DNA-Mediated Self-Assembly of Artificial Vesicles.* Plos One, **5**, no. 3.

[103] P. A. Beales, J. Nam, and T. K. Vanderlick. *Specific adhesion between DNA-functionalized "Janus" vesicles: size-limited clusters.* Soft Matter, **7**, no. 5 (2011) 1747–1755.

[104] Y. M. Chan, B. van Lengerich, and S. G. Boxer. *Effects of linker sequences on vesicle fusion mediated by lipid-anchored DNA oligonucleotides.* Proceedings of the National Academy of Sciences of the United States of America, **106**, no. 4 (2009) 979–984.

[105] G. Stengel, R. Zahn, and F. Höök. *DNA-induced programmable fusion of phospholipid vesicles.* Journal of the American Chemical Society, **129**, no. 31 (2007) 9584–+.

[106] B. Städler, D. Falconnet, I. Pfeiffer, F. Höök, and J. V. *Micropatterning of DNA-Tagged Vesicles.* Langmuir, **20**, no. 26 (2004) 11348–11354.

[107] H. Kitano and H. Ringsdorf. *Surface Behaviors of Nucleic-Acid Base-Containing Lipids in Monolayer and Bilayer Systems.* Bulletin of the Chemical Society of Japan, **58**, no. 10 (1985) 2826–2828.

[108] E. Montanha, F. Pavinatto, L. Caseli, O. Kaczmarek, J. Liebscher, D. Huster, and O. Oliveira Jr. *Properties of lipophilic nucleoside monolayers at the air/water interface.* Colloids and Surfaces B: Biointerfaces, **77**, no. 2 (2010) 161–165.

[109] E. Montanha, L. Caseli, O. Kaczmarek, J. Liebscher, D. Huster, and O. Oliveira Jr. *Comparative study of liponucleosides in Langmuir monolayers as cell membrane models.* Biophysical chemistry, **153**, no. 2-3 (2011) 154–158.

[110] L. Caseli, P. Pascholati, F. Teixeira Jr., S. Nosov, C. Vebert, A. Müller, and O. Oliveira Jr. *Interaction of oligonucleotide-based amphiphilic block copolymers with cell membrane models.* Journal of Colloid and Interface Science, **347**, no. 1 (2010) 56–61.

[111] M. Anaya, M. Kwak, A. J. Musser, K. MÃ$\frac{1}{4}$llen, and A. Herrmann. *Tunable Hydrophobicity in DNA Micelles: Design, Synthesis, and Characterization of a New Family of DNA Amphiphiles.* Chemistry - A European Journal, **16**, no. 43 (2010) 12852–12859.

[112] T. Oguchi, K. Sakai, H. Sakai, and M. Abe. *AFM surface morphology and friction force studies of microscale domain structures of binary phospholipids.* Colloids and Surfaces B: Biointerfaces, **79**, no. 1 (2010) 205–209.

[113] M. Kwak, I. J. Minten, D. Anaya, A. J. Musser, M. Brasch, and M. . *Virus-like Particles Templated by DNA Micelles: A General Method for Loading Virus Nanocarriers.* Journal of the American Chemical Society, **132**, no. 23 (2010) 7834–.

[114] J. Rodríguez Patino, A. Caro, M. Rodriguez Niño, A. Mackie, A. Gunning, and V. Morris. *Some implications of nanoscience in food dispersion formulations containing phospholipids as emulsifiers.* Food Chemistry, **102**, no. 2 (2007) 532–541.

[115] A. M. Goncalves da Silva, R. S. Romao, A. Lucero Caro, and J. M. Rodriguez Patino. *Memory effects on the interfacial characteristics of dioctadecyldimethylammonium bromide monolayers at the air-water interface.* Journal of Colloid and Interface Science, **270**, no. 2 (2004) 417–425.

[116] M. Nino, A. Lucero, and J. Patino. *Relaxation phenomena in phospholipid monolayers at the air-water interface.* Colloids and surfaces. A, Physicochemical and engineering aspects, **320**, no. 1-3 (2008) 260–270.

[117] J. G. Petrov, T. D. Andreeva, and H. Möhwald. *Fluorination of the Hydrophilic Head Accelerates the Collapse of the Monolayer but Stabilizes the Bilayer of a Long-Chain Trifluoroethyl Ether on Water.* Langmuir, **22**, no. 9 (2006) 4136–4143.

[118] J. Zhou, S. Gregurick, S. Krueger, and F. Schwarz. *Conformational Changes in Single-Strand DNA as a Function of Temperature by SANS.* Biophysical Journal, **90**, no. 2 (2006) 544–551.

[119] G. Nelles, H. Schönherr, M. Jaschke, H. Wolf, M. Schaub, W. Tremel, E. Bamberg, H. Ringsdorf, and H. Butt. *Two-Dimensional Structure of Disulfides and Thiols on Gold(111).* Langmuir, **14**, no. 4 (1998) 808–815.

[120] J. Garnaes, T. Bjornholm, and J. A. N. Zasadzinski. *Nanoscale lithography on Langmuir-Blodgett films of behinic acid.* In *The 1993 international conference on scanning tunneling microscopy*, volume 12, pp. 1839–1842. AVS, **1994**.

[121] M. Jaschke and H. Butt. *Deposition of Organic Material by the Tip of a Scanning Force Microscope.* Langmuir, **11**, no. 4 (1995) 1061–1064.

[122] R. D. Piner, J. Zhu, F. Xu, S. Hong, and C. A. Mirkin. *Dip-Pen Nanolithography.* Science, **283**, no. 5402 (1999) 661 –663.

[123] H. Tsai and Y. Lee. *Manipulation ordered and close-packed nanoparticle monolayers at air/liquid interface coupling Langmuir-Blodgett and self-assembly techniques.* Soft Matter, **5**, no. 15 (2009) 2962.

[124] E. Meyer, K. Rosenberg, and J. Israelachvili. *Recent Progress in Understanding Hydrophobic Interactions.* **103** 15739–15746.

[125] E. Meyer, Q. Lin, T. Hassenkam, E. Oroudjev, and J. Israelachvili. *Origin of the Long-Range Attraction Between Surfactant-Coated Surfaces.* Proceedings of the National Academy of Sciences of the United States of America, **102**, no. 19 (2005) 6839–6842.

[126] S. Vannoort, K. Vanderwerf, B. Degrooth, N. Vanhulst, and J. Greve. *Height anomalies in tapping mode atomic force microscopy in air caused by adhesion.* Ultramicroscopy, **69**, no. 2 (1997) 117–127.

[127] Y. Ebenstein, E. Nahum, and U. Banin. *Tapping Mode Atomic Force Microscopy for Nanoparticle Sizing: Tip-Sample Interaction Effects.* Nano Letters, **2**, no. 9 (2002) 945–950.

[128] M. A. Frommer and I. R. Miller. *Adsorption of DNA at the Air-Water Interface.* Journal of physical chemistry, **72**, no. 8 (1968) 2862–1866.

[129] F. E. Alemdaroglu, K. Ding, R. Berger, and A. Herrmann. *DNA-templated synthesis in three dimensions: Introducing a micellar scaffold for organic reactions.* Angewandte Chemie (International ed. in English), **45**, no. 25 (2006) 4206–4210.

[130] T. Wu, P. Gong, I. Szleifer, V. Subr, and J. Genzer. *Behavior of Surface-Anchored Poly(acrylic acid) Brushes with Grafting Density Gradients on Solid Substrates: 1. Experiment.* Macromolecules, **40**, no. 24 (2007) 8756–8764.

[131] P. Gong, T. Wu, J. Genzer, and I. Szleifer. *Behavior of Surface-Anchored Poly(acrylic acid) Brushes with Grafting Density Gradients on Solid Substrates: 2. Theory.* Macromolecules, **40**, no. 24 (2007) 8765–8773.

[132] G. L. Eichhorn and Y. A. Shin. *Interaction of metal ions with polynucleotides and related compounds. XII. The relative effect of various metal ions on DNA helicity.* J. Am. Chem. Soc., **90**, no. 26 (1968) 7323–7328.

[133] S. L. Lippard and S. M. Berg. *Bioanorganische Chemie.* Spektrum Akademischer Verlag, 1st edition, **1995**.

[134] R. G. Pearson. *Hard and Soft Acids and Bases. 1. Fundamental Principles.* Journal of chemical education, **45**, no. 9 (1968) 581–.

[135] K. Mortensen. *Structural studies of aqueous solutions of PEO-PPO-PEO triblock copolymers, their micellar aggregates and mesophases; A small-angle neutron scattering study.* Journal of physics. Condensed matter, **8**, no. 25A (1996) A103–A124.

[136] J. Sadoc and N. Rivier. *Foams and Emulsions.* Kluwer Academic Press, Dordrecht, **1997**.

[137] R. Pugh. *Foaming, foam films, antifoaming and defoaming.* Advances in Colloid and Interface Science, **64**, no. 0 (1996) 67 – 142.

[138] D. Weaire and S. Hutzler. *The Physics of Foams.* Oxfod University Press, 1st edition, **February 1999**.

[139] I. Kralova and J. Sjöblom. *Surfactants Used in Food Industry: A Review.* Journal of Dispersion Science & Technology, **30**, no. 9 (2009) 1363–1383.

[140] J. Bezelgues, S. Serieye, L. Crosset-Perrotin, and M. Leser. *Interfacial and foaming properties of some food grade low molecular weight surfactants.* Colloids and Surfaces A: Physicochemical and Engineering Aspects, **331**, no. 1-2 (2008) 56–62.

[141] P. J. Halling. *Protein-stabilized Foams and Emulsions.* Critical reviews in food science and nutrition, **15**, no. 2 (1981) 155–203.

[142] J. Davis and E. Foegeding. *Comparisons of the foaming and interfacial properties of whey protein isolate and egg white proteins.* Colloids and Surfaces B: Biointerfaces, **54**, no. 2 (2007) 200–210.

[143] A. R. Cox, D. L. Aldred, and A. B. Russell. *Exceptional stability of food foams using class II hydrophobin HFBII.* Food Hydrocolloids, **23**, no. 2 (2009) 366–376.

[144] P. Erni, E. J. Windhab, P. Fischer, and P. . *Emulsion Drops with Complex Interfaces: Globular Versus Flexible Proteins.* Macromolecular materials and engineering, **296**, no. 3-4 (2011) 249–262.

[145] B. P. Binks. *Particles as surfactants - similarities and differences.* Current opinion in colloid & interface science, **7**, no. 1-2 (2002) 21–41.

[146] R. G. Alargova, D. S. Warhadpande, V. N. Paunov, O. D. Velev, and R. . *Foam superstabilization by polymer microrods.* Langmuir, **20**, no. 24 (2004) 10371–10374.

[147] A. C. Martinez, E. Rio, G. Delon, A. Saint Jalmes, and D. Langevin. *On the origin of the remarkable stability of aqueous foams stabilised by nanoparticles: link with microscopic surface properties.* Soft matter, **4**, no. 7 (2008) 1531–1535.

[148] Z. Du, M. Bilbao-Montoya, B. Binks, E. Dickinson, R. Ettelaie, and B. Murray. *Outstanding stability of particle-stabilized bubbles.* Langmuir, **19**, no. 8 (2003) 3106–3108.

[149] J. M. Rodriguez Patino, C. Carrera Sanchez, and M. R. Rodriguez Niño. *Implications of interfacial characteristics of food foaming agents in foam formulations.* Advances in Colloid and Interface Science, **140**, no. 2 (2008) 95–113.

[150] N. Duerr Auster, T. Eisele, R. Wepf, R. Gunde, and E. Windhab. *Influence of pH on colloidal properties and surface activity of polyglycerol fatty acid ester vesicles.* Journal of colloid and interface science, **327**, no. 2 (2008) 446–450.

[151] B. S. Murray. *Stabilization of bubbles and foams.* Current Opinion in Colloid & Interface Science, **12**, no. 4-5 (2007) 232–241.

[152] N. Duerr Auster, R. Gunde, R. Mader, and E. Windhab. *Binary coalescence of gas bubbles in the presence of a non-ionic surfactant.* Journal of colloid and interface science, **333**, no. 2 (2009) 579–584.

[153] E. Reimhult, B. Kasemo, and F. Höök. *Rupture Pathway of Phosphatidylcholine Liposomes on Silicon Dioxide.* International Journal of Molecular Sciences, **10**, no. 4 (2009) 1683–1696.

[154] M. A. V. Axelos and F. Boue. *Foams As Viewed by Small-Angle Neutron Scattering.* Langmuir, **19**, no. 17 (2003) 6598–6604.

[155] K. Dimitrievski, M. Zach, V. P. Zhdanov, and B. Kasemo. *Imaging and manipulation of adsorbed lipid vesicles by an AFM tip: Experiment and Monte Carlo simulations.* Colloids and surfaces. B, Biointerfaces, **47**, no. 2 (2006) 115–125.

[156] G. Andreatta, Y. J. Wang, F. K. Lee, A. Polidori, P. Tong, and G. . *Molecular transfer of surfactant bilayers: Widening the range of substrates.* Langmuir, **24**, no. 12 (2008) 6072–6078.

[157] J. Benattar, M. Nedyalkov, F. K. Lee, and O. K. C. Tsui. *Adhesion of a Free-Standing Newton Black Film onto a Solid Substrate.* Angewandte Chemie International Edition, **45**, no. 25 (2006) 4186–4188.

[158] X. Zhang, G. Tang, S. Yang, and J. Benattar. *Two-Dimensional Self-Assemblies of Silica Nanoparticles Formed Using the Bubble Deposition Technique.* Langmuir, **26**, no. 22 (2010) 16828–16832.

[159] G. Reiter. *Dewetting of thin polymer films.* Physical Review Letters, **68**, no. 1 (1992) 75–78.

[160] R. Seemann, S. Herminghaus, and K. Jacobs. *Dewetting Patterns and Molecular Forces: A Reconciliation.* Physical Review Letters, **86**, no. 24 (2001) 5534–5537.

[161] P. Müller-Buschbaum. *Dewetting and pattern formation in thin polymer films as investigated in real and reciprocal space.* Journal of Physics: Condensed Matter, **15**, no. 36 (2003) R1549–R1582.

[162] N. Müller-Fischer, H. Bleuler, and E. Windhab. *Dynamically enhanced membrane foaming.* Chemical Engineering Science, **62**, no. 16 (2007) 4409–4419.

[163] W. Hanselmann and E. Windhab. *Flow characteristics and modelling of foam generation in a continuous rotor/stator mixer.* Journal of Food Engineering, **38**, no. 4 (1998) 393–405.

List of Publications and Presentations

Accepted Publications:

B. Lorenz, R. Keller, E. Sunnik, B. Geil, A. Janshoff, *Colloidal Probe Microscopy of Membrane-Membrane Interactions: From Ligand-Receptor Recognition to Fusion Events*, Biophysical Chemistry **150**, p. 54 (2010).

L. de Viguerie , R. Keller, U. Jonas, R. Berger, C. G. Clark, Jr., C. O. Klein, T. Geue, K. Müllen, H.-J. Butt, D. Vlassopoulos, *Effect of Molecular Structure on the Hierarchical Self-Assembly of Semifluorinated Alkanes at the Air/Water Interface*, Langmuir **27**, p. 8776 (2011).

C. Curschellas , R. Keller, R. Berger, U. Rietzler, D. Fell, H.-J. Butt, H.-J. Limbach, *Scanning Force Microscopy as a Tool to Investigate the Properties of Polyglycerol Ester Foams*, Journal of Colloid and Interface Science **347**, p. 164 (2012).

Manuscripts submitted:

R. Keller, M. Kwak, C. Sawaryn, J. Wang, M. Anaya, K. Müllen, H.-J. Butt, A. Herrmann, R. Berger, *Properties of Amphiphilic DNA Films at the Air/Water Interface and after Film Transfer*, submitted to Colloids and Surfaces B: Biointerfaces.

Oral Presentations at International Conferences and Meetings:

02.2011 Zsigmondy-Kolloquium der Kolloidgesellschaft, Münster, Germany: "Organization of Amphiphilic Molecules at the Air/Water Interface".

05.2012 International Association of Colloid and Interface Scientists Conference, Sendai, Japan: "Self-Assembly of Amphiphilic DNA Hybrid Molecules at the Air/Water Interface".

Poster Presentations at International Conferences and Meetings:

06.2009 Scanning Probe Microscopies and Organic Materials XVII: "Influence of Synapsin I on Synaptic Vesicles".

06.2009 Scanning Probe Microscopies and Organic Materials XVII: "DNA Block Copolymers as Building Units for Self-Assembled Structures".

09.2011 MPI-P Posterday, Mainz, Germany: "Atomic Force Microscopy as a Tool to Investigate the Properties of Polyglycerol Ester Foams", Best Poster Award.